INFORMATION TO USERS

This manuscript has been reproduced from the microfilm master. UMI films the text directly from the original or copy submitted. Thus, some thesis and dissertation copies are in typewriter face, while others may be from any type of computer printer.

The quality of this reproduction is dependent upon the quality of the copy submitted. Broken or indistinct print, colored or poor quality illustrations and photographs, print bleedthrough, substandard margins, and improper alignment can adversely affect reproduction.

In the unlikely event that the author did not send UMI a complete manuscript and there are missing pages, these will be noted. Also, if unauthorized copyright material had to be removed, a note will indicate the deletion.

Oversize materials (e.g., maps, drawings, charts) are reproduced by sectioning the original, beginning at the upper left-hand corner and continuing from left to right in equal sections with small overlaps. Each original is also photographed in one exposure and is included in reduced form at the back of the book.

Photographs included in the original manuscript have been reproduced xerographically in this copy. Higher quality 6" x 9" black and white photographic prints are available for any photographs or illustrations appearing in this copy for an additional charge. Contact UMI directly to order.

UMI

A Bell & Howell Information Company
300 North Zeeb Road, Ann Arbor MI 48106-1346 USA
313/761-4700 800/521-0600

Synthesis and Characterization of Ti_3SiC_2

A Thesis

Submitted to the Faculty

of

Drexel University

by

Tamer S. El-Raghy

in partial fulfillment of the

requirement for the degree

of

Doctor of Philosophy

June 1997

DREXEL UNIVERSITY

Thesis Approval Form
(For Masters and Doctoral Students)

This thesis, entitled Synthesis and Characterization of Ti_3SiC_2 and authored by Tamer S. El-Raghy, is hereby accepted and approved.

Signatures:

Chairman, Examining Committee:

Supervising Professor:

Committee Members:

Peter F. Barnes

Graduate Advisor:

Department Head:

Form T-1

DEDICATION

To my Father and my Mother

To Nour and Nahla

Thank you.

ACKNOWLEDGMENT

The author would like to express his sincere gratitude to his advisor Prof. M. W. Barsoum for his continuous scientific and moral support. Working with him is a great honor. The author greatly appreciates the contribution of his co-advisors Dr. A. Zavaliangos and Dr. S. Kalidindi to this work. The author is also grateful to Dr. L. Ogbuji, NASA-Lewis, for his contribution to the oxidation study. The author would like to thank Prof. P. Davies, Prof. R. Doherty, and Dr. W. Shih for their time and interest in reviewing this thesis and participating in the author's defense committee.

Special thanks are due to Mr. D. Von Rohr for his great help with the SEM and to Mr. M. Shiber for doing a great job in machining dies for this work. Also the author would like to than Mr. S. McCollum. for his help during the author's first six months. Special thanks are due to Judy Trachtman for her help and advice. Special thanks are also due to all the faculty members of the Materials Engineering Department.

The author aiso thanks all the graduate students, and the MAGNET officers, in the Materials Engineering Department for making this work an enjoyable and unforgettable experience. Special thanks are due to Dr. D. Brodkin for his help during the last two years.

Finally, the author would like to thank all the teachers and professors, back in Egypt, who taught the author and transferred their knowledge to him since his first day in the never ending education path.

Table of Contents

List of Tables

List of Figures

Abstract

Synthesis and Characterization of Ti_3SiC_2

Tamer S. El-Raghy

Prof. Michel M. Barsoum

This work aimed to characterize the physical properties of Ti_3SiC_2 as well as to investigate the microstructure evolution and its effect on the mechanical properties, the deformation mechanism, the high temperature oxidation, and surface treatment (carburization, siliconization, and nitridation).

For the first time, bulk, single phase, fully dense Ti_3SiC_2 samples were fabricated by hot pressing or HIPing of Ti, SiC, and C powders. This compound is as readily machinable as graphite. The room temperature electrical conductivity is 4.5×10^6 $ohm^{-1}\ m^{-1}$, roughly twice that of pure Ti. The thermal expansion coefficient in the temperature range 25 to 1000 °C, the room temperature thermal conductivity, and heat capacity are respectively, 9.2×10^{-6} $°C^{-1}$, 43 W/m.K, and 588 J/kg K. Young's modulus of 325 GPa was measured.

By controlling the process, the final grain size can be either fine (3-5 μm), or coarse (100-200 μm). For both microstructures the failure is brittle at room temperature. A brittle to ductile transition temperature of 1200 °C was measured. At 1300 °C, both microstructures exhibited high levels of plasticity (> 20 %). Both the fine and the coarse grained materials was found to be damage tolerant. Although the coarse grains material is not susceptible to thermal shock up to 1400 °C, the fine grains material was found to thermal shock between 750 and 1000 °C.

Oriented macro-grains (1-4 mm) of Ti_3SiC_2 were fabricated to study the deformation mechanism. We have shown conclusively that there is an active slip system (across the basal planes) at room temperature which results in the room temperature

plasticity. It was found that grain buckling and cavities formation are the mechanisms by which the material can accommodate the strain.

The oxidation was parabolic with parabolic rate constants, k_p, that increased from 1 x 10^{-9} (comparable to that of Cr metal) to 1 x 10^{-4} $kg^2m^{-4}s^{-1}$ as the temperature increased from 900 to 1400 °C, respectively, which yielded an activation energy of 370±20 kJ/mol. The scale that forms was dense, adhesive, resistant to thermal cycling and layered. The outer layer was pure TiO_2 (rutile), and the inner layer consisted of mixture of SiO_2 and TiO_2. The results are consistent with a model in which growth of the oxide layer occurs by the inwards diffusion of oxygen and the simultaneous outwards diffusion of titanium and carbon.

By surface treatment, the hardness was measured to be 10-25. and 7-15 GPa in the case of carburization, and nitridation respectively. In siliconization, while the surface hardness values of 10-12 GPa were measured, the oxidation resistance was found to be enhanced more than 3 orders of magnitude. Activation energies of 370 and 130 kJ/mol were measured in carburization and siliconization respectively.

1. Introduction

Ceramic materials are primary candidates for numerous critical applications due to their hardness, excellent wear resistance and chemical stability, along with high modulus and specific strength. Ceramic compounds could be used at high temperatures or in environments beyond the reach of their metal or intermetallic counterparts. However, the inherent disadvantages of monolithic (single phase) ceramics are their brittleness and hence tendency to catastrophic failure, as well as the very high machining costs, and their tendency to thermal shock.

The need for a material that can stand the severe conditions in high temperature structural applications is essential. Such a material should be strong at high temperatures with a non-catastrophic failure. It should be thermal shock resistant, damage tolerant, as well as chemically stable at high temperatures (ex. oxidation resistance). Since the costs of machining ceramics and superalloys are quite high, the desired material should be engineered so that the machining costs can be reduced.

In the last two decades, the ternary compound, Ti_3SiC_2, was reported as an interesting material that could be the desired " ductile ceramic". Due to the difficulties in fabricating monolithic, bulk and dense samples of Ti_3SiC_2, very little is known about it. Very recently, for the first time, we have reported on the processing of Ti_3SiC_2 in monolithic bulk and essentially dense form. As described in this work, the material was found to posses the desired properties to render it a promising candidate for high temperature applications. It is as machinable as graphite, damage tolerant and at temperatures as high as 1300 °C, is plastic with yield points that are higher than the best

superalloy available in the market today. Also Ti_3SiC_2 can be fabricated so that it is not susceptible to thermal shock up to 1400 °C. Ti_3SiC_2 is relatively soft (4 GPa) compared to other structural ceramics, but we have shown that it can be surface treated to bring the surface hardness to values of 20 GPa. Although it has a good oxidation resistance up 1000 °C (comparable to that of Cr metal), siliconizing the surface enhances the oxidation resistance and makes it comparable to those of ultra oxidation resistant ceramics such as $MoSi_2$, SiC, and $TiSi_2$.

This thesis is a collection of published (chapters 2* and 4), accepted for publication (chapter 5) or in preparation (chapters 3, 6, 7, and 8) papers. In chapter 2 the preliminary results of the processing and properties of Ti_3SiC_2 are reported. Chapter 3 discusses the reaction path and the microstructure evolution during the processing. Chapter 4 describes the damage mechanisms around the hardness indentation and also the damage tolerance. Chapters 5 and 6 investigate the high temperature oxidation and the surface treatment, respectively. Chapters 7 and 8 discuss the effect of microstructure on the mechanical properties and the deformation mechanisms, respectively. Chapter 9 proposes some recommendations for future work.*

* Please note that references 15, 17, 18, 24, 53 and 54 refer to chapters 2, 7, 4, 6, 5 and 3 respectively.

2. A Remarkable Ceramic: Ti_3SiC_2

Polycrystalline bulk samples of Ti_3SiC_2 were fabricated by reactively hot pressing Ti, graphite and SiC powders at 40 MPa and 1600 °C for 4 hours. This compound has remarkable properties. Its compressive strength, measured at room temperature, was 600 MPa, and dropped to 260 MPa at 1300 °C in air. Although the room temperature failure was brittle, the high temperature load-displacement curve shows significant plastic behavior. The oxidation is parabolic and at 1000 and 1400 °C the parabolic rate constants were, respectively, 2×10^{-8} and 2×10^{-5} $kg^2.m^{-4}$ s^{-1}. The activation energy for oxidation is thus ≈ 300 kJ/mol. The room temperature electrical conductivity is 4.5 x 106 ohm^{-1} m^{-1}, roughly twice that of pure Ti. The thermal expansion coefficient in the temperature range 25 to 1000 °C, the room temperature thermal conductivity, and heat capacity are respectively, 10×10^{-6} $°C^{-1}$, 43 W/m.K, and 588 J/kg K. With a hardness of 4 GPa and a Young's modulus of 320 GPa, it is relatively soft, but reasonably stiff. Furthermore, Ti_3SiC_2 does not appear to be susceptible to thermal shock; quenching from 1400 °C into water does not affect the post-quench bend strength. As significantly, this compound is as readily machinable as graphite. Scanning electron microscopy of polished and fractured surfaces leaves little doubt as to the its layered nature.

2.1 Introduction

Ti_3SiC_2 was first synthesized by Jeitschko and Nowotny [1] via a chemical reaction between TiH_2, Si and graphite at 2000 °C. The crystal structure is hexagonal and comprised of planar Si-layers linked together by TiC octahedra [1,2,4]. Its theoretical density is 4.51 gm/cm^3. To date pure Ti_3SiC_2 has only been synthesized by chemical

vapor deposition techniques in small quantities [2,3]. Attempts to synthesize it in bulk form always resulted in composites containing either TiC or SiC [5-10]. Consequently, very little is known about this compound. Its melting point has been reported to be in excess of 3000 °C [5]. Pampuch et al. [10] measured a Young's modulus of 326 GPa and a hardness of about 6 GPa, the latter in agreement with Goto and Hirai's [2] value of 6 GPa. Both groups have shown that the Vickers microhardness was a function of indentation load and concluded from that observation that Ti_3SiC_2 was a "ductile" ceramic. Interestingly enough Nickl et al. [3], indicated that while Ti_3SiC_2 formed by powder metallurgical processes did not show plastic behavior, their vapor deposited compound did show unusual plastic behavior similar to graphite. Knoop hardness measurements on small CVD single crystals by the same authors indicated a high anisotropy that was compatible with its layered structure.

Over the past several years we have been processing ultra-refractory ceramic-ceramic composites in the Ti-B-C and Zr-B-C systems using transient plastic phase processing or TPPP [11-13]. In TPPP, we start with a mixture of powders of a transient plastic phase (TPP) and a reactant phase (RP). The transient plastic phase is defined as a phase with a wide range of stoichiometry and a yield point that is a strong function of that stoichiometry. The reactant phase is one that will react with the transient phase according to:

"soft" transient plastic matrix + reactant phase fi hard matrix + reinforcement phase,

in such a way as to shift the composition of the TPP towards its harder and more refractory composition. The presence of the "soft" phase allows for densification to occur more readily. This approach has allowed us to fully densify ceramic/ceramic composites that otherwise were difficult or impossible to fabricate. The work reported here is a natural extension of this approach; we start with a mixture of Ti, C and SiC powders. We know

from previous work that the Ti and C react together during heating to form substoichiometric TiC_x, which we believe plays an important role in the overall process.

2.2 Processing

Bulk polycrystalline samples (final dimensions ≈ 76.2 x 25.4 x 7 mm) were fabricated by mixing Ti, C and SiC powders, the characteristics of which are listed in Table I, to yield the desired stoichiometry (3:1:2, Ti:Si:C). The powders were cold pressed at 180 MPa and then hot pressed at 1600 °C for 4 hours under a pressure of 40 MPa. The heating rate was 10 °C/min. X-ray diffraction of powdered samples indicated the presence of only Ti_3SiC_2 (Fig. 1). However, back scattered SEM micrographs of polished cross-sections indicated that there was less than 2 vol% SiC and TiC_x in the final samples, but no porosity. The measured density was 4.5 gm/cc, which is > 99 % of theoretical. We believe, at this time, that the presence of SiC and TiC_x in the final composite is not related to an incomplete reaction, but rather a shift of the overall chemistry to a higher C-content by the diffusion of C from the dies. To test this hypothesis we fabricated samples by hot isostatic pressing at 1600 ° and obtained significantly purer samples, with a total SiC and TiCx content that was less than 1%

In contrast to some reports in the literature [7,14] that Ti_3SiC_2 is thermally unstable and dissociates to TiC_x and gaseous Si at temperatures above ≈ 1400 °C, the ternary fabricated here was found to be quite stable up to 1600 °C. Post-fabrication anneals for 8 hrs in a vacuum (≈ 10^{-3} Pa) hot press at 1600 °C resulted in a weight loss of less than 1 %.

2.3 Microstructure

Optical microscopy on polished and etched (20 seconds in a 1:1:1 by volume solution of H_2O, HNO_3 and HF) cross sections and SEM microscopy on fractured surfaces were carried out. A typical optical micrograph is shown in Fig. 2a. An SEM of the black grains apparent in the bottom left of Fig. 2a, is shown in Fig. 2b at a higher magnification, which unequivocally confirms the layered nature of Ti_3SiC_2. The fractured surface is shown in Fig. 2c, where once again the cleavage planes are readily apparent.

2.4 Oxidation Resistance

To measure the oxidation kinetics the time dependence of the weight changes of small cubes in air were measured at 1000 and 1400 °C. At both temperatures the kinetics were parabolic, with a parabolic rate constant, K_w, calculated to be 2×10^{-8} kg^2 $m^{-4}s^{-1}$ at 1000 °C, which is comparable to Cr metal. X-ray diffraction and SEM of the oxidized surfaces indicated the presence of rutile and SiO_2, in accordance with Racault et al. [7]. At 1400 °C the parabolic rate constant was 2×10^{-5} $kg^2m^{-4}s^{-1}$, implying that the activation energy for oxidation is ≈ 300 kJ/mole. It is interesting to compare our oxidation results with those previously reported. For example, Tong et al. [14] working with 95 % dense samples report a parabolic rate constant that is roughly three orders of magnitude higher than the one reported here. The reason for the discrepancy is not clear at this point, but could be due to the presence of significant amounts of unreacted TiC and/or the fact that their samples were not fully dense.

2.5 Mechanical Properties

The Young's modulus of Ti_3SiC_2 was estimated using the resonance frequency technique to be ~320 GPa, which is in good agreement with the only previously reported value of 326±11 GPa [9]. The Vickers hardness was measured to be 4 GPa, which, as far as we are aware, is the lowest value reported to date. This is not too surprising given the purity of our samples.

The flexural strength or modulus of rupture, MOR, was determined by four-point bending of electron discharged machined samples with approximate dimensions of 1.5 x 2.0 x 25 mm^3. The tensile surfaces of the specimens were polished down to 0.03 μm alumina powder and the edges were beveled to minimize edge effects. The tests were performed on a servo-hydraulic machine using a cross-head displacement rate of 0.0033 mm/s. The flexural strength was measured to be 260±20 MPa. While this value may not be very high it is quite respectable considering that some of the larger grains in our samples were of the order of 100 μm (see Fig. 2a). It is not unreasonable to assume that reducing the grain size should, in principle, significantly enhance the MOR (see chapter 7).

Small parallelepipeds (2.7x1.8 mm cross section and 4.3 mm high) were electron discharged machined and the compressive strength was measured at room temperature and at 1300 °C in air using a cross-head displacement rate of 0.0033 mm/s. At room temperature, the compressive strength was 580 ± 20 MPa. Since no attempt was made to reduce the friction between the samples and the compression platens, these values have to be considered a lower bound. At 1300 °C, the compressive strength was 260 ± 5 MPa. The stress-strain curves, however, indicate substantial yield at that temperature (see Fig. 3). It is worth noting that the yield point at this temperature is significantly higher than that of the best superalloys available today.

The susceptibility to thermal shock was evaluated by quenching small parallelepipeds (2 x 1.5 x 25 mm^3) from successively higher temperatures into ambient temperature water. The samples were inserted into the hot furnace and held at temperature approximately 5-10 mins. The quenched surfaces were then lightly polished to remove the oxide layer that may have formed and the retained four-point bend strength was measured as described above. The effect of the severity of the quench on the retained strength is plotted in Fig. 4, where each bar represents a different sample. It is obvious from the data that Ti_3SiC_2 is not susceptible to thermal shock, an unprecedented conclusion for a ceramic . Typically resistance to thermal shock is related to a combination of low thermal expansion coefficient, high fracture toughness and thermal conductivity. Given that the thermal expansion and conductivity (see below) are not extreme, the excellent thermal shock resistance of Ti_3SiC_2 is probably related to a high fracture toughness. We are currently attempting to measure the fracture toughness and the results will be published shortly (see chapter 4).

2.6 Machinability

As remarkable as the non-susceptibility to thermal shock and of great technological importance, is the fact that this material is very readily machinable. Holes are easily drillable in our samples using commonly available high-speed steel drill bits with no lubrication. These holes, in turn, are easily hand tapped to form very precise internal thread screws as shown in Fig. 5. Interestingly enough no burrs are evident, but the feel of the shavings were reminiscent of graphite.

2.7 Thermal and Electrical Properties

The thermal conductivity and specific heat capacity of a sample which had a density of 4.48 $gm.cm^{-3}$, were measured at 27 °C using a laser flash technique to be, respectively, 43 W/m K and 588 J/kg K. These values are similar of those of pure Ti, namely, 31 W/m K and 523 J/kg K, respectively.

The thermal expansion coefficient was measured in a dilatometer (Model TDA-H1, Harrop Industries, Columbus, OH) in the temperature range 25-1000 °C. To avoid oxidation the samples were covered with a TiC powder and the runs were carried out under Ar. The coefficient of thermal expansion was measured to be $9.2\pm0.5 \times 10^{-6}$ $°C^{-1}$ in the temperature range 25-1000 °C. This value is slightly lower than that of pure TiC.

The electrical resistance was measured at room temperature using a microohmeter (Model 5600 AEMC Instruments), from which the electrical conductivity was calculated to be 4×10^6 ohm^{-1} m^{-1} and found to increase with decreasing temperature. The temperature coefficient of resistivity was measured to be 0.019 $°C^{-1}$ in the 50-300 K temperature range. The fact that the electrical conductivity of Ti_3SiC_2 is higher than either pure Ti (2.3×10^6 S/m) or TiC (1.6×106 S/m), is important since it is a strong indication that delocalized electrons parallel to the Si planes are contributing to the overall conductivity. This fact together with the ease of machinability, relative softness, and layered nature of the compound leads us to conclude that Ti_3SiC_2 and graphite have much in common.

2.8 Technological Importance

Ti_3SiC_2 is a remarkable material in that it combines many of the best attributes of both metals and ceramics. Like metals it is an excellent electric and thermal conductor,

easily machinable, relatively soft, not susceptible to thermal shock and behaves plastically at higher temperatures. Like ceramics it is oxidation resistant, extremely refractory, and, most importantly, it maintains its strength to temperatures that render the best superalloys available today unusable. As far as we are aware, the combination of machinability, strength and ductility at elevated temperatures and non-susceptibility to thermal shock has never been observed in any other material. Additionally, it is worth noting that the values reported here are far from optimized; once the deformation mechanisms are better understood, it is not unreasonable to expect enhancements in the mechanical properties.

We believe that the technological impact of this material, even with the limited set of data reported here, as a structural ceramic for high temperature applications, a graphite or a machinable ceramic substitute will not be inconsequential. Furthermore, Ti_3SiC_2 is much stronger in compression than graphite, very easily machinable and oxidation resistant, in other words, a potentially ideal material for any application, such as bearings, that demands lubricity at elevated temperatures in air or other oxidizing environments. Such a material does not exist at this time.

The high yield points and plasticity at 1300 °C, together with its oxidation resistance and non susceptibility of thermal shock, renders Ti_3SiC_2 a likely candidate for structural applications at elevated temperatures, such as turbine blades and stators. If one compares the properties of Ti_3SiC_2 reported above with those of other materials that are being considered today for the fabrication of ceramic engines, most notably Si_3N_4, it is obvious that Ti_3SiC_2 is the more promising candidate at a comparable level of development.

The ease of machinability, together with the retention of strength at high temperatures renders it an excellent replacement for currently available machinable ceramics

such as Maycor^{TM}. It is important to note that in contrast to currently machinable ceramics, Ti_3SiC_2 does not require firing after machining. Furthermore, the thermal shock resistance and good electrical conductivity render it an excellent candidate for electrodes used for metal smelting in general, and Al in particular. Finally the ease by which this compound can be strengthened by thermodynamically stable inclusions, such as SiC, TiC, $TiSi_2$ and $Ti_5Si_3C_x$, is an extra dimension that will indubitably render Ti_3SiC_2, and its composites, solids of great technological importance.

3. Reaction Path and Microstructure Evolution During the Processing of Ti_3SiC_2

This work was conducted to study the reaction path and microstructure evolution during the reactive hot isostatic processing of Ti_3SiC_2, starting with Ti, SiC and graphite powders. A series of interrupted and completed hot isostatic press runs were made at different temperatures in the range of 1200 - 1600 °C, for different periods of time (0 - 24 hours). Based on x-ray diffraction and SEM-EDS results, it has been shown that the main phases present at ≈ 1200 °C are TiC_x and $Ti_5Si_3C_x$. Ti_3SiC_2 appears to nucleate and grow within the $Ti_5Si_3C_x$ phase. Fully dense, essentially single phase samples can be produced over the temperature range 1450 - 1600 °C, and various times (1-8 hrs depending on temperature). The time-temperature processing envelope for fabricating, small (≈ 5μm), large (≈300 μm) and a duplex microstructure in which large grains of Ti_3SiC_2 are embedded in a much finer matrix has been delineated. The effect of the starting powders and the fabrication process (HIP vs hot press) on the final material was studied. Ti_3SiC_2 was found to be thermally stable under vacuum and Ar atmosphere at temperatures as high as 1600 °C for up to 24 hours.

3.1 Introduction

Recently, the fabrication of bulk polycrystalline single phase Ti_3SiC_2 was reported on [15]. Based on the results obtained to date, Ti_3SiC_2, appears to be a very promising candidate material for high temperature structural applications. This compound was found to be as machinable as graphite, not susceptible to thermal shock and posses good oxidation resistance, especially up to 1100 °C [16]. It is a good thermal (43 w/m.K) and a

good electrical conductor (4.5 x 10^6 $\Omega^{-1}m^{-1}$) . Its thermal expansion coefficient is 9.2 x 10^{-6} $°C^{-1}$.

Mechanically, Ti_3SiC_2 posses a Vickers hardness of 4 GPa and a Young's modules of 320 GPa, respectively [15]. The ductile-to-brittle transition is fairly sharp and occurs around 1200 °C [17 (see chapter 7)]; above that temperature the material showed large strains to failure (> 20 %). The modulus of rupture, compressive strength and K_{IC}, at ambient temperatures were reported to be 330 MPa, 720 MPa and 6.7 MPa $\sqrt{m}$. To date most, if not all, the mechanical properties characterizations were carried out on large (> 100 μm) grained samples. In the accompanying paper the effect of grain size on the mechanical properties is addressed [17 (see chapter 7)]. Ti_3SiC_2 was found to be damage tolerant [18 (see chapter 4)] where many energy absorption mechanisms were found to operate around the hardness indentation.

Ti_3SiC_2 was first synthesized by Jeitschko and Nowotny [1] via a chemical reaction between TiH_2, Si, graphite at 2000 °C. Because previous attempts [2, 3, 6-10, 19] to synthesize Ti_3SiC_2 in bulk form resulted in non-single-phase materials, little data are available about Ti_3SiC_2. Okano et al [9], working with bulk samples that contained some secondary phases (TiC_x and Ti-silicides), and were 95 % of the theoretical density, fabricated by hot pressing Ti_3SiC_2 powders that were synthesized via a solid state reaction, reported the flexural strength and K_{IC} at room temperature to be 580 MPa and 6.9 MPa$\sqrt{m}$, respectively. Also they reported preliminary results of the oxidation behavior at 1000 °C (porous non protecting TiO_2 layer). Pampuch et al [6,10], working with samples that contained anywhere from 10 - 20 % TiC, that were fabricated by hot pressing Ti_3SiC_2 powders synthesized by self-propagating high temperature synthesis, reported Young's modulus and the hardness values to be 326 and 6 GPa respectively. Gotto et al [2] and Nickel et al [3] reported the production of small quantities of Ti_3SiC_2 by means of CVD

and reported that Ti_3SiC_2 behaves as a "ductile" ceramic. Lis et al.[19] measured the hardness of Ti_3SiC_2 - TiC composites as a function of their TiC contents and estimated that the hardness of pure polycrystalline Ti_3SiC_2 should be about 4 GPa. Racault et al [7], by solid state reaction and then leaching ended with Ti_3SiC_2 powder, reported the thermal expansion coefficient and also the oxidation behavior (was found to be better than that of TiC) but on the other hand they reported that Ti_3SiC_2 becomes unstable at temperatures as low as 1400 °C. By arc melting and then leaching, Arunajatesa and Carim [8] reported the synthesis of Ti_3SiC_2 powders. Sambasivan [20] reported the isothermal section of the ternary system Ti-Si-C at 1200 °C, see Fig. 6.

This work was conducted to understand the reaction path and microstructure evolution during the processing of Ti_3SiC_2.

3.2 Experimental Details

3.2.1 Starting Powders

Most of the work was carried out using powder mixtures of Ti, SiC and C to yield a final composition of 3:1:2 of Ti:Si:C. The powders used and their purities are listed in Table II. High purity Ti and SiC (see Table II), henceforth will be called M1, were used to study the reaction path, microstructure evolution and thermal stability. The other mixture was Ti / Si / C ,henceforth will be called M2, to study the effect of the starting powders on the final composition by comparing it with M1. To study the effect of the purity of the starting powders on the formation of Ti_3SiC_2, a third mixture , M3, was used using less pure Ti and SiC (see Table II). Completed and interrupted HIP runs were done and the resulting samples were tested using X-ray diffraction, SEM-EDS, and optical microscopy.

3.2.2 Processing procedure

The powders were dry mixed in a V-blender for 2 hr. The mixture was then cold pressed under 180 MPa into 69 x 12 x 12 mm bars. To study the reaction path and microstructure evolution, interrupted and completed hot isostatic press (HIP) runs were conducted. For the HIP runs, the green body was encapsulated in a glass tube under vacuum and then placed in a HIP under an argon atmosphere of 60 MPa pressure at different temperatures (1200 - 1600 °C) for different time periods (0 - 24 hr). The HIPed samples were then soaked in HF acid (48 %) to dissolve the glass (HF does not dissolve Ti_3SiC_2). After HIPing the samples were cut using a diamond wheel and polished down to 1 μm diamond powder for microscopic evaluation.

More than 10 runs were carried out as shown in Fig. 7, where each circle represents a different run. The heating rate in all cases was 10 °C/min and in Fig. 7, zero time refers to samples that were heated to the temperature indicated and immediately cooled as the desired temperature was reached.

To measure the grain growth kinetics, the samples were etched using HF : HNO_3 :H_2O in equal volume fractions and observed under both optical and scanning electron microscopy; SEM. For the X-ray measurements, a drill was used to obtain powder samples from the bulk of the samples. Siemens D-500 x-ray diffractometer was used using a scanning step (2θ) of 0.05 ° with a scanning speed of 0.1 ° / s.

In order to study the effect of the processing technique on the final composition and microstructure, some samples, M1, were hot pressed. The green body was placed in a graphite split die which was placed in a vacuum hot press and heated in vacuum (10^{-3}Pa) under 40 MPa pressure at 1600 °C for 4 hr. The surface of both the hot pressed and HIPed

samples was then machined and the samples were then tested using x-ray diffraction and SEM.

3.3 Results and Discussion

Figure 8 shows the x-ray diffraction patterns of the different phases that form during heating of the M1 mixture (Ti, SiC and C). At 1200 °C and 0 time (i.e. no soak time) the x-ray diffraction pattern shows that the main phases present are TiC_x , $Ti_5Si_3C_x$ and some unreacted Ti. Some small peaks of Ti_3SiC_2 are also visible. This x-ray result was confirmed by SEM and EDS mapping of Ti and Si as shown in Fig. 9. Given that the average initial particle size of the Ti powders was about 40 μm, the micrograph shown in Fig. 9, clearly demonstrate that both C and Si atoms diffuse into the Ti particles forming TiC_x and $Ti_5Si_3C_x$ as intermediate phases. This conclusion is similar to Brodkin et al. who have shown that during the heating of Ti, B_4C and graphite powders, the reaction occurs by the diffusion of B and C into the Ti particles [21].

At 1400 °C and zero time, the x-ray diffraction pattern shows that Ti_3SiC_2 is now the major phase, while TiC_x is a secondary phase. Since the main peaks of Ti_3SiC_2 overlap those of $Ti_5Si_3C_x$, it is not clear from the x-ray if the latter is present at that temperature. However, mass balance considerations dictate that TiC_x cannot be the only secondary phase present since it contains no Si. The presence of $Ti_5Si_3C_x$ at 1400 °C, is confirmed in the SEM micrograph shown in Fig. 10. Figure 10a is a cross-section of an unetched sample, where the dark phase is Ti_3SiC_2, and the light phase is $Ti_5Si_3C_x$. Figure 10b is a micrograph of a similar area after the sample was placed in concentrated HF for 10 s. The $Ti_5Si_3C_x$ readily dissolved and what remained is the Ti_3SiC_2 phase. This micrograph is important for another reason; it strongly suggests that nucleation and growth of Ti_3SiC_2 phase occurs within the $Ti_5Si_3C_x$ phase.

According to the x-ray results (Fig. 8) heating to 1600 °C and cooling, is insufficient to obtain single phase Ti_3SiC_2, since some of the TiC peaks are still apparent. One hour at 1600 °C, however, is sufficient to obtain single phase samples (Fig. 8). This was corroborated with SEM back scattered images in which the only phase present is Ti_3SiC_2 (Fig. 11).

By comparing these results with those reported by Morozumi et al [22] and Cockeram and Rapp [23] on the bonding of SiC by Ti foil and Ti / Si diffusion couples respectively, the following was found. In the case of Ti / SiC the reaction products are Ti_3SiC_2, $Ti_5Si_3C_x$ and $TiSi_2$. In our case $TiSi_2$ was not observed at any stage because of the early formation of TiC_x, besides which, the only products were found to be Ti_3SiC_2 and $Ti_5Si_3C_x$. In the case of Ti / Si five layers, $TiSi_2/TiSi/Ti_5Si_4/Ti_5Si_3/Ti_3Si$, were found to form at 1150 °C after 14 h. In our case the fact that C is introduced to the system in the form of graphite and SiC, which shifts the reaction towards the carbon rich corner in the ternary diagram forming carbon rich phases (TiC_x). The only silicide that was found to form in this study is $Ti_5Si_3C_x$.

3.3.1 Effect of Processing Technique and Starting Powders

Repeating the same experiment (1600 °C for 4 hr) in a graphite die that was placed in a vacuum hot press to compare it with the HIPed sample resulted in samples that contained 2-3 % TiC_x as a secondary phase. This is believed to be due to the diffusion of C from the die to the sample. TiC_x is known to form as a product of the surface reaction of C and Ti_3SiC_2 [24 (see chapter 6)]. In that work it was found that, at 1600 °C for 4 hrs, carbon can diffuse into the Ti_3SiC_2 matrix forming a TiC layer of the order of 40 μm. TiC was also formed at the grain boundaries to a depth of about 100 μm in the matrix. This small amount of TiC_x was found to have a deleterious effect on the oxidation kinetics of

Ti_3SiC_2; the details are discussed elsewhere [16 (see chapter 5)]. It is interesting to note that there was no significant texture to the hot pressed sample.

For reasons that are not entirely clear and which are currently under investigation, the extent of reaction is sensitive to the nature of the starting materials. This is shown in Fig. 12, where the x-ray diffraction patterns of samples that were pressureless sintered under vacuum (10^{-3} Pa) at 1600 °C for 4 hr starting with Ti, SiC and C are compared with those where the starting powders were Ti, Si and C. The latter clearly contains TiC_x as a secondary phase. One possible explanation is the loss of elemental Si, which has a relatively high vapor pressure at its melting point. This loss would effectively shift the equilibrium composition into the Ti_3SiC_2 and TiC_x phase fields (see Fig. 6).

It is well established that the formation of some phases are sensitive to the purity of the initial powders. For example, Brodkin et al [25] have shown that the nucleation and growth of Ti_3B_4 is quite sensitive to the purity of the initial Ti powders used. To examine the sensitivity of the formation of Ti_3SiC_2 on impurities, samples were fabricated starting with low purity, grit-grade SiC (main impurities were SiO_2; see Table II). The samples were HIPed at 1600 °C for 4 hr using 60 MPa pressure. The x-ray diffraction patterns were almost identical to ones obtained from the higher-purity starting powders; in either case, the product was single phase Ti_3SiC_2 (Fig. 12). It therefore appears that the formation of Ti_3SiC_2 is not sensitive to the impurities present in the initial powders used here. These impurities, however, adversely affected the room and high temperature mechanical properties [17], but enhanced the oxidation resistance as discussed elsewhere [16].

One of the advantages of reaction processing is that densification and reaction occur simultaneously or sequentially [21,26]. The presence of soft phases during the reaction process have been found to be very beneficial to the attainment of full density . Figure 13

shows a secondary SEM image of the microstructure at different stages of the process. At 0 time, It is obvious from these micrographs that the porosity level decreases with increasing temperature. By 1600 °C, the sample is almost fully dense. As discussed below, fully dense samples can be obtained at various combinations of temperature and time.

3.3.2 Grain Growth

The grain growth study was carried out in the temperature range of 1450 - 1600 °C. The effect of soaking time at 1450 °C on the microstructure is shown in Fig. 14. Since Ti_3SiC_2 grains have a high aspect ratio, thereafter the grain size will be referred as to the longest dimension of the grain. In Fig. 14-a, after 8 hours the microstructure is uniform with an average grain size of ≈ 3-5 μm. After 16 hours, the microstructure contains abnormal grains that reached a size of ≈ 100 μm, embedded in a matrix of ≈3-5 μm grains (Fig. 14-b). After 24 hours, the number of grains that exhibited abnormal grain growth has increased, the microstructure is more uniform and the average grain size increased to ≈300 μm (Fig. 14-c). From these micrographs, it is clear that Ti_3SiC_2 exhibits anisotropic and abnormal (exaggerated) grain growth behavior.

In ceramics, anisotropic grain growth is poorly understood. In various ceramic systems different reasons for anisotropic grain growth, often connected with abnormal G.G., were proposed, such as anisotropic surface energies for different crystal planes, layers of impurities or dopant ions on certain crystallographic planes which prevent growth in some directions , different wetting of anisotropic grains with liquid phase or the presence of impurities which form new compounds [27-30]. The lack in the knowledge about the surface energies of the different planes of Ti_3SiC_2 makes it very difficult to understand the behavior at the grain boundaries. A detailed TEM study is being conducted to study the nature of the grain boundaries.

Even though the grain growth behavior is not entirely clear, the following evidence were observed. As shown in (Fig. 15-a), an etched microstructure shows a wide region attacked around the grain boundaries. The nature of that region around the grain boundaries is unknown, but most likely unreacted phases (as noted above, $Ti_5Si_3C_x$ dissolves in the etchant while TiC does not) that can pin the grain boundaries and inhibit grain growth. The grain boundaries regions in the case of the large grains are much thinner (see Fig. 15-b). The other evidence was found in a long term hot press run. It was found that the outer layer is TiC_x (Fig. 16) and moving towards the center of the sample the TiC_x concentration decreases. Simultaneously the grain size of Ti_3SiC_2 increases dramatically towards the center of the sample. This leaves little doubt that TiC_x particles at the grain boundaries inhibit the grain growth of Ti_3SiC_2.

Ti_3SiC_2 can be produced in three microstructures depending on the processing temperature and time. Figure 17 summarizes the processing domains that result in the various microstructures shown in Fig. 14. The duplex microstructure means that some large grains (100-300 μm) are embedded in a finer (3-5 μm) matrix. These varieties of microstructures affect both room and high temperature mechanical properties which are discussed in detail elsewhere [17 (see chapter 7)].

The question of the thermal stability of Ti_3SiC_2 is of some importance if it ultimately to be used in vacuum or reducing atmospheres at high temperatures. There have been more than one report in the literature claiming that Ti_3SiC_2 dissociates at temperatures as low as 1400 °C depending on the atmosphere resulting in TiC and Si gas [2,7]. Also, Nowotny et al [31] reported that Ti_3SiC_2 dissociates at 1720 °C.

To investigate the thermal stability of Ti_3SiC_2 bulk and powdered samples were annealed in under vacuum (10^{-3} Pa) for 24 hr at 1600 °C. In another experiment (- 325

mesh) Ti_3SiC_2 powders were annealed under Ar at 1600 °C for up to 4 hr. In all cases, x-ray results showed Ti_3SiC_2 as the only present phase. This shows that Ti_3SiC_2 is stable up to 1600 °C under these atmospheres.

2.4 Conclusions

This work has shown that TiC_x and $Ti_5Si_3C_x$ are the intermediate phases in the processing of Ti_3SiC_2, if the starting powders are Ti, SiC and graphite. For reasons that are not entirely clear, heating Ti / Si / C to 1600 °C for four hours, results in a two-phase mixture of TiC_x and Ti_3SiC_2, whereas starting with Ti / SiC / C yields single phase Ti_3SiC_2. Dense single phase Ti_3SiC_2 samples can be produced over a wide range of temperatures (1450 -1600 °C) and times (1-8 hours depending on the temperature). Ti_3SiC_2 was found to exhibit exaggerated grain. The final microstructure can be in the form of fine grains (3-5 μm), duplex, or coarse grains (100-300 μm). Ti_3SiC_2 was found to be thermally stable at temperatures as high as 1600 °C under vacuum and Ar atmospheres.

4. Damage Mechanisms Around Hardness Indentations in Ti_3SiC_2

Microstructural observations of damage around indentations in Ti_3SiC_2 are presented. The Vickers hardness decreased with increasing load and asymptotically approached 4 GPa at the highest loads. No indentation cracks were observed even at loads as high as 300 N. Preliminary strength versus indentation plots indicate that, at least for the large-grained material (≈ 100 μm) studied here, Ti_3SiC_2 is a damage tolerant material able to contain the extent of microdamage to a small area around the indent The following multiple energy-absorbing mechanisms have been identified from scanning electron micrographs of areas in the vicinity of the indentation: diffuse microcracking, delamination, crack deflection, grain push-out, grain pull-out and the buckling of individual grains are several of the microstructural features .

4.1 Introduction

Ti_3SiC_2 was first synthesized by Jeitschko and Nowotny [2] via a chemical reaction between TiH_2, Si and graphite at 2000 °C. The unit cell, shown in Fig. 18, is hexagonal and consists of planar Si layers linked together by TiC octahedra [1,2, and 4]. Until recently, very little was known about the properties of Ti_3SiC_2 primarily owing to the difficulty of fabricating fully dense bulk samples [2,3,,4,6,7,8,9,10,14, and 19]. Pure, single phase Ti_3SiC_2 has only been synthesized by chemical vapor deposition techniques in

small quantities [2,3]. Previous attempts to synthesize it in bulk form resulted in multiphase ceramics containing either TiC, SiC, or titanium silicides [3,6,7,8,9,10,14, and 19]. Working with small single crystals prepared by CVD, Nickl et al. [3] report anisotropic Knoop hardnesses normal and parallel to the basal planes of 12- 15 and 3-4 GPa, respectively. Pampuch et al. [10], using hot pressed samples that contained some hard phase impurities, measured a Young's modulus of 326 GPa and a hardness of about 6 GPa, the latter in agreement with Goto and Hirai's value on CVD samples [2]. Both groups have shown that the Vickers microhardness was a function of indentation load and concluded from that observation that Ti_3SiC_2 may exhibit "ductile" behavior. In a more recent paper Lis et al. [19] measured the hardness of Ti_3SiC_2-TiC composites as a function of their TiC content and estimated that the hardness of pure Ti_3SiC_2, should be about 4 GPa. Pampuch et al. [6,10] further noted that since the ratio of the Vickers hardness, H_V, to Young's modulus, E was low, this suggested that the mechanical properties of Ti_3SiC_2 were somewhat similar to those of ductile metals.

Recently, we fabricated and characterized pure single phase, fully dense, bulk polycrystalline samples of Ti_3SiC_2 by reactively hot pressing Ti, graphite and SiC powders at 40 MPa and 1600°C [15]. Preliminary characterization has shown that Ti_3SiC_2 possessed a combination of unique properties. Its electrical and thermal conductivities were higher than those of pure Ti. The material was not susceptible to thermal shock and at 1000 °C had an oxidation resistance comparable to $MoSi_2$. Furthermore, its machinability was comparable to that of graphite. At temperatures about 1300 °C, large plastic deformations in compression were observed with yield points of the order of 300 MPa [15]. More recently we also fabricated Ti_3GeC_2, and some of the so-called H-phases, including Ti_2GeC, Ti_2AlC and Ti_2AlN. In all cases the resulting compounds were as

readily machinable as graphite and possessed electrical conductivities in the range of 3-15 x 10^{-6} $\Omega^{-1}m^{-1}$ and hardnesses in the range of 3-6 GPa [32].

Based on our work to date there is little doubt that interplanar bonding between the transition metal and the B-metal in these ternary compounds, while relatively weak when compared to primary covalent or ionic bonds, is significantly *stronger* than that in graphite, and most probably possesses a metallic character. In this paper we present microstructural observations on damage mechanisms active around a microhardness indentation on Ti_3SiC_2 as a means to elucidate the operative deformation and fracture mechanisms and their association with the microstructural and atomistic features of this material. Our results indicate that Ti_3SiC_2 is a damage tolerant material able to contain the extent of microdamage in a small area via multiple energy absorption mechanisms.

4.2 Experimental Details

Polycrystalline samples of Ti_3SiC_2 were fabricated using the procedure detailed in Ref. [15]. Briefly Ti, SiC and C powders were mixed in the proper molar ratio, cold pressed and then hot pressed in graphite dies at 1600 °C for four hours under a pressure of 40 MPa. Samples for the hardness measurements were ground using SiC grinding paper and polished using diamond paste down to 1 μm. Figure 19 shows an SEM micrograph of the microstructure of the as-fabricated and etched (20 s in a 1:1:1 by volume solution of water, nitric and hydrofluoric acid) specimen. The Vickers hardness test was measured using loads of 100, 200, and 300 N. The microhardness was measured using Leco M-400 tester at 0.5, 1, 3, 5, 10 N. The results summarized in Fig. 20 represent the average of at

least 10 individual measurements at each load. Measurements at 0.1 N or less did not result in a measurable indent under

Indentations on bend specimens were performed using a Vickers indenter under loads of 1, 10, 100, 200, 300 N [1]. The dimensions of the specimens conformed to ASTM C1161 type A (25 mm x 2 mm x 1.5 mm). One diagonal of the indenter was parallel to the length of the specimen. The flexural strength after indentation was determined by four-point bending according to procedure outlined in ASTM C1161 and ASTM C1211. The specimens were cut using a diamond wheel without any additional surface polishing. The tests were performed in a semiarticulating SiC fixture with outer span of 20 mm and inner span of 10 mm on a servo-hydraulic MTS testing machine with load resolution of 5N at a strain rate of 10^{-4} s^{-1}. The results are plotted in Fig. 23.

For an estimate of fracture toughness, single edge notched beam bars were electric discharge machined to bars of the dimensions of 25 x 2 x 1.5 mm^3. A notch of the width of 80 μm and depth of 500 μm was made using a diamond wheel. The bar was then loaded until fracture using an MTS testing machine with crosshead speed of 0.02 mm/sec.

4.3 Results and Discussion

Figure 20 shows the microhardness of Ti_3SiC_2 as a function of the applied load. At higher loads, the microhardness asymptotes to a value of about 4 GPa, which is identical to the value extrapolated to by Lis et al.[19] and that reported by Nickl et al [3]. At lower loads, the microhardness was found to decrease with increasing load levels and a

[1] Specimens could not sustain a load of 500N without breaking.

significant scatter was observed in the microhardness values. This scatter is attributed to the anisotropic structure of Ti_3SiC_2. As the size of the indentation becomes comparable to the grain size, the effect of anisotropy becomes much more pronounced as observed.

SEM micrographs of the indentation surfaces are shown in Figs. 21 a-c for different loads. These micrographs reveal many unique and characteristic features of the indentation surfaces in Ti_3SiC_2. There is a distinct upheaval of the region around the indentation, and more often than not the indentation is clearly asymmetric. The damage region around the indentation extends to about 1.0-1.5 indentation diameters from the indentation mark. There are, however, no dominant cracks emanating from the corners of the indentation even at the highest load levels applied - an observation made by others as well [2,10, and 19].

Preliminary measurements of the fracture toughness and modulus of rupture of this compound at room temperature yielded 6 MPa $m^{1/2}$ and 290 MPa, respectively. It should, however, be noted that a fracture toughness of 6 MPa $m^{1/2}$ is surprisingly high for Ti_3SiC_2, since it seems to be highly prone to delamination. The presence of multiple energy dissipative mechanisms discussed below, however, apparently play a critical role in enhancing the fracture toughness of this compound.

The asymmetry of the damage around the indentations in Fig. 21 can be attributed to the anisotropy of the mechanical properties of Ti_3SiC_2. As noted above, based on our previous work there is little doubt that slip along the basal planes is the dominant deformation mode. Therefore, as the material is subjected to a high triaxiality stress during

the indentation, compressive stresses parallel to the surface are relieved by deforming and pushing grains in the vicinity of the indentation towards the surface - the grains that are appropriately oriented such that the shear is maximized along their basal planes are more easily pushed out in contrast to the rest of the grains. This effect is best seen in Fig. 21a (left hand side), where the grains that are pushed out are not directly adjacent to the indentation mark.

Various micromechanisms of damage can be observed clearly in the SEM micrographs shown in Fig. 22. These micrographs were taken from regions adjacent to the indentation impression. Extensive delamination on the basal planes was observed in the grains in this region (Fig. 22a). There are also clear indications of crack deflection along the basal planes, debonding, pull-out and deformation of single grains (see Fig. 22b). In particular, a significant number of the delaminated grains were seen to buckle leading to "wavy" or "kinked" grains (Fig. 22c). A closer look at the kinks in these grains revealed a remarkable feature - the microlaminates while debonded are not fractured (i.e. across the basal planes). The kinking of these micro-laminates and the absence of cracking at the kinks once again suggests that Ti_3SiC_2 is capable of exhibiting micro-scale plasticity at room temperature. Grain sub-division was also noted in some of the micrographs (not shown here) and is believed to be a consequence of extensive kinking or breakup of the grains.

The pile-up of the material seen in Figs. 21 a-c around the micro-hardness indentations is unusual for non-metals. Indentations on ceramics often produce sink-in which are attributed to densification below the tip of the indention [33,34]. On the other hand, in metals the material in the neighborhood of the indentation often rises above the

unindented surface level by plastic deformation. The type of damage seen in Figs. 21 or 22, clearly cannot be related to classic macroscopic plasticity that occurs in ductile metals, but rather to a combination of buckling, bending and "push-out" of favorably oriented grains.

The increased microhardness at low loads (Fig. 20) and the nature of the pile-ups and damage observed in the neighborhood of the indentations (Fig. 21) are believed to be indications of the ability of Ti_3SiC_2 to exhibit micro-scale plasticity. This conjecture is corroborated by both the relatively low value of the H_V/E ratio as well as the photomicrographs showing damage mechanisms in the region adjacent to the indentations (Fig. 22). The H_V/E values for most ceramics are in the range of 0.02 - 0.1 [33,35], whereas most metals possess values in the range of 0.001-0.03. It follows that the H_V/E value of 0.012 for Ti_3SiC_2 is lower than that for most if not all ceramics, and is comparable with the values exhibited by low ductility high strength metals such as Ti.

The aforementioned observations suggest that Ti_3SiC_2 should be a damage tolerant material. To test this hypothesis the four-point flexural strength was measured as a function of indentation loads (Fig. 23). From such graphs the asymptotic slope at higher indentation loads is used as an indicator of the damage tolerance of a material - for perfectly brittle materials that slope corresponds to -1/3 [36]. Given that the asymptotic slope in Fig. 23 is less than 1/3, this suggests that Ti_3SiC_2 is a damage tolerant material. Needless to say, more experiments on samples with smaller grains are needed to determine the slope at high loads with more accuracy (see chapter 7). However, this evidence when taken together with the microstructural observations around the indentation reinforce the conclusion that Ti_3SiC_2 is capable of sustaining and locally confining the damage due to external loads by a variety of mechanisms, that in turn render Ti_3SiC_2 a damage tolerant

material when compared to other structural ceramics. This is consistent with the observation that Ti_3SiC_2 is not sensitive to thermal shock (i.e. the bending strength does not decrease after quenching from temperatures as high as 1400°C [15]). Finally it is worth noting that in its ability to tolerate damage Ti_3SiC_2 is reminiscent of other damage tolerant mica-glass composites [37]. To the best of our knowledge Ti_3SiC_2 is the only single phase ceramic material that exhibits this behavior.

4.4 Summary and Conclusions

Preliminary measurements of the fracture toughness of Ti_3SiC_2 gave ≈ 6 MPa $m^{1/2}$. Indentation cracks, typical in other structural ceramics with comparable levels of fracture toughness, were not observed. Even at the highest indentation loads applied (300 N) no median or lateral cracks were detected - the damage was found to be confined to the immediate vicinity of the indentations. Furthermore, instead of the usual sink-in around indentations typical for most ceramics, the material in the vicinity of the indentations was piled-up as a result of a combination of grain push-out, pullout, breakup and buckling. Ti_3SiC_2 appears to be a damage tolerant material able to contain the extent of damage in a small area via a number of multiple energy-absorbing mechanisms herein identified namely: diffuse microcracking, delamination, crack deflection, grain buckling, grain pull-out and grain push-out.

5. Oxidation Of Ti_3SiC_2 in Air

Polycrystalline samples of Ti_3SiC_2 were oxidized in air in the 900-1400 °C temperature range. The oxidation was parabolic with parabolic rate constants, k_p, that increased from 1 x 10^{-9} to 1 x 10^{-4} $kg^2m^{-4}s^{-1}$ as the temperature increased from 900 to 1400 °C, respectively, which yielded an activation energy of 370±20 kJ/mol. The scale that forms was dense, adhesive, resistant to thermal cycling and layered. The outer layer was pure TiO_2 (rutile), and the inner layer consisted of mixture of SiO_2 and TiO_2. The results are consistent with a model in which growth of the oxide layer occurs by the inwards diffusion of oxygen and the simultaneous outwards diffusion of titanium and carbon. The presence of small volume fractions (≈ 2%) of TiC_x in Ti_3SiC_2 were found to have a deleterious effect on the oxidation kinetics.

5.1 Introduction

Recently, we reported on the fabrication of fully dense, single phase, bulk, polycrystalline samples of Ti_3SiC_2 [15]. The unique properties exhibited by this material, such as easy machinability, non-susceptibility to thermal shock, excellent ductility and high yield points at 1300 °C, suggest that this compound could be an excellent structural material for high temperature applications. Our preliminary data on the oxidation of Ti_3SiC_2 indicated that the oxidation was parabolic, with a parabolic rate constant of 2 x 10^{-8} kg^2 m^{-4} s^{-1} at 1000 °C and 2 x 10^{-5} kg^2 m^{-4} s^{-1} at 1400 °C, which translates to an activation energy of ≈ 300 kJ/mol [15].

Prior to our work, all attempts to produce bulk single phase polycrystalline samples of Ti_3SiC_2, resulted in the presence of second phases most notably TiC [6,7,9,10, and 14]. Consequently, very little information about the intrinsic oxidation resistance of Ti_3SiC_2 exists. As far as we are aware, the only study that attempted to measure the oxidation resistance of bulk samples of Ti_3SiC_2 is that of Okano et al. [9] who were working with samples that were 95 % of theoretical density and contained a few volume percent of TiC and SiC. They reported that a porous non-protective oxide layer consisting of rutile and amorphous silica formed upon oxidation. They also report a weight gain of $\approx$ 100 mg/cm^2 after 600 mins. at 1000 °C in air. The only other report on the oxidation of Ti_3SiC_2 is that of Racault et al. [7] who carried out thermogravimetric experiments on powders. They report that while the oxidation kinetics of Ti_3SiC_2 were slower than those of TiC, total oxidation was achieved between 1050 and 1250 °C resulting in titania (rutile) and silica (cristobalite).

Apart from these two references there are apparently no other reports in the literature on the oxidation behavior of Ti_3SiC_2. Accordingly comparison can only be made to compounds with comparable chemistries such as $TiSi_2$, Ti, Si, TiC and SiC; some of which exhibit oxidation properties and oxide scale morphologies that are similar to those found in this study.

The oxidation of Ti is complicated by the fact that blistering and scaling of the oxide layer occurs at elevated temperatures and by the large solubility of oxygen in titanium metal that tends to complicate the analysis [38]. Despite this complication it is now reasonably well established that the oxidation in the temperature range from 700-1000 °C is parabolic and occurs by the inwards diffusion of oxygen through the layer [39] in spite of titanium's larger diffusion coefficient in TiO_2 [40]. Typical values for the parabolic rate constants are listed in Table III.

Interestingly enough there is very little information on the oxidation of TiC. Kosalopova [42] reports that at 900 °C the weight gain after 1 hour was 1.21 kg/m^2 which translates to a k_p of 4 x 10^{-4} kg^2/m^4 s. Tampieri and Bellosi [41] measured the oxidation resistance of 30 vol% of TiC or TiN in Al_2O_3 fabricated by hot pressing. At temperatures greater than 900 °C the oxidation kinetics were parabolic. In both cases a thick rutile layer formed on the surface of the composites and the activation energies for oxidation were calculated to be, respectively, 190 and 144 kJ/mol. The rate limiting step was again assumed to be the diffusion of oxygen through the TiO_2 layer.

It is well established that the oxidation of pure Si results in parabolic oxidation kinetics at temperatures greater than 1000 °C due to the formation of a dense adherent silica layer [43]. Typical values of the parabolic rate constants at 1000 and 1200 °C are listed in Table III. The rate limiting step in this case is the inwards diffusion of molecular rather than ionic oxygen [43-46]. Similarly, the good oxidation resistance of SiC is attributed to the formation of a dense silica layer. However, the apparent activation energies reported for the oxidation of SiC vary over a wide range (85-498 kJ/mol) but, in general, the greater the purity of the SiC, the closer the activation energies and absolute values of k_p approach those of pure silicon and the more reproducible the results between investigators [e.g. 44-46]. It is also interesting to note that the fate and role of the C during the oxidation of SiC, even after numerous investigations, remains somewhat elusive [44]. However, there is now a mounting body of evidence that suggests that, especially for high purity SiC, the C reacts with oxygen and diffuses out of the layer as CO [44]. This is important here because for the oxidation of Ti_3SiC_2 to proceed, the C also has to diffuse out through the reaction layer.

The most relevant compound to this study is $TiSi_2$. As far as we are aware, there are only two reports on the oxidation of bulk $TiSi_2$ in the literature [47,48]. The first was

carried out on pressureless sintered 95-98 % dense samples in the temperature range of 600-1400 °C [47]. In the 1000-1300 °C temperature range the oxidation was parabolic with an activation energy of ≈ 90 kJ/mol [47]. The results were consistent with a model in which the rate-limiting step was the diffusion of oxygen through a silica film that forms on the surface with the simultaneous diffusion of Ti from the substrate to islands of rutile growing on top of the amorphous silica. More recently Becker et al. [48] measured the oxidation of hot isostatically pressed $TiSi_2$ samples in the temperature range 1100-1400 °C in air. The oxidation was linear at 1100 °C, but parabolic at 1200 °C and 1300 °C. At 1100 °C the scale formed consisted of an outer layer of titania and an inner layer of a mixture of silica and titania. Increasing the temperature increased the silica content in the outer layer and at temperatures > 1200 °C a silica scale with precipitates of Ti-Si oxides was found. The parabolic rate constants at the higher temperatures are listed in Table III, and, comparable to the ones determined by Schwettmann et al. [47].

The purpose of this paper is to report on the oxidation kinetics of Ti_3SiC_2 in air, as well as the effect of the different fabrication processes and the purity of the starting powders on the oxidation.

5.2 Experimental Details

To study the effect of the powder purity on the oxidation resistance two types of mixtures were used. The first mixture, henceforth, referred to as M1, consisted of Ti (99%, -325 mesh, Johnson Matthey), SiC abrasive grains (97.5%, -325 mesh, Carborandum), and C (99%, d_m =1 μm, Aldrich). The second purer mixture, henceforth refereed to as M2, consisted of Ti (dehydrided, 99.99%, -325 mesh, Alta Group), SiC (99.5%, d_m =2 μm, BET = 10.56 m^2/g, Johnson Matthey), and C (99%, d_m =1μm,

Aldrich). Both mixtures had the same stoichiometry: Ti_3SiC_2. The major impurities found in the two SiC powders used are listed in Table IV.

The mixtures were dry mixed in a V-blender for 2 hr and then cold pressed in 69 x 12.5 x 15 mm^3 bars under 180 MPa. The green bodies were then either hot-pressed or hot isostatically pressed (HIPed) to study the effect of the processing route on the oxidation resistance. One set of samples were placed in a graphite die in a vacuum hot press at 1600 °C for 4 hr under a pressure of 40 MPa. The second set was sealed under vacuum in glass tubes and HIPed using Argon under a pressure of 60 MPa at 1600 °C for 4 hr. These samples were then soaked in concentrated HF to dissolve the glass. It is worth noting here that Ti_3SiC_2 does not react with, or dissolve in, concentrated HF.

The outer surfaces of both the hot-pressed and HIPed samples were removed by electric discharge machining (EDM) and the samples were further cut into 25 x 2 x 1.5 mm^3 bars. The bars were then polished down to 600 grit SiC paper. All samples were fully dense as evidenced by scanning electron microscopy of the polished surfaces prior to oxidation. However, X-ray and SEM back scattered images showed that the hot-pressed samples contained ≈ 2 vol % of TiC_x, while the HIPed samples had less than 1 vol% TiC_x.

For the oxidation study, the samples were suspended in a vertical thermobalance (CAHN D101-2) with a Pt wire and heated at 100 °C/min up to the test temperature. Upon reaching the requisite temperature, the weight gained was measured as a function of time. The tests were held at 1100, 1240, and 1400 °C. At 900 and 1000 °C the noise level in the thermobalance was too high. Instead the parabolic rate constants were measured by intermittently interrupting the runs and weighing the samples.

The oxidized samples were characterized using X-ray diffraction (Siemens D-500) to determine the phases in the oxide layers. Scanning electron microscopy (SEM) of the oxide layer was also carried out on scanning electron microscopes (AMRAY 1830, and JOEL-JSM 840) equipped with an energy dispersive spectroscopy or EDS system.

Another set of samples, were isothermally heated at 1240 °C for 0.5, 1, 4 and 12 hours. The oxidized samples were cross-sectioned, mounted, polished and the time dependence of the oxide thicknesses both the inner and outer layers, see below, were determined. The thickness measurements were made at regular intervals along the topscale/subscale boundary: 25 measurements in each case. By sampling at regularly marked intervals, sampling bias was minimized. The standard deviations for the 25 measurements were calculated and found to be below 5% in all cases (see Table V).

5.3 Results

5.3.1 Parabolic Rate Constants:

Figure 24a shows the isothermal weight gained per unit area as a function of time for the M1 samples at four different temperatures. The parabolic nature of the oxidation is confirmed in Fig. 24b in which the square of the normalized weight gain is plotted versus time. The parabolic rate constant, k_p, was found to increase from 1×10^{-9} to 1×10^{-4} $kg^2m^{-4}s^{-1}$ as the temperature increased from 900 to 1400 °C, respectively. The M2 samples exhibited the same parabolic behavior in the studied temperature range, but with slightly higher values for k_p (see Fig. 25 and Table III). That the processing route affected the oxidation kinetics is also shown in Fig. 26; the oxidation resistances of the HIPed samples are slightly better than the hot pressed ones.

The Arrhenian plots for k_p are shown in Fig. 25. The purity of the initial powders not only affected the absolute value of the oxidation rate but also influenced the activation energies. The activation energies for the oxidation of M1 and M2 samples were calculated to be, respectively, 320 ± 5 and 370 ± 20 kJ/mol.

As discussed below, the oxidation proceeds with the formation of two strata: an outer layer comprised of almost pure rutile and an inner layer composed of titania and silica. Figures 27a and b are, respectively, a linear plot of the functional dependence of the thicknesses of the various strata on time for M2 samples oxidized at 1240 °C in air, and a plot of the same data as square of the oxide scale thicknesses versus time. These results indicate that not only is the overall oxidation rate parabolic, but also, the thickening rates of each separate stratum after a short initial transient. The parabolic rate constants, k_x, values calculated from Fig. 27b are 1210 $\mu m^2/h$ for the outer layer, and 1740 $\mu m^2/h$ for the inner layer.

Table V summarizes the thickness data of the oxide films that form on Ti_3SiC_2 at various temperatures and times, together with the corresponding parabolic rate constants, expressed in units of kg^2/m^4 s. One set of parabolic rate constants (last column) are those determined from the thermogravimetric results (i.e. Table III). The second set (column 7) were calculated starting with the thickness data and assuming the overall reaction to be reaction I (see next section). Good agreement was found between the two sets of data especially at higher temperatures. At lower temperatures, for reasons that are not clear, the agreement is not as good.

The following factor allows the conversion of parabolic scale constants from total scale thickness to net weight gain in the temperature range 1000-1400 °C:

$$1\ (\mu m^2/h) \approx 4.33 \times 10^{-10}\ (kg^2/m^4\ s)$$

In other words, to convert from $\mu m^2/h$ to kg^2/m^4 s multiply by to 4.67×10^{-10}. (see Appendix C for details) For comparison's sake, the corresponding factor for SiC is 1.74×10^{-10}. The assumptions made to derive this relationship were that the oxide layers are fully dense and pore free and do not dissolve in each other The exact value of the constant depends on the density chosen for the silica-rich phase. Given that silica dissolves some titanium, the density chosen here is 2.5 gm/cm^3. (The density of silica varies slightly depending on the its polymorphic form, but in general varies from 2.2 gm/cm^3 for fused silica to 2.65 for quartz [40]. The exact value of the constant is thus a weak function of the value chosen).

Figure 27c is a plot of the ratio of the inner to outer oxide thickness as a function of time at 1240 °C, which shows that the inner mixed oxide layer is always thicker than the outer TiO_2 layer. Furthermore, with the exception of the 1400 °C runs, the ratios of the inner to outer layer thicknesses, were found to be more or less constant at about 1.5 (column 6, Table V). At 1400 °C the inner to outer layer thickness ratio increases to ≈ 3.

The upturn in subscale to topscale ratio at shorter times (Fig. 27c) suggests that the inner layer of mixed oxides forms first. After the initial transient the thickness ratio becomes essentially constant (Fig. 27c). This conclusion is consistent with our observation that for short times, the samples had an off-white color with a slight yellowish tint. We now know that this color is associated with the two phase-mixture of silica and titania. At longer times, the color of the samples changed noticeably to a more reddish-yellow color, which we now associate with pure titania. A careful examination of a back scattered SEM micrograph of a sample that was oxidized at 900 °C (Fig. 28) , shows that a very thin (< 0.5 μm) lighter phase, titania, is forming atop a darker phase which is a two phase mixture of silica and titania.

5.3.2 Microstructural Observations:

a. At 900 °C the oxide scale is monolithic, compact and dense (Fig. 28) and, according to XRD, entirely comprised of rutile or TiO_2. The XRD failed to detect any evidence of crystalline silica due to the combination of it being present in low concentrations (≈ 17 at % Si) to begin with, and, if present, would, more likely than not, be amorphous. Back scattered and EDS analysis confirmed the presence of a Si-containing phase in the scale. Figure 28 also shows that the oxide scale is demarcated by more or less straight boundaries both at its inner and outer surfaces.

b. At 1000 °C the oxide layer is stratified (Fig. 29). And while the outer layer is readily identified as dense TiO_2, the nature of the inner layer is less clear. It also consists of TiO_2 (XRD again detected no crystalline SiO_2); however, EDS of that layer indicated the presence of Si. Back scattered SEM micrographs (Fig. 29) clearly show that the subscale is distinct from the TiO_2 topscale and appears to retain a shadow of the morphological texture of the underlying substrate. The subscale is separated from the topscale by a zone of high porosity.

c. At 1100 °C the oxide layer is stratified as shown in Fig. 30a. At 1400 °C, (Fig. 31a) the separate layers have well developed morphological and compositional peculiarities. The same morphology was also observed for samples oxidized at 1240 °C (not shown). Figures 32b and 32c are EDS maps of the elements in an oxide scale that was formed as a result of annealing in air for 12 hours at 1400 °C (Fig. 32a). At these temperatures the oxide layer consists of:

¤ a dense outer layer which consists of large (> 300 μm) columnar TiO_2 as evidenced by the dark-field optical micrograph shown in Fig. 31b.

¤ an inner oxide layer or subscale of duplex composition comprised of a mixture of SiO_2 and TiO_2 (Fig. 33). In Fig. 33 the light gray phase is TiO_2, the dark gray is SiO_2 and the darkest patches are pores. The pores in this case lie within the subscale and not, in contrast to the situation at 1000 °C, at the subscale/topscale boundary.

At both 1100 and 1240 °C, the outermost surface of the oxide exhibited a rough outer surface, while the topscale/subscale boundary marked by the porosity remains straight (planar). The subscale/substrate boundary again has a ragged appearance.

5.4 Discussion

The parabolic nature of the oxidation kinetics leaves little doubt that a protective oxide layer forms on Ti_3SiC_2. At all temperatures the oxide layers formed are stratified (Figs. 29-32), consisting of external rutile layers and internal subscales comprised of rutile and silica; at lower temperatures the silica is amorphous, but at temperatures greater than ≈ 1240°C, cristobalite peaks appear in the X-ray diffraction patterns and become stronger at higher temperatures. Based on these observations it is concluded that oxidation takes place according to the following overall reaction:

$$Ti_3SiC_2 + 4.5\ O_2 = 3\ TiO_2 + SiO_2 + 2\ CO\ (g)$$

Figure 31a is an SEM micrograph of a sample that was oxidized in air at 1400 °C for 12 hrs. Marked on the figure are the dimensions of the original sample, from which it is apparent that the oxide layer grows on *either* side of that demarcation. Consequently there is little doubt that the oxidation proceeds by the diffusion of Ti outwards and oxygen inwards. Without that conclusion it would be difficult to rationalize the presence of an external layer comprised of almost pure titania and very little or no silica.

This conclusion is further confirmed, when it is recognized that the Si sublattice remains essentially immobile, the evidence for which can be seen in any of the micrographs shown in Figs. 29 or 31a. Figure 29 is especially telling since the oxide layer that forms appears to have retained a shadow of the morphological texture of the underlying substrate. This shadowing effect serves as an "internal" marker that the inwards diffusion of oxygen is occurring. Furthermore, evidence that the Si sublattice is essentially immobile can also be seen in Fig. 31a; the sharp corners of the original sample are retained after oxidation, a fact that could not be easily reconciled with a scenario in which the Si diffuses. The apparent shift outwards of the location of the original interface shown in Fig. 31a, is not due to diffusion of Si, but rather to the increase in volume associated with the formation of the oxide (Appendix A). Furthermore, the fact that the inner oxide layer forms first (Fig. 28) can also be taken as indirect evidence that the oxygen in diffusing inwards.

Needless to say, there must also be a flux of electronic defects, the nature of which is unknown at this time, to maintain overall charge neutrality.

Given that there are apparently no detailed reports on the oxidation of Ti_3SiC_2 in the literature, the only comparison that can be made is with other compounds that share some of the same atoms such as $TiSi_2$, SiC and TiC. As a first approximation it is not unreasonable to assume that the oxidation kinetics of Ti_3SiC_2 should fall somewhere between the oxidation kinetics of pure Ti metal or TiC, on the one hand, and pure Si or SiC, on the other; a conclusion that is borne out by the results shown in Table III.

Based on the nature and morphology of the oxide layers, the oxidation of Ti_3SiC_2 and $TiSi_2$ are similar in that both form layered oxide structures that grow by the inwards

diffusion of oxygen and the outwards diffusion of Ti [47,48]. The major differences between the two, however, are:

i) In contrast to $TiSi_2$ the oxidation of Ti_3SiC_2 cannot proceed without the, presumably, concomitant outwards diffusion of a carbonaceous species. The exact mechanism of how the C-atoms diffuse through the reaction layer is presently not known, and more work is required before this question can be answered. Experimentally this is not a trivial problem. For example, it remains unresolved for the oxidation of SiC, which has been extensively studied and is simpler than Ti_3SiC_2 in that it is a binary compound.

It should be pointed out that another mechanism by which the C atoms can be accommodated is their rejection at the oxide/substrate interface by diffusion into the bulk. This is the less likely mechanism, for two reasons. The first is the affinity of C for oxygen. Second such a rejection should result in an increase in the C activity at the interface, that should in time result in the formation of TiC and SiC near the interface, neither of which have been observed.

ii) The concentration of silicon atoms in Ti_3SiC_2 is insufficient to form a continuous silica layer. This in turn has the following consequences.

iii) The parabolic rate constants for the oxidation of Ti_3SiC_2 are roughly four to five orders of magnitude higher than those of $TiSi_2$ in the temperature range studied (Table III).

iv) At 370 kJ/mole, the activation energy for oxidation of Ti_3SiC_2 is roughly four times that of the oxidation of pure Si, $TiSi_2$ or SiC, and almost double that of Ti or TiC. It is also $\approx$ 1.5 times the activation energy for the diffusion of Ti and oxygen in titania [49-51]. This is a high value, and it is not clear what physical rate-limiting step it represents. Based on that value, however, it is unlikely that the rate limiting step is the diffusion of oxygen through silica, as is most probably the case in $TiSi_2$, or that it is the diffusion of titanium or oxygen ions through titania.

A caveat to be kept in mind when considering the activation energies and the absolute rates of oxidation is the sensitivity of these values to the presence of impurities. In SiC it is now well established that unless the SiC is extremely pure the results from one study to another are quite irreproducible, and the activation energies reported have ranged from 85-498 kJ/mol [e.g. Ref 44]. In this work there is a hint of the importance of the purity of the starting powders on the oxidation kinetics and activation energies (see below), but as noted above a more systematic study is required before any definitive conclusions can be reached. Oxidation studies on ultra high purity, chemically-vapor deposited Ti_3SiC_2 samples would be invaluable in answering some of the outstanding questions raised here.

The mechanisms of oxidation of Ti_3SiC_2 and $TiSi_2$ may be similar, but the rates at which they oxidize are orders of magnitude apart (Table III). Based of the respective k_p values, the diffusion of Ti or oxygen through silica must be orders of magnitude lower than the diffusion of the same specie in titania. It thus follows that it is mostly through the titania phase that the diffusion of the species responsible for oxidation of Ti_3SiC_2 is occurring. Furthermore, given that the volume fraction of silica in the inner layer is ≈ 0.53 (Appendix C) implies that the flux of atoms through the inner layer is roughly half that through the outer titania layer.

It one makes the plausible assumption that the inner layer grows as a result of the inwards diffusion of oxygen and the outer layer as a result of the outwards diffusion of titanium, it is possible to answer one of the more intriguing questions raised by this work, namely: the weak dependence of the ratio of the thicknesses of the inner-to-outer oxide layers formed on temperature (column 6. Table V). This observation implies that the *fluxes* of oxygen and titanium ions are comparable over the temperature range 1000-1400 °C. This, in turn, implies that the activation energies and absolute values of the diffusivities of

both oxygen and titanium are also comparable over the same temperature range. The data available for the diffusivities of Ti and O in titania tend to support this conclusion. The reported values for the activation energy for the diffusion of O in titania vary, but in general fall in the range of 233 to 251 kJ/mol [49,50]. The activation energy for the diffusion of Ti in titania is 257 kJ/mol [51]. Furthermore, the diffusion coefficient of Ti is roughly 30 times higher than that of oxygen over the 1000-1400 °C temperature range [40].

The concentration of oxygen ions in titania is double that of titanium ions, consequently the ratio of the fluxes, assuming the driving forces are identical (which is a good assumption since the activities of oxygen and titanium in the titania phase are inter-related by the Gibbs-Duhem relationship), should be of the order of 15, with that of titanium being greater. This in turn implies that the location of the original interface after oxidation should be closer to the external surface, which is consistent with the results shown in Fig. 31a. The ratios of inner to outer thicknesses, however, are not 15 to 1, but closer to being equal for reasons that are not known. It is hereby acknowledged that more work is needed to further understand the exact mechanisms responsible for the growth of these stratified oxide layers, and while the aforementioned calculation, does not prove the mechanism proposed, it is consistent with it.

The presence of the pores in the oxide layers can also be understood if it is postulated that the outward diffusional flux of Ti ions is greater than the inwards flux of oxygen. For thin films plastic flow is usually sufficient to prevent the growth of pores. As the oxide layers gets thicker, however, plastic flow is insufficient to eliminate all the pores and they will form. Comparing Figs. 28 and 29, it is obvious that as the oxide layers got thicker pores formed. At higher temperatures the size and density of the pores decrease noticeably once again (compare Figs. 29 to 30, 31 or 32), most probably as a result of the viscous flow of the silica that becomes more fluid at higher temperatures.

The samples fabricated with the purer starting powders resulted in poorer oxidation resistance than their less pure counterparts (Fig. 25). The impurities influence more than the rate of oxidation - they also affect the activation energies. The activation energies for M1 and M2 are, respectively, 320±5 and 370±20 kJ/mol. Given that the M2 samples are purer than M1, the higher of the two values has to be considered closer to the intrinsic value. The reason for this difference is not understood at this time and a detailed study of the role of impurities in the original starting powders on the oxidation kinetics would have to be carried out before a definitive answer can be given. A perusal of Table IV, however, suggests that the enhanced oxidation resistance of the M1 samples is due to the higher content of silicon, whether as free Si or in the form of silica, in the starting powders. The increased silicon content would increase the volume fraction of silica in the oxide scale, which reduces the area through which the species responsible for the oxidation of Ti_3SiC_2 are diffusing, which in turn should enhance the oxidation resistance, as observed. This is also consistent with our high temperature deformation work that has shown that the deformation of M1 samples occurred at lower yield points and resulted in significantly more cavitation than the M2 samples - both observations consistent with the M1 samples having a larger volume fraction of a viscous phase.

The indication that the oxidation can be enhanced by increasing the Si content, suggests that fabricating composites with increasing volume fractions of a high silicon-containing Ti-silicide phase, such as $TiSi_2$, should enhance the oxidation resistance, especially if sufficient amounts of that phase are present to form a continuos silica layer. We have preliminary results that indeed show that to be the case; the oxidation resistance of Ti_3SiC_2, was enhanced by 4 orders of magnitude by siliconizing the surface. The details will be published shortly (see chapter 6).

As noted above, X-ray and SEM back scattered images showed that the hot-pressed samples contained ≈ 2 vol % of TiC_x (most probably as a result of C diffusion from the graphite dies into the sample which shifts the overall chemistry of the sample towards the C-rich corner of the ternary phase diagram), while the HIPed samples were much more single phase. Given that the only discernible difference between the two samples was the TiC content and that the oxidation kinetics of TiC are inferior to those of Si or SiC (see Table III), it is not surprising that k_p for the hot pressed samples, 4.5 x 10^{-6} $kg^2m^{-4}s^{-1}$, is higher than that of the HIPed samples, 2.9 x 10^{-6} $kg^2m^{-4}s^{-1}$. This conclusion could also explain the poor oxidation resistance reported by Okano et al. whose samples contained more than 5 vol.% TiC [9].

In many long term applications of high temperature structural materials, such as turbine engines, internal combustion engines or reaction vessels in the chemical industry, the parts are subjected to thermal cycling. If the oxide layer does not adhere and remain on the surface of a part during cycling, that severely limits its use in such applications. To study the effect of cycling on the formed oxide, a sample was cycled from 1100 °C to room temperature six times for a cumulative time at temperature of 12 hrs (Fig. 30b). Another sample was held isothermally for the 12 hours at the same temperature (Fig. 30a). A comparison of the oxide layer after the cycling to one that was formed on a sample that was not cycled but held at the same temperature as the cycled samples for the same time, clearly shows that the cycling does not significantly affect the thickness or coherence of the oxide layer. The results shown in Fig. 24 (top curve) also confirm that the protective nature of the oxide is maintained after cooling and reheating the sample from 1400 °C - the weight gain simply continues as if the interruption had not occurred. This very important characteristic must be attributed to the presence of silica in the oxide layer. To confirm this we carried out some preliminary oxidation experiments on Ti_2AlC, in which case the oxidation forms TiO_2 and Al_2TiO_5. And whereas these oxides rendered the oxidation

parabolic, it quickly became apparent that was only true for the first heating. Upon cooling, the oxide layer crumbled into a fine dust, most probably because of the high anisotropic thermal expansion coefficient of Al_2TiO_5 that results in its spontaneous microcracking.

5.5 Summary and Conclusions

The oxidation kinetics in air of hot pressed and HIPed polycrystalline samples of Ti_3SiC_2 in the temperature range of 900-1400 °C, are parabolic with an activation energy of 370 kJ/mol. The protective oxide scales that form are layered. The inner layer is comprised of silica and titania, while the outer layer is pure rutile. The results are consistent with a model in which growth of the oxide layer occurs by the outwards diffusion of titanium and carbon, and the inwards of oxygen. The oxidation resistance appears to be a function of TiC content, among other factors: HIPed samples that had less TiC, had a slightly better oxidation resistance than the less pure (≈2 vol % TiC) hot-pressed ones.

6. Surface Carburization, Siliconization, and Nitridation of Ti_3SiC_2

This work aimed to study the surface treatment of Ti_3SiC_2 by means of carburization, siliconization, and nitridation in order to improve the surface hardness and oxidation resistance. Both carburization and siliconization showed parabolic behavior. In carburization a surface layer of TiC was formed in the temperature range of 1400 - 1600 °C. The activation energy was found to be 370 kJ/mol . Carburized surface hardness values of 10-25 GPa were measured. In the case of siliconization, a layer of $TiSi_2$ and SiC was formed on the surface in the temperature range of 1200 - 1350 °C. The activation energy was found to be 130 kJ/mol. Surface hardness values of 10-12 GPa were measured and the oxidation resistance was found to be enhanced more than 3 orders of magnitude in the temperature range of 1240 - 1400 °C in air. In the case of nitridation, non-parabolic behavior was observed and an outer layer of porous, non-uniform TiN was formed over a more uniform inner layer of TiC_x, and SiC. Surface hardness of as nitrided samples was 7 - 12 GPa. The hardness of the underlying TiC_x-SiC layer was ≈ 20 GPa.

6.1 Introduction

Recently, for the first time, we fabricated and characterized single-phase, fully-dense, bulk polycrystalline samples of Ti_3SiC_2 by reactively hot pressing or HIPing of Ti, SiC, and graphite powders at 1600 °C for 4 hr [15]. It was found that Ti_3SiC_2 has a combination of unique properties. The material was not susceptible to thermal shock up to 1400 °C and as machinable as graphite with hardness value of 4 GPa. At 1300 °C, large plastic deformation was observed with yield points of the order of 300 and 100 MPa in compression and bending, respectively. In more recent work [18], we reported on the

energy absorption mechanisms that were observed around the hardness indentation (grain pull out, grain break up, and microplasticity) which make the material a damage tolerant one. Also we reported on the effect of grain size on the room temperature and elevated temperatures mechanical [17 (see chapter 7)]. It was found that despite the grain size, Ti_3SiC_2 is a damage tolerant material while the fine grained material (3-5 μm) was found to thermal shock in the temperature range of 750-1000 °C unlike the coarse grained material (≈ 100 μm) which is not susceptible to thermal shock up to 1400 °C. Yield points of 500 and 120 MPa were measured in compression and bending, respectively, for the fine grained material at 1300 °C.

The parabolic rate constants of oxidation, k_p, was found to vary from 1 x 10^{-9} to 1 x 10^{-5} $kg^2.m^{-4}.s^{-1}$ in the temperature range of 900 -1400 °C in air. At lower temperatures the k_p values are comparable to those of Cr metal, but because of the large activation energy for oxidation (370 kJ/mol) at higher temperatures the k_p values are about five orders of magnitude higher than those for other very oxidation resistance materials such as $TiSi_2$, $MoSi_2$, and SiC. A detailed oxidation study is discussed elsewhere [53 (see chapter 5)]. We have also reported the reaction path and microstructure evolution during the processing of Ti_3SiC_2 [54 (see chapter 3)].

Due to the combination of its properties, Ti_3SiC_2 is considered a new and promising candidate for high temperature applications. Even though it possesses a unique combination of properties, for some applications the surface hardness and the high temperature oxidation resistance would need to be enhanced.

Given that this is the first report on the surface modification of Ti_3SiC_2 there is no previous work to compare. The best that can be done here is to review the surface modifications of related or similar compounds such as titanium metal and its alloys, or

compounds where there have been a few reports on their surface siliconization, nitridation and carburization [23, 54-58]. Using halide-activated pack cementation or HAPC, Cockeram and Rapp [23] reported the surface siliconization of commercial pure titanium in the temperature range of 950 -1150 °C. In this process titanium was imbedded in a mixture of silicon, Al_2O_3, and fluoride activator salt (MgF_2, AlF_3, or CuF_2). They reported a multilayer of $TiSi_2$, TiSi, Ti_5Si_4, Ti_5Si_3, and Ti_3Si. The growth kinetics of each layer was parabolic. Munro and Gleeson [55] reported on the surface aluminization and siliconization of γ-TiAl using the HAPC technique. They reported that silicide coating was non uniform and porous, consisting primarily of $TiSi_2$, TiSi and Ti_5Si_4, with the rate-controlling step for the coating growth to be the diffusion of aluminum into the γ-TiAl ahead of the silicide/γ-TiAl interface. Langauer [56], studied the nitridation of Ti by nitrogen diffusion and showed that the rate of oxidation increases with increasing the nitrogen content. Buscaglia et al [57] studied the nitridation of niobium - 46% Ti alloy in nitrogen atmosphere at 1300 °C and reported a parabolic behavior. Wu et al [58], reported the surface carburization of Ti-6Al-4V alloy by $BaCO_3$ molten salt at 860 °C for different periods of time. They reported the formation of small amounts of TiC on the surface.

The general aim of this work was to investigate the mechanisms, kinetics, and the effect on surface properties of surface carburization, siliconization, and nitridation of Ti_3SiC_2.

6.2 Experimental Procedures

Ti_3SiC_2 was produced by hot pressing of Ti, SiC, and graphite powders as was explained in details elsewhere [15 (see chapter 2)]. The outer surfaces were then machined off and the remaining material was cut by a diamond wheel into coupons of approximate

dimensions of 5 x 5 x 2 mm. The coupons surfaces were ground to a 1200-grit finish and cleaned with methanol.

6.2.1 Carburization

The coupons were placed between two graphite foils (Fiber materials) and a dead load of 2.5 kg (equivalent to ≈ 1 MPa) was placed on the diffusion couple to ensure good contact. The sandwich was then placed in a graphite-element heated vacuum furnace. The diffusion anneals were carried out at 10^{-3} Pa at 1400, 1500, 1550 and 1600 °C; the heating rate in all runs was 10 °C/min. and the samples were furnace cooled. The diffusion time was varied between 1 to 16 hours. Three different runs on different samples were carried out at each anneal time and temperature.

The surfaces of the samples (after peeling off the graphite foil) were then examined by x-ray diffraction using a Siemens D-500 diffractometer. The samples were then cross-sectioned using a diamond wheel, mounted, and polished down to 1 μm diamond grit. Both the surfaces and the cross sections of the samples were examined using an AMRAY 1830 scanning electron microscope (SEM) equipped with an energy dispersive spectroscopy (EDS). The layers thicknesses were measured using the SEM and up to 10 measurements were carried out on each sample. The microhardness was measured using a Leco M-400 tester at 5 and 10 N. The reported microhardness measurements are the average of at least 10 measurements for each sample.

6.2.2 Siliconization

Siliconized samples were prepared by setting up diffusion couple between single crystal Si wafers (Virginia Semiconductors, Inc., Virginia) and the Ti_3SiC_2 coupons. The

siliconization was studied at 1200, 1250, 1300, and 1350 °C and the soak time varied was between 2 - 16 hours. The heating rate was 10 °C/min. The siliconized samples was subjected to the same characterization and testing as the carburized ones.

6.2.3 Nitridation

For the nitridation experiments, the samples were placed in an alumina boat which in turn was placed in a horizontal alumina tube furnace. The nitriding atmosphere was 99.999 pure N_2 gas (B.O.C. gases, N.J.). The nitridation was studied at 1400, 1500 and 1600 °C and the soak time was varied between 1 - 8 hours. The heating rate was again 10°C/min. To see if there is any effect of the N_2 pressure on the nitridation kinetics, a nitridation run was conducted in a hot isostatic press with a pressure of 40 MPa at 1500 °C for 4 hours. The nitrided samples were tested the same way as described above.

6.3 Results and Discussion

6.3.1 Carburization

According to the Ti-Si-C phase diagram shown in Fig. 34 (line 1), the addition of carbon to Ti_3SiC_2 shifts the composition towards the Ti_3SiC_2 - TiC - SiC compatibility triangle. In other words, TiC_x - SiC should form. Consequently carburization should in principle result in TiC_x and SiC according to the following reaction:

$$Ti_3SiC_2 + (3x-1)\,C = 3\,TiC_x + SiC \qquad \Delta V \approx 12.2\,\% \qquad (1)$$

However, X-ray diffraction of the carburized layer indicated the presence of only TiC_x. This was confirmed by the SEM micrographs of the layer shown in Fig. 35. The

layer was porous and EDS confirmed the absence of SiC. Given the aforementioned evidence, the following reaction is proposed for the carburization of Ti_3SiC_2:

$$Ti_3SiC_2 + (3x-2)C = 3\,TiC_x + Si \qquad \Delta V = -15.7\ \% \qquad (2)$$

It is important to note that in contradistinction to reaction 1, where the volume change upon reaction is positive, the volume change for reaction 2 is negative. A conclusion that is in agreement with the fact that the carburized layer is porous. The porosity was estimated to be about 15 vol %.

Interestingly enough, the top view of the carburized layer, shown in Fig. 36b, clearly reveals that there is an epitaxial growth relationship between the carburized layer and the underlying Ti_3SiC_2 grains. The original Ti_3SiC_2 grains are quite large as shown in Fig. 36a. In other words, Ti_3SiC_2 acts as a template for the growth of the TiC. At higher magnification, Fig. 36c, the TiC appears to form a continuous network.

Further microstructural evidence for the presence of TiC at the grain boundaries of Ti_3SiC_2, Fig. 35, in the bulk suggests the mechanism of carburization to be the diffusion of C into Ti_3SiC_2 forming TiC.

The fate of the Si formed as a result of reaction 2 is unclear at this time, but there are two, non-exclusive, possibilities. The first is the rejection of Si at the interface; the second is its vaporization in the vacuum environment in which the carburization was carried out. To differentiate between the two scenarios, a mixture of Ti_3SiC_2 and graphite powders was placed in a vacuum furnace at 1600 °C for 8 hours. X-ray of the resulting mixture clearly showed the presence of both TiC and SiC. In other words, the Si did not diffuse or evaporate from the sample. This result confirms that TiC and SiC are the equilibrium phases resulting from the reaction of Ti_3SiC_2 and graphite.

The other evidence that Si did not evaporate is the formation of TiC in the bulk material at the grain boundaries (where it is impossible for the Si to evaporate) without SiC . More work is needed to be done in order to fully understand the behavior of the Si atoms.

A plot of the thickness squared of the carburized layer as a function of time at 1600 °C is shown in Fig. 37. To obtain a measure of the parabolic rate constant, k_p for the reaction, the data can be fitted to an equation of the form:

$$x^2 = 2\, k_p\, t \qquad (3)$$

where x is the thickness (cm), and t is the time (s). Figure 38 is an Arhenius plot of the parabolic rate constants from which the activation energy of carburization was calculated to be 370 kJ/mol. The parabolic nature of the carburization is consistent with a mechanism which is diffusion controlled. The nature of the rate limiting step is unknown at this time and further work is required before that question can be satisfactorily answered.

The effect of the carburization temperature and time on the surface microhardness are shown in Figs. 39a and b. Increasing the carburization temperature and time increases the carburized layer thickness and hence increases the surface hardness. Increasing the indentation load decreases the measured surface hardness values due to the presence of porosity and the thin nature of the carburized layer.

To study the effect of the applied pressure on carburization, a sample was carburized at 1600 °C for 24 hr under a uniaxial pressure of 40 MPa. With an applied pressure of only 1 MPa, and using the value of k_p at 1600 °C, the thickness of the carburized layer after 24 h should be 80±5 μm. Under 40 MPa of uniaxial pressure, the carburized layer was found to be fully dense with a thickness of 65±5 μm (Fig. 40). As noted above, the carburized layer that formed under 1 MPa was porous with ≈ 15 %

porosity. That results in that the carburized layer under 40 MPa pressure (fully dense) is equivalent to an 85% dense layer of a thickness of ≈ 75±5 μm which is comparable to the value that was predicted using only 1 MPa (80±5 μm). It can be concluded that the applied pressure (in the studied pressure range) has no effect on the thickness of the carburized layer .

6.3.2 Siliconization

According to Fig. 34 (line 2), the reaction of Si with Ti_3SiC_2 should shift the overall composition into the Ti_3SiC_2 - $TiSi_2$ - SiC compatibility triangle. Consequently, the following reaction is proposed for the siliconization process:

$$Ti_3SiC_2 + 7\ Si = 3\ TiSi_2 + 2\ SiC \qquad \Delta V = 120\ \% \qquad (4)$$

X-ray diffraction and SEM micrographs of the reaction layers at elevated temperatures (1200 °C-1350 °C) confirm that the siliconized surfaces consist of $TiSi_2$ and SiC, in total agreement with reaction 4. In contrast to the carburized layer, the siliconized surfaces are fully dense, in part due to the fact that the volume change upon reaction is large and positive. The second reason is the siliconization temperatures are very close to the melting point of the $TiSi_2$ (≈ 1520 °C) where creep or sintering is operative.

The microstructure of a siliconized surface, Fig. 41, shows equiaxed grains of $TiSi_2$ (as is) where, as will be shown, the SiC at the surface is so fine so that it does not appear at this magnification. The microstructure of the siliconized layer depends on the siliconization temperature and time. At low siliconization temperature and short time, (e.g. 1200 °C for 2 hours) the siliconized layer consists of $TiSi_2$ and very fine SiC. At higher temperature, 1350 °C, the siliconized layer was comprised of layered $TiSi_2$ and SiC as shown in Fig. 42. The SiC,. however, appears in two distinct morphologies; in the inner

layer the SiC is coarse (≈ 10 μm). In the outer layer, the morphology of the SiC is in the submicron scale.

Based on the micrograph shown above (Fig. 42) it can be concluded that the reaction occurs by the diffusion of C and Ti outwards for the following reasons:

I. If it is postulated that the morphology of the SiC in the inner layer is due to coarsening, this implies that the SiC in the inner layer formed first and the one in the outer layer formed later. Consequently, C-atoms must be diffusing outwards through the reaction layer. It is only be making that assumption that the formation of the fine SiC in the outer layer can be accounted for.

II. The fact that the outer layer ($TiSi_2$ / SiC) grows with time points out that Ti atoms diffuse outwards too, because it is impossible to form $TiSi_2$ in the outer layer without a flux of Ti atoms. Note that the outer layer can not grow on the expense of the inner one: that is fine SiC can not be produced from coarser one.

In order to confirm that the SiC particles do indeed coarsen with time a sample was siliconized for 16 hours at 1350 °C. The resulting microstructures are shown in Figs. 43a b, and c, from which it is clear that whereas the bimodal distribution in the morphology of the SiC is maintained, coarsening of both layers occurred readily; the average SiC particle size in the outer layer increased to 1 - 3 μm, while in the inner SiC coarsened to 15 - 20 μm.

The reason for the bimodal distribution of the SiC particles is not entirely clear at this time, but an intriguing possibility is that the interface between the coarse and fine areas (which is quite sharp) is the original interface. In other words, the SiC particles that form in the original material are different in morphology than the ones that form as a result of the diffusion of C outwards. It is hereby acknowledged that more work is needed to

understand this difference. It is worth noting, Radhakrishnan et al [26], studying TiSi2/SiC composite made by displacive reaction between TiC and Si, reported that SiC was formed in two different morphologies; a fine needle-like shape and blocky one. The reason behind this difference in the morphology of SiC was not clearly understood.

A possible overall mechanism could be as follows. Ti and C atoms diffuse out of the Ti_3SiC_2 substrate increasing the activity of Si which then leads to the precipitation of $TiSi_2$ and SiC in the vicinity of the substrate forming the inner layer. At the same time, the outward diffusing Ti and C atoms react with the Si on the surface forming the $TiSi_2$ and SiC outer layer. These two different SiC formation mechanisms could explain the two different morphologies of SiC that were observed.

Figure 44 is a plot of the square of the thickness of the siliconized layer, as a function of time at 1350 °C, from which it is clear that the kinetics are parabolic. From the graph k_p was calculated to be 5.5 x 10^{-9} cm^2/s at 1350 °C. By plotting the parabolic rate constant as a function of the siliconization temperature as shown in Fig. 45, the activation energy was calculated to be 130 kJ/mol. This value is comparable with the value of 167 kJ/mol obtained by Cockeram and Rapp [23] for the siliconization of Ti. Interestingly enough, the k_p values of the $TiSi_2$ layer reported in this work are roughly an order of magnitude lower than these reported by Cockeram and Rapp [23]. The reason for the differences observed is not entirely clear at this time, but could be related to the fact that in this work the reaction layer consisted of $TiSi_2$ and SiC, rather than just $TiSi_2$.

As a preliminary study, a thin siliconized sample, 10 x 20 x 2 mm^3, (siliconized at 1350 °C for 8 hours) was oxidized in air at 1240 and 1400 °C for 12 hours. A comparison of the values of the parabolic rate constants of oxidation of Ti_3SiC_2, siliconized Ti_3SiC_2, $TiSi_2$ and SiC in Table VI. It is worth noting that the siliconization by means of this

technique results in non-uniform layers specially at the sides of the samples. Hence, the values of the parabolic rate constants can be considered as a lower bound. The use of siliconizing gaseous atmospheres should yield more uniform layers and consequently better oxidation resistance. Measuring the microhardness of the siliconized layers resulted in the value shown in Table VI. The values of the microhardness are identical to those reported by Radhakrishnan et al for a $TiSi_2$ / SiC composite with 32.5 % of volume [26].

6.3.3 Nitridation

The Ti-Si-C-N quaternary phase diagram is unavailable and consequently the phases one would expect as a result of the nitridation of Ti_3SiC_2 are unknown. The x-ray diffraction measurements, optical and SEM micrographs of nitrided layers, however, indicate that the nitridation of Ti_3SiC_2 resulted in the formation of two distinct layers: an outer porous layer of TiN, separated from an inner layer composed of TiC and SiC (Fig. 46). In other words, the overall nitridation reaction is:

$$Ti_3SiC_2 + 2N = 2\ TiN + TiC_x + SiC \qquad \Delta V = 10.5\ \% \qquad (5)$$

The exact mechanism for the nitridation is unclear at this time. However the following observations are consistent with a mechanism in which Ti diffuses out of the substrate. The evidence for the outwards diffusion of Ti in indirect but compelling. Thermodynamically, the formation of TiC_x and SiC upon nitridation can only occur by the lowering of the activity of Ti. In other words, for TiC_x and SiC to form, the overall composition must follow line 3 in Fig. 34. As the Ti diffuses outwards, the activities of Si and C increase until eventually TiC_x and SiC precipitate out. At which point three phases are present in equilibrium, namely TiC_x , SiC and Ti_3SiC_2. Other evidence that Ti

diffuses outwards, is shown in Fig 47, where a layer of Ti deficient is formed around the grains which tend to be consumed by the formation of TiC and SiC.

The kinetics of nitridation was found to obey a power law behavior (Fig. 48), instead of the parabolic one observed during carburization and siliconization. A least square analyses of a log-log plot of the results shown in Fig. 48, results in a slope of 0.209. It follows that the following relationship best describes the kinetics of nitridation of Ti_3SiC_2 at 1400 °C.

$$x^{4.8} = 2\ k_p\ t \qquad (6)$$

Clearly in this case the process is not diffusion controlled. Consistent with the fact that the process is not diffusion controlled, is the fact that the layer thickness is a function of the total pressure of nitrogen. By increasing the pressure of the nitriding atmosphere from 0.1 MPa to 40 MPa at 1500 °C, the thickness of the nitrided layer increased from 85 to 220 μm. No discernible differences in the morphology were observed.

Given the nature of the reaction sequence proposed it is not too surprising that the nitridation kinetics are non-parabolic. Since the nitridation occurs by the outwards diffusion of Ti, initially through Ti_3SiC_2, the formation of a TiC/SiC layer in which the diffusion of Ti is, presumably, reduced should in principle reduce the nitridation kinetics.

The surface hardness was measured as a function of the nitridation time at 1400 °C and plotted in Fig. 49. The values ranged from ≈ 7-12 GPa due to the increase in the nitrided layer thickness. Measuring the surface hardness after gently removing the porous TiN layer, resulted in values in the range of 15 - 25 GPa (microhardnesses of the TiC /SiC sublayer) depending on the nitridation time and temperature.

6.4 Conclusions

In this paper the surface carburization, siliconization, and nitridation of Ti_3SiC_2 were investigated. The following conclusions were reached

1- Carburization of Ti_3SiC_2 in the temperature range of 1400 - 1600 °C resulted in a diffusion controlled process (parabolic behavior) that resulted in the formation of a TiC_x surface layer. An activation energy of 370 kJ/mol was measured. Surface hardness values in range of 10 -25 GPa were measured.

2- In the siliconization of Ti_3SiC_2 in the temperature range of 1200 - 1350 °C, the process was found to be diffusion controlled where the C and Ti atoms diffuse outwards of the Ti_3SiC_2. The net result was found to be two layers, both consisting of $TiSi_2$ and SiC, where the SiC has a bimodal distribution; fine in the outer layer and coarse in the inner one. An activation energy of 130 kJ/mol was measured. The surface hardness of the siliconized samples was measured to be 10-12 GPa, which is three times that of the bare Ti_3SiC_2 . The parabolic rate constants of oxidation of the siliconized samples were found to decrease by more that three orders of magnitude at 1240 and 1400 °C in air.

3- In the nitridation of Ti_3SiC_2 in the temperature range of 1400 - 1600 °C, it was found that it is not diffusion controlled (power low instead of parabolic). Two layers were formed. A porous non adherent TiN outer layer and more dense TiC / SiC inner one. It is believed that nitrogen dissociates at the surface reacting with Ti_3SiC_2 to form TiN. At the same time the Si and C atoms are rejected into the substrate forming TiC and SiC. Increasing the nitrogen pressure 400 times increased the nitrided layer 2.6 times.

7. Effect of Grain Size on the Room and Elevated Temperature Mechanical Properties of Ti_3SiC_2

This work aimed to investigate the effect of the grain size on the room temperature and elevated temperatures mechanical properties such as compression, four point bending, thermal shock and damage tolerance. The comparison was made between two materials with different grain sizes; fine grains (3-5 μm) and coarse grains (100-200 μm). For the fine grained material at room temperature the failure is brittle and the compressive strength and the MOR were measured to be 1050 and 600 MPa, respectively. The corresponding values for the coarse grained material were decreased to be 720 and 330 MPa. At elevated temperatures, the strength was decreased with increasing the temperature with a BDTT (brittle to ductile transition temperature defined as the temperature at which the material exhibits plasticity ≈ 2 %) of 1200 °C . At 1300 °C, both microstructures exhibited high levels of plasticity (> 20 %). In the case of the fine grained material, yield points of 540 and 120 MPa were measured in compression and bending, respectively. In the case of the coarse grained material, values of 320 and 100 MPa were measured. Using low purity SiC powders in the processing of the coarse grains resulted in a decrease in the compressive and flexural strengths at both room and elevated temperatures. Both the fine and the coarse grained materials was found to be damage tolerant. Although the coarse grains material is not susceptible to thermal shock up to 1400 °C, the fine grains material was found to thermal shock between 750 and 1000 °C. The microhardness was found to be a function of the indentation load in the two cases.

7.1 Introduction

The need for new materials that can stand the aggressive conditions in the high temperature applications is increasing tremendously. Ti_3SiC_2 can be considered as a new candidate for high temperature applications, even though very little was known till very recently about it due to the difficulties in producing it in bulk dense single phase [1,2,3,6,7,8,9,10, and 19]. Recently, we reported on the fabrication and characterization of bulk fully dense single phase Ti_3SiC_2 [15 (see chapter 2)]. It was found that Ti_3SiC_2 possesses a unique combination of properties. Ti_3SiC_2 is as machinable as graphite and is not susceptible to thermal shock up to 1400 °C (with grain size ≈ 100 μm). Hardness of 4 GPa was measured. At 1300 °C, large plastic deformation was reported with yield points of the order of 300 and 100 MPa in compression and bending respectively. Also, we have reported the energy absorption mechanisms that were observed around the hardness indentation and the damage tolerance of Ti_3SiC_2 [18 (see chapter 4)]. A detailed oxidation study in the temperature range of 900 -1400 °C in air was also reported [53 (see chapter 5)]. Also, the reaction path and microstructure evolution during the processing of Ti_3SiC_2 was discussed in details elsewhere [54]. The effect of surface carbonization, siliconization, and nitridation on the properties of Ti_3SiC_2 were also reported elsewhere [59].

The influence of grain size on the mechanical behavior of intrinsically brittle solids, particularly of alumina, magnesia and other noncubic ceramics, has been documented [36, 60-67]. Generally, the strength is observed to decline with coarsening of the grain structure. Understanding the strength/grain-size dependence is very important factor in the microstructural design of structural ceramics. Studying the strength-grain size behavior of $MgAl_2O_4$, Rice [61] suggested that the nonzero intercept of σ_f vs $1/\sqrt{G}$ curves may be the consequence of flow sizes which are larger than the grain size. Davidge [62] showed that, for dense MgO, the fracture strength as a function of the grain size depends strongly on the

surface finish where the largest grain is the most important one not the average grain size. Studying the thermal shock of mica glass-ceramics, Chyung[63] showed that increasing the grain size decreased the fracture strength and increased ΔT_c of thermal shock.

In this work, the authors aimed to study the effect of the grain size on the mechanical properties (compression and bending) at room temperature and elevated temperatures. The effect of the grain size on thermal shock, hardness, as well as on damage tolerance were also studied.

7.2 Experimental Details

The detailed procedure of producing Ti_3SiC_2 with different grain sizes is discussed in the accompanying paper [13 (see chapter 3)]. Briefly, Ti (99.99 %, -325 mesh, Johnson Matthey), SiC (99.5 %, d_m = 2 μm, Johnson Matthey), and C (99 %, d_m = 1 μm, Aldrich) powders were reactively HIPed (in glass tubes, for details see chapter 3) at 1450 and 1600 °C for 4 hours to produce fine and coarse grained samples, respectively. As shown in Fig. 50, the grains were found to have aspect ratios anywhere from 2 - 10. Thereafter, the grain size will be described by the longest dimension of the grains. Thus the small and large grained materials will be referred to as "3 μm" or "100 μm" material, respectively.

Most of the samples discussed in this paper was fabricated using the aforementioned powders. However, in order to investigate the effect of the powders' purity on the mechanical behavior, low purity SiC (97.5 %, d_m = 44 μm, Carborundum abrasive grains, where the major impurities were SiO_2 and Si, were used to produce coarse-grained material (Table IV).

After HIPing, the samples were soaked in concentrated HF (48%) to dissolve the glass. The sample surfaces were then machined off using a diamond wheel. Samples for mechanical testing were machined using a diamond wheel. In contrast to typical ceramics, no additional surface polishing or beveling of the edges was used prior to testing. Cubes of the dimensions of 2 x 2 x 2 mm^3 were machined for both the room and elevated temperatures compression tests. A servo-hydraulic MTS testing machine was used for all tests. The cross head speed chosen was to be 0.01 mm/s. In the elevated temperatures compression tests, a heating rate of 20 °C/min was used to reach the test temperatures. The sample was held at that temperature for 5 minutes prior to testing to insure thermal equilibrium. Three samples were tested at each temperature.

For the four point bending tests, the dimensions of the specimens conformed to ASTM C1161 type A (25 x 2 x 1.5 mm^3) using a SiC fixture with outer span of 20 mm and an inner span of 10 mm. The same cross head speed and heating rates were used as in the case of compression. All the elevated temperatures tests were conducted in air.
Flexure strength, σ, was calculated using:

$$\sigma = 3 P (L_1 - L_2) / (2 B W^2) \qquad (1)$$

where P is the load at fracture, L_1 and L_2 are the outer and the inner span respectively, B is the specimen width (2 mm), and W is the specimen thickness (1.5 mm). For tests where the specimens exhibited plastic deformation, P was taken as the load for the onset of non-linearity in the load-displacement curve. Three samples were tested at each temperature.

The microhardness was measured using Leco M-400 tester at 0.5, 1, 5 and 10 N. The hardness was measured by averaging at least 10 measurements at each load.

To measure the damage tolerance, the flexural strength was measured as a function of the indentation load after introducing the hardness indentation on the tensile surfaces.

Vickers indentations were made using loads of 0.5, 5, 10, 100 and 300 N. Three samples were tested for each point shown in Fig. 56.

For the thermal shock measurements, bend samples with the same dimensions as described above were used. The furnace was preheated to the desired temperature, T_{quench}, and the samples were inserted in the hot furnace, held at temperature for 10 mins and then quenched in ambient temperature water. The post-quench retained strengths were measured as a function of the severity of the quench, or $\Delta T = T_{quench} - T_{water}$. Four samples were tested at each temperature.

7.3 Results and Discussion

7.3.1 Compression and Bending

Typical microstructures of the two materials tested in this study are shown in Figs. 50a and b. The effect of the grain size on compressive strength is shown in Fig. 51. At room temperature, despite the fact that microplasticity was reported [18] the overall failure is brittle in both cases with compressive strengths of 720±40 and 1050±50 MPa for the coarse and the fine grained materials, respectively. This difference in the strength is a Griffth effect, these results however are not enough to verify a relation between σ_f and G. S.

At 1150 °C, both materials exhibited brittle failure at slightly (≈ 15 %) lower compressive stresses. At 1200°C, macroplasticity (≥ 2 %) was apparent in the stress-strain curves. The yield stresses for the fine and coarse grained samples were, respectively, of 600±30 and 420±25; MPa. Given that the onset of plasticity occurred at 1200 °C, that temperature can be considered the BDTT for this material.

As shown in Fig. 52, at 1300 °C, both materials showed high levels of plasticity (> 20%) with yield points of 500±20 and 320±15 MPa for the fine and coarse grains, respectively. It is worth noting that in obtaining the data in Fig. 52, the MTS was preprogrammed to displace the platens by the displacement shown, at which point the runs were interrupted; in other words, they were not run to failure.

Figure 53 shows the load - displacement curve and the bent sample at 1300 °C in the case of the coarse grains (the fine grained material showed the same behavior). No cracks were observed on the surface of the bent sample.

The effect of temperature on the behavior of the two materials in four point bending is shown in Fig. 54. Once again at room temperature, the failure was brittle and the flexural strengths were measured to be 330±20 and 600±30 MPa for the coarse and fine grained material, respectively. The BDTT was again found to be in the vicinity of 1200 °C. The yield stress was 150±10 MPa for the fine grained material and 120±10 MPa for the coarse grained. At 1300 °C, both materials exhibited large plasticity levels (≈ 10 %) with yield stresses of 100±5 and 120±5 MPa for the fine and coarse grained materials, respectively.

The effect of the impurities in the starting SiC on the flexural strength at 1300 °C is clearly shown in Fig. 53. The less pure sample yielded at 60 MPa and the load bearing capability dropped beyond the yield point. The purer samples, the yield point is about 100 MPa, and the load bearing capability increases with increasing deformation. The purity of the starting powders also affected the room temperature flexural strengths: 260 MPa for the less pure powders compared to 330 MPa for the purer ones. The compressive strengths were also reduced from 720 MPa to 560 MPa. Similarly, at 1300 °C, the compressive yield stress decreased from 320 MPa to 260 MPa.

Post-deformation examination of the less pure bend specimens showed that cracks were initiated on the tensile surface of the sample and that cavities are formed ahead of the crack tip. This type of cavity formation under the application of tensile loads is known in the case of viscous grain boundary films [68]. Even though a TEM study is needed to identify the nature of the grain boundaries, this is believed to be the case because the main impurity in the starting SiC powders is SiO_2. To test this hypothesis, two samples (10 x 10 x 100 mm^3) with the two purity levels were placed on graphite rolls with a span of 80 mm and annealed in a vacuum furnace at 1600 °C for 4 hours. Under its own weight, the less pure sample slumped, whereas the pure one did not, which indirectly confirms the glassy nature of the grain boundaries in the case of the less pure sample. At this time it is acknowledged that more work is needed to understand the effect of impurities on the load-displacement curves at elevated temperatures.

7.3.2 Microscopic Observations

After 20 % deformation, the coarse grained material was found to form cavities and the grains showed break-up where the deformed grains were in the order of 10 μm. In some areas, as shown in Fig. 55a,b, grains with the original size (≈100 μm) were found to exhibit buckling which leads to cavities formation, and hence grain bending, and then grains break-up. In the case of the fine grains no major changes were observed in the microstructure. As shown in Fig. 52, the drop in the stress after small strain level is due to the grains buckling and then break up.

The microstructure of the bent samples did not show any difference than before bending. The reason why the yield stress under bending is lower than that under compression is not clearly understood.

7.3.3 Damage Tolerance and Thermal Shock

The need to produce ceramics that are damage tolerant is essential in order to render them insensitive to the initial flaw sizes and/or subsequent in-service damage. Ti_3SiC_2, with 100 μm grains, was reported to be a damage tolerant material [18 (see chapter 4)]. In this work, the flexural strength of the pre-indented samples as a function of the indentation load is shown in Fig. 56. At different flexural stress levels, both of the coarse and fine grained materials showed a small degradation of the strength with increasing the indentation load and hence the indentation size. In both cases, the slopes of the curves were significantly lower than -1/3 (which is a typical value for brittle materials [36]. Noting that Ti_3SiC_2 is relatively soft and has a hardness of 4 GPa that resulted in indentations and damaged areas as large as 700 μm which is more than two orders of magnitude larger than the fine grains (3 - 5 μm). Where in the case of alumina or hard ceramics, the indentation (surface flaw) that is produced under the same load will be much smaller [36]. This indicates how severe and valid this test is in the case of Ti_3SiC_2. The reason why Ti_3SiC_2 is damage tolerant is due to the ability of the material to absorb the energy within a small area in the form of several damage mechanisms as was discussed in details elsewhere [18 (see chapter 4)].

Thermal shock resistance is another very important property needed if the material is to be used as a high temperature structure material. Usually ceramics have a good thermal shock resistance if they have low thermal expansion coefficients, high thermal conductivities, low elastic moduli, and high fracture toughness . We reported that Ti_3SiC_2 with 100 μm grain size does not susceptible to thermal shock up to 1400 °C [15 (see chapter 2)]. This is believed to be due to the ability of the material to absorb the energy within a localized area by different mechanisms like grain pull-out, breakup, and buckling (micro plasticity) as was reported previously [18 (see chapter 4)]. Figure 57 shows the

thermal shock resistance of the fine and coarse grained materials. For the fine grained material, it is clear that at $\Delta T \approx 750$ °C, the retained strength decreased by about 10 % compared to the unquenched samples. Where at 1000 °C the material lost about 50 % of its strength. Generally speaking in ceramics, ΔT_c is defined as the temperature at which a sudden (step function) drop occurs in the retained strength after quenching [69]. In the case of fine grained Ti_3SiC_2, it is believed that the gradual decrease in the retained strength is due to the damage tolerance of the material which was explained before. In the case of alumina, it was reported that increasing the grain size improved flaw tolerance [36,60].

7.3.4 Hardness

Figure 58 shows the microhardness, as well as macrohardness, of Ti_3SiC_2 as a function of the applied load for the two different grain sizes. At higher loads (100 N) the value of the hardness was found to be 4 GPa and independent on the grain size. This value is the same as that was extrapolated by Lis et al [19]. For the coarse grains, the microhardness decreased dramatically (from 8 to 4 GPa) with increasing load with a significant scatter in the values at lower load levels. In the case of the fine grain size, the same behavior was observed, but the decrease in the hardness values was not as dramatic As the indentation size becomes comparable to the grain size, the effect of the anisotropy becomes more pronounced as observed in the case of the coarse grain sized material. In the case of the fine grain size, the indentation is larger than the grain size even at lower loads.

7.4 Conclusions

The major findings of our study are:

a) In compression, the room temperature failure was found to be brittle with compressive strengths of 1050 and 720 MPa for the fine grained material and the coarse grained material, respectively. The compressive strength was found to decrease with increasing the temperature. The BDTT was about 1200 °C. At 1300 °C, both materials exhibited large plastic deformation levels (> 20 %) with yield points of 320 and 500 MPa for the coarse and fine grained materials, respectively.

b) At room temperature, the flexural strengths were found to be 330 and 600 MPa for the coarse and fine grains, respectively. At 1300 °C, associated with high levels of plastic deformation (≈ 10 %), yield points of 100 and 120 MPa were measured for the coarse and fine grains respectively. As in the case of compression, the BDTT was found to be about 1200 °C.

c) Both of the fine and coarse grained materials was found to be damage tolerant.

d) Even though the coarse grained material was found to be thermal shock resistant up to 1400 °C, the fine grained material was found to lose its strength gradually. Quenching from 750 °C results in a 10 % drop in strength, while quenching from 1000 °C results in a 50 % drop in strength.

e) The hardness values were found to decrease by increasing the applied load due to the anisotropy of the material

8. Ambient and Elevated Temperature Deformation Mechanisms of Oriented Macro-Grains of Ti_3SiC_2

Large oriented grains, 1 - 4 mm in length with aspect ratios of 20-40, were fabricated by a forging-grain growth route in order to study the deformation mechanisms of Ti_3SiC_2 in compression at 25 and 1300 °C. The grains were arranged in an X-shaped pattern with the basal planes making an angle of ≈ 25° with the loading axis. Slip was found to occur readily on the basal planes at both room temperature and 1300 °C. The dominant deformation mechanisms observed were grain shearing along the basal planes and grain buckling. Both mechanisms resulted in the formation of cavities. At 1300 °C cavities formation were found to be less severe than that at room temperature. Grain curling, a first for a ceramic material, was also observed at room temperature. The yield stress was found to decrease from 170 to 120 MPa as the temperature increased from ambient to 1300 °C. The critical resolved shear stress along the basal planes is estimated to be of the order of 50 - 60 MPa.

8.1. Introduction

Recently we have shown that Ti_3SiC_2 combines a unique combination of properties especially at temperatures in excess of 1200 °C where polycrystalline samples deformed plastically [15,17 (see chapters 2 and 7)]. Prior to our reports, there had been very few reports on the intrinsic properties of Ti_3SiC_2, partially as a result of the difficulty of fabricating single phase fully dense samples of Ti_3SiC_2. This compound was first synthesized in 1967 [1]. Okano et al [9], working with a material that has some secondary phases (TiC_x and Ti-silicides) and was 95 % of the theoretical density reported a flexural strength of 580 and 500 MPa at room temperature and 1000 °C, respectively. At 1200 °C

the strength decreased dramatically and the samples exhibited plastic behavior. Pampuch and coworkers [6,10], working with hot pressed samples that contained 10 - 20 % TiC reported a Young's modulus of 326 GPa and a Vickers hardness of 6 GPa, and noted that since the ratio of the Vickers hardness to Young's modulus was low, that suggested that the mechanical properties of Ti_3SiC_2 were somehow similar to those of ductile metals. A similar conclusion was also reached from carrying out microhardness measurements as a function of the applied load [2,10].

Recently, we reported on the fabrication and characterization of bulk fully dense single phase samples of Ti_3SiC_2 [15 (see chapter 2)]. It was found that Ti_3SiC_2 is as machinable as graphite, is not susceptible to thermal shock up to 1400 °C, and has a hardness of 4 GPa. At 1300 °C, large plastic deformation was observed with yield points of the order of 300 and 100 MPa in compression and bending, respectively. Furthermore, we reported on the various energy absorption mechanisms that were observed around the hardness indentation and the damage tolerance of Ti_3SiC_2 [18 (see chapter 4)]. In that work we showed that some grains around the hardness indentation were pulled-out, buckled (microplasticity), and delaminated across the basal planes.

Studying the effect of the grain size (3 - 5 vs. 100 - 200 μm grains) on the mechanical properties [17 (see chapter 7)], it was found that the room temperature failure is brittle where the strength decreased with increasing the temperature. The BDTT (brittle-to-ductile transition temperature) was found to be 1200 °C. At 1300 °C the material exhibited high levels of plasticity (>20 %). The material was found to be damage tolerant independent of the grain size. Even though the coarse size grained material does not susceptible to thermal shock up to 1400 °C, the fine grained one was found to lose its strength gradually starting at ΔT of about 750 °C. .

In this work we report on the compressive behavior of oriented macro-grains of Ti_3SiC_2 at room temperature and 1300 °C. By measuring the compressive yield point for different orientations the resolved critical shear stress was estimated. The ultimate aim of this study is to understand the intrinsic deformation mechanisms of this material in order to better understand its overall mechanical behavior of this material.

8.2. Experimental Details

Titanium (99.99 %, -325 mesh, Alta Group), SiC (99.7 %, d_m = 4 μm, Performance Ceramics), and C powders (99%, d_m = 1 μm, Aldrich) were weighed and dry mixed in a V-blender for 2 hours to yield the Ti_3SiC_2 stoichiometry. The mixture was cold pressed into a 76 x 20 x 25 mm^3 green body, which in turn was placed in a vacuum furnace (10^{-3} Pa) and heated to 1450 °C at 10 °C/min and held at that temperature for 8 hours. The resulting body comprised of single phase of Ti_3SiC_2, was approximately 65 % dense and had an average grain size of ≈ 3 μm. The reason for choosing this temperature and soaking time is discussed in details below.

A 15 x 20 x 25 mm^3 piece was cut and placed in a 50 x 25 mm^2 channel graphite die that was presprayed with BN to prevent the sample from sticking to the die walls. The sample was centered in the die in such a way that the hot and cold pressing directions were the same. The height of the sample was 20 mm. Given that at 15 mm the length of sample was shorter than the die (50 mm), the idea was to deform the porous preform under plane strain conditions. That is both deformation and densification occur simultaneously.

The die was then placed in a vacuum hot press under a vacuum of (10^{-3} Pa) and processed using the heating and loading protocols shown schematically in Fig. 59. The sample was heated to 1300 °C before applying any load. At that temperature the preform is ductile and consequently will not break upon the application of the load. The one hour

soak at 1450 °C allows the sample to deform and fill the die cavity and densify, but is insufficient to cause much grain growth [54 (see chapter 3)]. The extensive deformation, however, results in the observed texture. The final anneal at 1600 °C under a pressure of 42 MPa for 24 hours allows the grains to grow in the preferred orientation produced by the deformation. The final height of the sample was ≈ 4 mm, which implies that the total reduction in height was therefore ≈ 80 %.

The surfaces of the sample were then machined off to remove the outer layer which was contaminated by TiC resulting from the diffusion of C from the graphite die. TiC was found to inhibit the grain growth in the outer layer which was discussed in details elsewhere (see chapter 3; Fig. 16). Cubes of the dimensions of 2 x 2 x 2 mm^3 were machined for both the room temperature and 1300 °C compression tests. A servo-hydraulic MTS testing machine was used for all tests. The cross head speed chosen was to be 0.01 mm/s. In the 1300 °C compression tests, a heating rate of 20 °C/min was used to reach the test temperatures. The sample was held at that temperature for 5 minutes prior to testing to insure thermal equilibrium. Three samples were tested at each temperature.

The fabricated parts were characterized by x-ray diffraction, optical microscopy, and SEM.

8.3. Results and Discussion

Optical micrographs of the material are shown in Fig. 60b and c. Referring to Fig. 60a, the micrograph shown in Fig. 60b is that of plane 23. Similarly, the micrograph shown in Fig. 60c is for plane 13. X-ray diffraction patterns of plane 23 are shown in Fig. 61a from which it is clear that the prismatic plane (110) (the intensity should be only 13 %, see Fig. 8) shows strong preferred orientation. When this evidence is taken together

with the morphology of the fracture surfaces (Fig. 61b where cleavage is always along the basal planes), the conclusion is that the grains are in the shape of plates oriented such that their prismatic plane are parallel to the hot pressing direction and their basal planes make an angle of $\approx 25°$ with the horizontal axis (Fig. 60a).

It thus appears that when the grains are still fine, the forging operation rotates them so that their basal planes are in the direction of maximum shear. At 1600 °C the grains prefer to grow in the direction of the basal planes with a high aspect ratio, which leads directly to the microstructure shown in Fig. 60. It is worth noting that, that under identical conditions (1600 °C, 24 hrs.) randomly oriented grains will only grow to a final size of 100 - 400 μm [9]. In other words, the forging operation is needed to orient the grains and allow them to grow to the very large dimensions observed.

Vickers microhardness measurements normal to the prismatic plane using an indentation load of 10 N, yielded a hardness of 3 GPa, in agreement with that measured on single crystals made by CVD [3].

Referring once more to Fig. 60a, the compression tests were conducted in three directions namely: 1-1, 2-2, and 3-3. Figure 62a shows the engineering stress-strain behavior at room temperature in compression in directions 1-1 and 3-3. The yield stresses for these two directions are 230 and 170 MPa respectively. In 1-1 direction, at room temperature, the material exhibited higher strength than in the case of 3-3. Instability was observed in the form of delamination between the layers and buckling at the corner of the sample . Figure 63 shows the compressed sample in 1-1 direction at room temperature with the buckled corner. In this orientation the basal planes are parallel to the direction of the applied load and thus cannot slip.

Figure 62b shows the engineering stress-strain behavior in compression in the direction 3-3 at both room temperature and 1300 °C. At both temperatures significant plasticity was observed. It is worth noting that the test was interrupted at the strain shown rather than run to failure. The yield stress of 120 MPa at 1300 °C was slightly lower than the room temperature yield stress of 170 MPa. There are three possible interpretations for the drop in the yield stress with increasing temperature. The possibilities in decreasing likelihood are

i) the reduction in shear modulus with increasing temperature, which in turn would reduce the yield point

ii) the critical resolved shear stress along the basal planes is thermally activated

iii) another slip system not active at room temperature becomes operative at 1300 °C with a lower yield point.

To differentiate between the first and second possibilities, the temperature dependence of the shear modulus has to be determined. However, to differentiate between the second and third possibilities, that is whether at elevated temperatures other slip systems are operative, compression tests were carried out in the 1-1 direction both at room temperature and 1300°C. At 1300 °C, the behavior is almost identical to that at room temperature (with the almost the same yield point) which implies that the deformation or failure mechanisms at both temperatures are the same.

The microstructures of the compressed samples at room temperature and 1300 °C, are shown in Figs, 64 and 65, respectively. Both samples exhibited deformation bands along the basal planes. Furthermore, some steps are apparent at the sides of the samples due to the relative slipping of the basal planes of some of the grains at the surface. The formation of cavities was observed at both temperatures, but the density of cavities that formed at room temperature was higher than those formed at 1300 °C. A correlation was

found between the total strain a sample was deformed to and the density and size of the cavities. both at room temperature and 1300 °C. more cavities were formed at higher strain levels. Also at the higher strain levels. the grains exhibited break up.

Based on the micrographs of the deformed samples two mechanisms for the formation of cavities have been observed and identified. The first due to the sliding of one grain relative to another. This mechanism is shown in Fig. 66. where two grains oriented in such a way that their basal planes are almost normal to each other. The resolved shear stress on the basal planes of each grain shears the grain in such a way that the strain cannot be accommodated by the neighboring grain. which ultimately forms a cavity at the grain boundary. The second mechanism is by the buckling of grains which are located in the deformation bands and due the constrain from the surrounding grains. the grain buckles and cavities form at the grain boundaries (see Fig. 67).

Grain curling that occurred at room temperature was also observed in this material as shown in Fig. 68. In addition to once again confirming the plasticity of this material at room temperature. this micrograph also confirms the flexibility of the layers that was first observed around hardness indentations [18 (see chapter 4)].

The basal planes slide past one another. presumably. as a result of the relatively weak bonding between the Si and Ti planes. Assuming that the slipping occur only in the basal planes and assuming that the yielding phenomenon is due to the slipping in the basal planes. the critical resolved shear stress can be calculated by resolving the yield stress in the basal plane. The yield stresses in compression in the directions 2-2 and 3-3 are 216 and 170 MPa respectively. were used to calculate the critical resolved shear stress. Even though more work is needed to be carried out on single crystals. resolving the yield stresses yielded a value of 50 ± 5 MPa for the critical resolved shear stress .

It is well known that five independent split and/or twinning systems are necessary for accommodating a general plastic deformation. Many non-cubic crystals (low symmetry crystals) have less than five independent systems by which these crystals can not accommodate an arbitrary plastic deformation . In the case of super conducting oxides, it was assumed that they accommodate strain by the means of crystallographic glide as the only mechanism that operates during the compression of 2223 BSCCO ($Bi_2Sr_2Ca_2Cu_3O_x$) powder (70). Also microcracks were found to be formed, in preferential crystallographic plane, and followed by crystal sliding. Schoenfeld et al (71) densifying BSCCO showed that the deformation mechanisms are crystallographic glide and porosity evolution.

8.4. Conclusions

This work aimed to investigate the behavior under compression of oriented macro grains of Ti_3SiC_2 (1-4 mm) that were fabricated via a forging - grain growth route, at both room temperature and 1300 °C for different orientations. The samples showed plasticity associated with cavities formation at room temperature where the yield stress decreased at 1300 °C. Grain shearing and buckling were observed at both room temperature and 1300 °C. In the case where the basal planes were in the directions of the applied stress, the material showed instability and delamination of the grains where the " yield stress" was found to be insensitive to the temperature up to 1300 °C. This concluded that the only active slip system up to 1300 °C is in the basal planes. For the first time in ceramics, as far as we aware of, grain curling was observed at room temperature.

9. Future Work

This study has shown that Ti_3SiC_2 possesses very interesting features both scientifically and technologically. The following are some recommendations for future work among other interesting points to be studied.

1. The production of oriented macro-grains can serve a wide range of investigations. Understanding the anisotropic behavior of this material is an essential need which can be carried out using such oriented microstructure. A basic-science oriented study to better understand the electrical and thermal properties of Ti_3SiC_2 can also be done on the same oriented grains.

2. Application-oriented tests of the material such as the visibility of mass production and testing the material in a real life test to prove positively the potential applications of Ti_3SiC_2.

3. Since Ti_3SiC_2 can be surface treated so that both surface hardness and oxidation resistance are improved significantly, studying the performance of the treated material (wear, long term oxidation study, etc..) would be of a great benefit.

4. The fact that Ti_3SiC_2 is thermodynamically in equilibrium with TiC, SiC, $TiSi_2$, and $Ti_5Si_3C_x$, which are as high temperature materials, makes it worth studying the composites of Ti_3SiC_2 with these compounds to obtain the desired properties.

LIST OF REFERENCES

1. W. Jeitschko and H. Nowotny, "Die Kristallstructur von Ti_3SiC_2 - Ein Neuer Komplexcarbid-Typ" Monatasch fur Chem., 98, 329-37 (1967).

2. T. Goto and T. Hirai, "Chemically Vapor Deposited Ti3SiC2", Mat. Res. Bull., 22, 2295-1202, (1987).

3. J. J. Nickl, K. K. Schweitzer and P. Luxenberg, "Gasphasenabscheidung im Systeme Ti-C-Si" J. Less Common Metals, 26, 283 (1972).

4. S. Arunajatesan and A. H. Carim, "Symmetry and Crystal Structure of Ti_3SiC_2", Materials Letters, 20, 319-324 (1994).

5. J. Panczyk, T Niemyski,.L. Winogradow & W. Sinelnikova, Szklo i Ceram., 23, (1972) (in Polish). [Idem, Chem. Ab., 77 (640884c)].

6. R. Pampuch, J. Lis, L. Stobierski & M. Tymkiewicz, "Ti_3SiC_2-Based Materials Produced by Self-propagating High-Temperature Synthesis (SHS) and Ceramic Processing", J. Eur. Ceram. Soc. 5, 283 (1989).

7. C. Racault, F. Langlais and R. Naslain, "Solid State Synthesis and Characterization of the Ternary Phase Ti3SiC2, J. Mater. Sci. 29, 3384-3392, (1994).

8. S. Arunajatesan and A. H. Carim, "Synthesis of Titanium Silicon Carbide", J. Amer. Cer. Soc., 78, 667 (1995).

9. T. Okano, T. Yano and T. Iseki, "Synthesis and Mechanical Properties of Ti3SiC2 Ceramic", Trans. Met. Soc. Jpn., 14A, 597 (1993).

10. R. Pampuch, J. Lis, J. Piekarczyk & L. Stobierski, "Ti_3SiC_2-based Materials Produced By Self-propagating High-temperature Synthesis (SHS) and Ceramic Processing", J. Mater. Synthesis & Processing, 1, 93 (1993).

11. M. Barsoum & B. Houng. "Transient Plastic Phase Processing of Ti-B-C Composites", J. Amer. Cer. Soc. 76. 1445-51 (1993).

12. M. Barsoum. "Methods for Densifying and Strengthening Ceramic-Ceramic Composites by Transient Plastic Phase Processing", U.S. Patent # 5,451,365 (1995).

13. M. Barsoum, A. Zavaliangos, S. Kalidindi, T. El-Raghy and D. Brodkin. "The Transient Plastic Phase Processing of Ceramic-Ceramic Composites", JOM, November 1995. p. 52.

14.. X. Tong, T. Okano, T. Iseki & T. Yano, "Synthesis and High Temperature Mechanical Properties of Ti_3SiC_2/SiC Composites", J. Mater. Sci.. 30, 3078 (1995).

15. M. W. Barsoum and T. El-Raghy, "Synthesis and Characterization of a Remarkable Ceramic : Ti_3SiC_2," J. Am. Ceram. Soc., **79** [7] 1953-56 (1996).

16. M. W. Barsoum, T. El-Raghy, and L. Ogbuji," Oxidation of Ti_3SiC_2 in Air," Accepted for Publication in J. of Electrochem. Soc.

17. T. El-Raghy, A. Zavaliangos, M. W. Barsoum, and S. Kalidindi," Effect of Grain Size on Mechanical Properties of Ti_3SiC_2", In preparation.

18. T. El-Raghy, A. Zavaliangos, M. W. Barsoum, and S. Kalidindi," Damage Mechanisms Around Hardness Indentation in Ti_3SiC_2," J. Am. Ceram. Soc., **80** [2] 513-516 (1997).

19. J. Lis, Y. Miyamoto, R. Pumpuch, and K. Tanihata, "Ti_3SiC_2 - Based Materials Prepared by HIP - SHS Techniques," Mater. Lett., **22**, 163-68 (1995).

20. S. Sambasivan, " Thermochemistry of Ceramic-Metal Reactions in Ti-Si-N and Ti-Si-C Systems at High Temperatures and Pressures "; Ph.D. Dissertation, Dept. of Chemistry, Arizona State University, Tempe, AZ, 1990.

21. D. Brodkin, S. Kalidindi, M. Barsoum, and A. Zavaliangos, " Microstructural Evolution During Transient Plastic Phase Processing of Titanium Carbide-Titanium Boride Composites," J. Am. Ceram. Soc., **79** [7], 1945-52 (1996).

22. S. Morozumi, M. Endo, M. Kikuchi and K. Hamajima, " Bonding Mechanism Between Silicon Carbide and Thin Foils of Reactive Metals ," J. Mater. Sci., 20, 3976-3982 (1985).

23. B. Cockeram and A. Rapp " The Kinetics of Multilayered Titanium-Silicide Coatings Grown by the Pack Cementation Method," Met. and Mater. Trans. A, **26A**, 777-791 (1995)

24. T. El-Raghy and M. W. Barsoum , " Surface Treatment of Ti_3SiC_2 ," In preparation.

25. D. Brodkin and M. W. Barsoum ," Isothermal Section of Ti-B-C Phase Diagram at 1600 °C ," . J. Am. Ceram. Soc., **79** [3], 785-87 (1996).

26. R. Radhakrishnan, C. H. Henager, J. L. Brimhall, and S. B. Bhaduri, " Synthesis of Ti_3SiC_2 / SiC and $TiSi_2$ / SiC Composites Using Displacement Reactions in the Ti-Si-C System.

27. U. Kunaver and D. Kolar ," Computer Simulation of Anisotropic Grain Growth in Ceramics , " Acat Metall. Mater., **41** [8], 2255-2263 (1993).

28. J. Rödel and A. Glaeser ," Anisotropy of Grain Growth in Alumina ," J. Am. Ceram. Soc., **72** [11] 3292-3301 (1990).

29. S. Bennison and M. Harmer , " Grain-Growth Kinetics for Alumina in the Absence of a Liquid Phase ," J. Am. Ceram. Soc., **68** [1] C-22 - C-24 (1985).

30. T. Fang , " Abnormal Grain Growth in Sintering Powders Compacts ," Scripta Metall., **22**, 9-11 (1988).

31. H. Nowotny and S. Windisch; p 171-194 in The Annual Review of Material Science, vol 3. Edited by R. Huggins, R. Bube, and R. Roberts. Annual Reviews Inc., California 1973.

32. M. Barsoum, D. Brodkin and T. El-Raghy " Layered Machinable Ceramics For High Temperature Applications ", Script. Met. et. Mater., 36,[5], 535-541, 1997.

33. D. B. Marshall, B. R. Lawn and A. G. Evans, "Elastic/Plastic Indentation Damage in Ceramics: The Lateral Crack System", J. Amer. Cer. Soc. **65**, 11, p. 561 (1982).

34. K. Zeng, E. Soederlund, A. E. Giannakopoulos, D. J. Rowcliffe, "Controlled Indentation: A General Approach to Determine Mechanical Properties of Brittle Materials", Acta Mater., **44**, p. 1127, (1996).

35. I. J. McColm, Ceramic Hardness, Plenum Press, New York (1990).

36. R. F. Cook, B. R. Lawn, and C. J. Fairbanks, "Microstructure-Strength Properties in Ceramics: I Effect of Crack Size on Toughness", J. Amer. Ceram Soc., **68**, 11, p. 604, (1985).

37. H. Cai, M. A. Kalceff, and B. R. Lawn, "Deformation and Fracture of Mica-Containing Glass-Ceramics in Hertzian Contacts", J. Mater. Res . **9**, p. 762, (1994).

38. P. Kofstad, High Temperature Oxidation of Metals, Wiley, N.Y., 1966.

39. K. Hauffe, Oxidation of Metals, Plenum Press, N.Y., 1965.

40. Y-M. Chiang, D. Birnie and W. D. Kingery, Physical Ceramics, Wiley, N.Y., 1996.

41. A. Tampieri and A. Bellosi, "Oxidation Resistance of Alumina-Titanium Nitride and Alumina-Titanium Carbide Composites", J. Amer. Cer. Soc., **75**, 1688-1690 (1992).

42. T. Ya. Kosolapova, Ed., Properties and Applications of Refractory Materials, (in Russian) Metallurgiya, Moscow, 1986.

43. B. E. Deal and A. S. Grove, "General Relationship for the Thermal Oxidation of Silicon", J. Appl. Phys., **36**, [12], 3370-78 (1965).

44. N. Jacobson, "Corrosion of Silicon-Based Ceramics in Combustion Environments", J. Amer. Cer. Soc., **76**, [1] 3, (1993).

45. E. Opilia, "Oxidation Kinetics of Chemically Vapor-Deposited Silicon Carbide in Wet Oxygen", J. Amer. Cer. Soc., **77**, [3] 730-736 (1994).

46. C. Ramberg, G. Cruciani, K. Spear and R. Tressler, "Passive Oxidation Kinetics of High-Purity Silicon Carbide from 800-1000 °C", J. Amer. Cer. Soc., **79**, [11] 2897, (1996).

47. F. N. Schwettmann, R. A. Graff and M. Kolodney, "Mechanism of the Oxidation of Titanium Disilicide", J. Electrochem. Soc., **118**, 1973-1977, (1971).

48. S. Becker, A. Rahmel and M. Schutze, "Oxidation of $TiSi_2$ and $MoSi_2$". Solid State Ionics, **53-56**, 280-289, (1992).

49. Y. Oishi and W. D. Kingery, J. Chem. Phys. **33**, 905 (1960).

50. P. Kofstad, Nonstoichiometry, Diffusion and Electrical Conductivity in Binary Metal Oxides, R. E. Krieger Publ. Co., p. 142-149 (1983).

51. D. L. Venkatu and L. E. Poceat, Mat. Sci. Eng., **5**, 258 (1969/70).

52. L. Ogbuji and E. Opilia, "A Comparison of the Oxidation Kinetics of SiC and Si_3N_4". J. Eletrochem. Soc., **142**, [3] 925-930 (1995).

53. M. Barsoum, T. El-Raghy, and L. Ogbuji," Oxidation of Ti_3SiC_2 in Air," Accepted for Publication in J. of. Electrochem. Soc.

54. T. El-Raghy and M. Barsoum, " Reaction Path and Microstructure evolution during the processing of Ti_3SiC_2," In preparation.

55. T. Munro and B. Gleeson, " The Deposition of Aluminide and Silicide Coatings on γ-TiAl Using the Halide - Activated Pack Cementation Method," Mettal . Mater. Trans. A, **27A**, 3761 3772 (1995)

56. W. Lengauer, " Properties of Bulk δ-TiN_{1-x} Prepared by nitrogen diffusion into titanium metal," J. Alloys and Compounds, **186**, 293 - 307 (1992).

57. V. Buscaglia, C. Bottino, R. Musenich, P. Fabbricatore, G. Gemme, R. Parodi, B. Zhang, and P. Parodi, " Nitridation of Niobium - 46 wt.% Titanium Alloy in Nitrogen at 1300 °C ," J. Alloys and Compounds, **226**,, 232-241 (1995).

58. T. Wu, W. Wei, F. Chen, F. Lai, and J. Wu, " Surface Hardening of Ti-6Al-4V Alloy by Molten Salt Carburization ." Mater. Manuf. Proc., **10** [4], 643-651 (1995).

59. T. El-Raghy, and M. Barsoum," Surface Carburization, Siliconization, and Nitridation of Ti_3SiC_2," In Preparation.

60. P. Chantikul, S. J. Bennison, and B. R. Lawn, "Role of Grain Size in the Strength and R-Curve Properties of Alumina," J. Am. Ceram. Soc., **73** [8] 2419-27 (1990).

61. R. W. Rice, pp 323-45 in Fracture Mechanics of Ceramics, Vol. 1. Edited by R. Bradt, D. Hasselman, and F. Lange., Plenum, New York., 1974.

62. R. Davidge, pp 447-468 in Fracture Mechanics of Ceramics, Vol. 2. Edited by R. Bradt, D. Hasselman, and F. Lange, Plenum, New York., 1974.

63. K. Chyung, pp 495-508 in Fracture Mechanics of Ceramics, Vol. 2. Edited by R. Bradt, D. Hasselman, and F. Lange, Plenum, New York., 1974.

64. R. Tressler, R. Langensiepen, and R. Bradt, "Surface-Finish Effects on strength-vs-Grain-size Relations in polycrystalline Al_2O_3," J. Am. Cer.. Soc., **57** [5] 226-227 (1974).

65. C. Seaton and S. Dutta, "Effect of Grain Size on Crack Propagation in Thermally Shocked B_4C," J. Am. Ceram. Soc., **57** [5] 228-229 (1974).

66. S. Carniglia, "Reexamination of Experimental Strength-vs-Grain-Size Data for Ceramics," J. Am. Ceram. Soc., **55** [5] 243-249 (1972).

67. T. Gupta, "Strength Degradation and Crack Propagation in Thermally Shocked Al_2O_3," J. Am. Ceram. Soc., **55** [5] 249-253 (1972).

68. M. Barsoum, Fundamentals of Ceramics, Ch. 12, P 453, McGraw-Hill, 1997

69. M. Barsoum, Fundamentals of Ceramics, Ch. 13, P 494, McGraw-Hill, 1997

70. S. Ahzi, R. Asaro, and D. Parks, " Application of Crystal Plasticity Theory for Mechanically Processed BSCCO Superconductors ," Mech. of Mater., **15**, p 201 222 (1993)

71. B. Schoenfeld, S. Ahzi, and R. Asaro ," The Bulk Processing of 2223 BSCCO Powders I. Densification and Mechanical Response ," Philos. Mag. A, **73** [6], p 1565-1590 (1996).

Appendix A (Tables)

Table I: Characteristics and sources of powders used in this work.

Powder	Purity	Particle	Source
Ti (hydride)	99.99	- 325 mesh	Alta Group, Fombell, PA
C (graphite)	99.0	dm = 1-2 μm	Aldrich Chemical, WI
SiC (hexagonal)	97.6 %	dm = 99 μm	Carborundum, NY ‡

‡ We acquired this SiC in the mid-eighties. Since then Carborundum has sold this division to Washington Mills Electrominerals, Niagara Falls, N.Y.

Table II. Starting Powders

Ti	-325 mesh	99 %	Johnson Matthey
Ti (dehydrided)	-325 mesh	99.99 %	Alta Group
SiC (abrasive grains)	-325 mesh	97.5 %	Carborundum
SiC	$d_m = 4\ \mu m$	99.5 %	Performance Ceramics
C	$d_m = 1\ \mu m$	99 %	Aldrich
Si	$d_m = < 20\ \mu m$	99.5 %	Elkem, New York

Table III: Parabolic rate constants, k_p, (kg^2/m^4 s) for the oxidation of Ti_3SiC_2, Si, Ti and SiC in air at various temperatures in °C.

	1000 °C	1200 °C	1300 °C	1400 °C	Activ. Energy kJ/mol	
Ti_3SiC_2 (M1)	1.31×10^{-8}	6.58×10^{-7}	2.7×10^{-6}	1.4×10^{-5}	320±5	This work
Ti_3SiC_2 (M2)	1.0×10^{-8}	1.92×10^{-6}	1.3×10^{-5}	1.0×10^{-4}	370±20	This work
Ti	$\approx 50 \times 10^{-8}$	25×10^{-6}	----	----	210-230	Ref. 7
$TiSi_2$	----	----	6×10^{-11} ‡‡‡	-----	-----	Ref. 17
$TiSi_2$	9.78×10^{-12}	2.4×10^{-11}	4.8×10^{-11}	-----	90	Ref. 16
Si	1.6×10^{-11} 1.9×10^{-11}	5.4×10^{-11} ----	---- -----	---- ----	119 95.7	Ref. 12 Ref. 15
SiC ‡	---- 1.25×10^{-12} ‡‡	3×10^{-12} ----	6.24×10^{-12} ----	1.75×10^{-11} ----	142 99.3	Ref. 14 Ref. 15
	----	8.5×10^{-12}	1.7×10^{-11}	2.7×10^{-11}	118	Ref. 21
TiC	4×10^{-4} (900°C)	----	----	----	----	Ref. 11

‡ The values reported here are those for high purity chemically vapor deposited SiC. The reference chosen is for comparison's sake only.

‡‡ Single crystal SiC.

‡‡‡ Becker et al. in Ref. 17 list a value of 6.1×10^{-7} without mentioning the units. We calculated our value from their Fig. 2.

Table IV: Manufacturer's data sheet for major impurities found in the SiC used in this study.

	Al	Fe	Na	Ca	Mg	Ti	K	Si (free)	Silica	C (free)	Source
SiC(M1)	0.3 %	0.2 %	----	----	----	----	----	0.8%	0.6 %	0.5 %	Carborundum
SiC(M2)	0.012%	0.023%	3 ppm	16 ppm	1 ppm	120 ppm	2 ppm	<0.05%	----	----	Alfa

Table V: Summary of inner, outer and total oxide thicknesses on M2 samples oxidized in air for times and temperatures shown. Columns 7 and 8, respectively, compare the parabolic rate constants in units of kg^2/m^4s calculated based on the oxide thicknesses listed in this table to those experimentally determined from the weight gain measurements (last column). In general the agreement is quite good. [ ] = standard deviation in μm.

Duration (h)	Temp. °C	Outer scale, μm	Inner scale, μm	Total scale, μm	inner/outer ratio	k_p total‡ kg^2/m^4s	k_p from Fig. 3.
96	900	----	----	25±1.2	----	----	----
96	1000	26±5	43 ± 8	69±6	1.65	$2.3x10^{-8}$	$1.3x10^{-8}$
12	1240	203±22	258 ± 48	461±42	1.27	$8.3x10^{-6}$	$3x10^{-6}$
12	1400	393±17	1203±66	1596±45	3.06	$1.0x10^{-4}$	$1.0x10^{-4}$

‡ Assumptions: Density of silica-rich phase is 2.5 gm/cm^3 and scale is dense and pore free.

Table VI. A comparison of the oxidation parabolic rate constants and surface hardnesses of Ti_3SiC_2, siliconized Ti_3SiC_2, $TiSi_2$, $TiSi_2$ / SiC composite and SiC.

	Parabolic rate constant of oxidation k_p ($kg^2.m^{-4}.s^{-1}$)		Surface μ hardness (GPa)	Reference
	1240 °C	1400 °C		
Ti_3SiC_2	1.9×10^{-6}	1×10^{-4}	4	Ref. 16
Siliconized Ti_3SiC_2 $TiSi_2$ / SiC (≈ 25 vol% of SiC)	4×10^{-10}	8.5×10^{-9}	10^{-12}	This work
$TiSi_2$ / SiC (32.5 vol% of SiC) [12]	----	----	12	Ref. 26
SiC	3×10^{-12}	1.75×10^{-11}	----	Ref. 45
$TiSi_2$	2.4×10^{-11}	----	----	47

Appendix B (Figures)

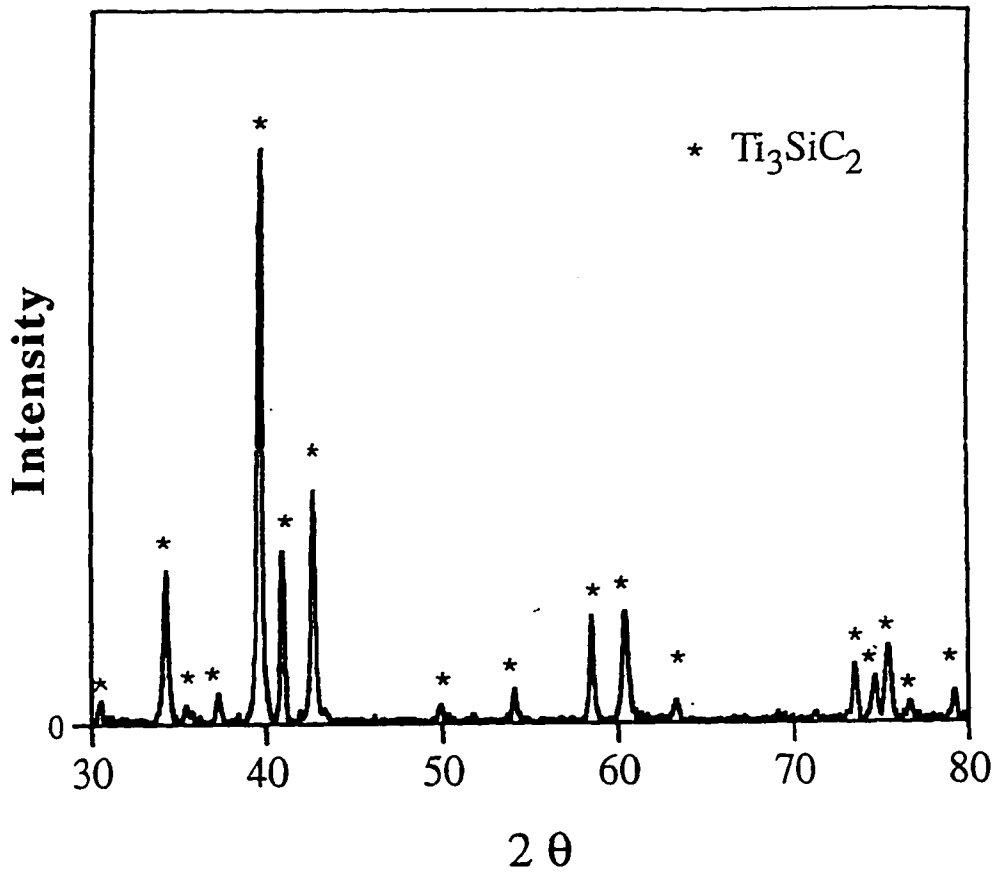

Figure 1. X-ray diffraction pattern of Ti_3SiC_2. No peaks other than those associated with Ti_3SiC_2 were observed even after very slow scans.

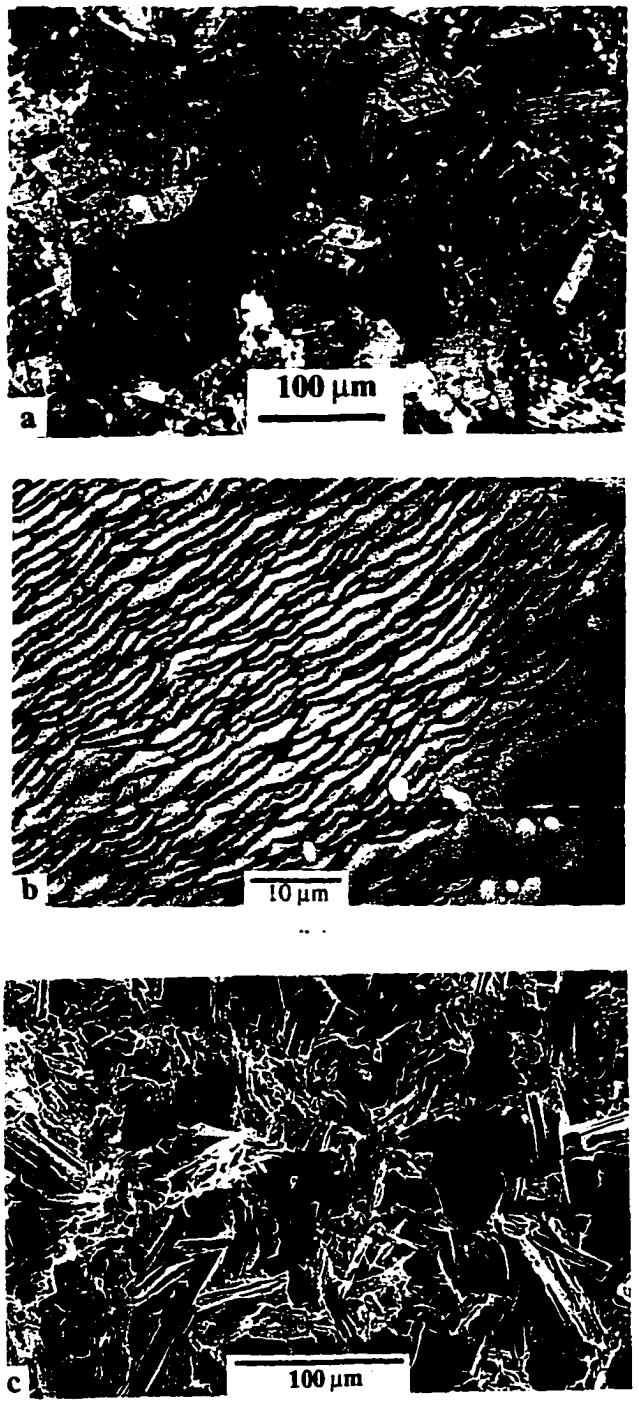

Figure 2. a) Optical micrograph (unpolarized light) of polished an etched surface of Ti_3SiC_2. b) Higher magnification micrograph of striated, black, grains clearly demonstrating layered nature of the material. c) SEM micrograph of fractured surface, where once again the layered nature is apparent.

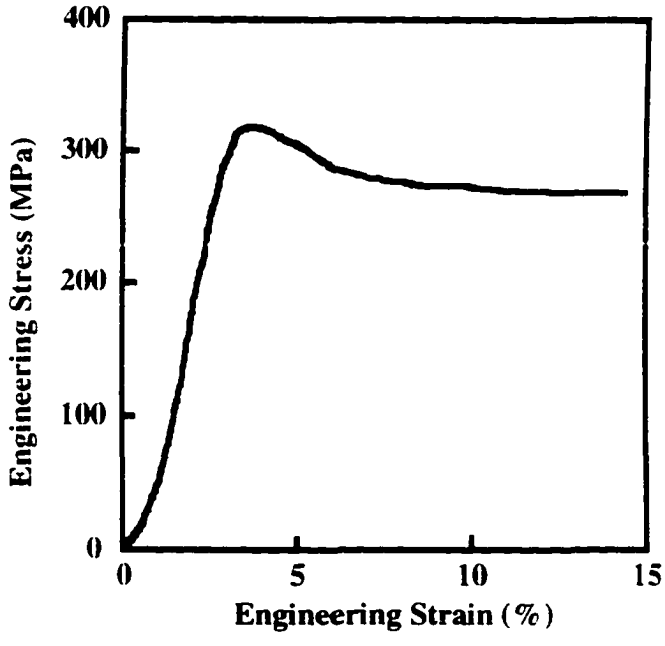

Figure 3. Engineering stress-strain curve for the deformation at 1300 °C in air of a 4.3 mm high parallelepiped of cross section 2.8 x 2.7 mm. Cross-head displacement rate was 0.0033 mm/s.

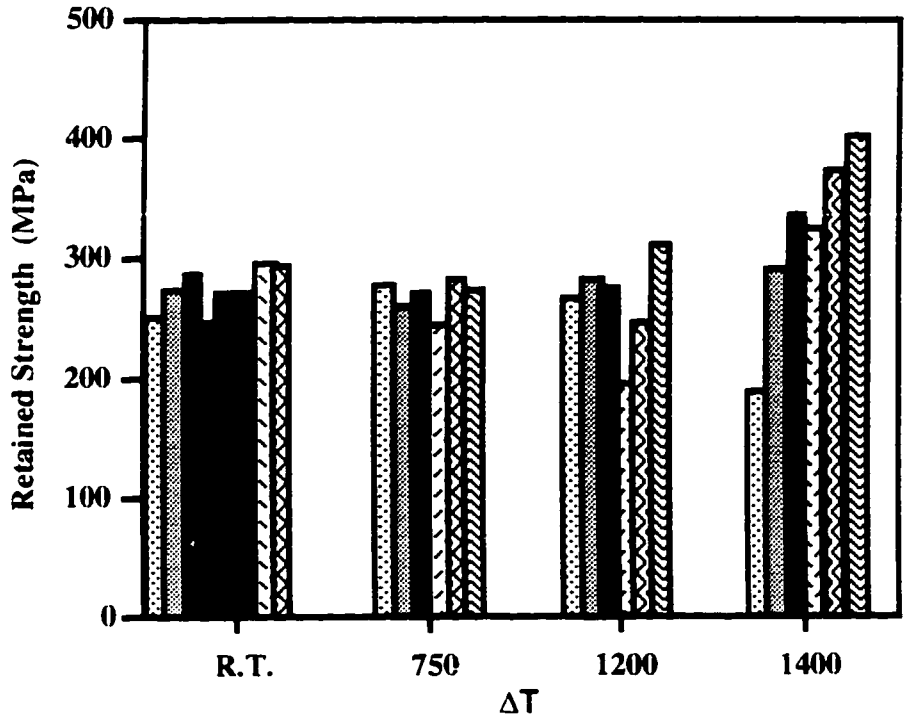

Figure 4. Functional dependence of retained strength after a water quench from temperature indicated.

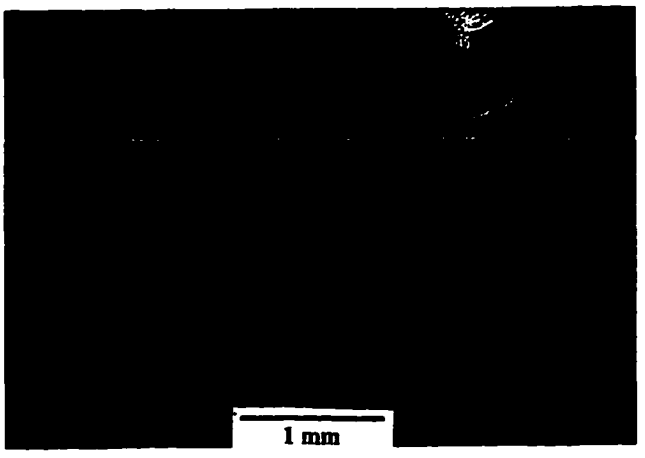

Figure 5. SEM micrograph of the cross-section of a threaded hole that was machined using regular high-speed drill bits and hand tapped without lubrication.

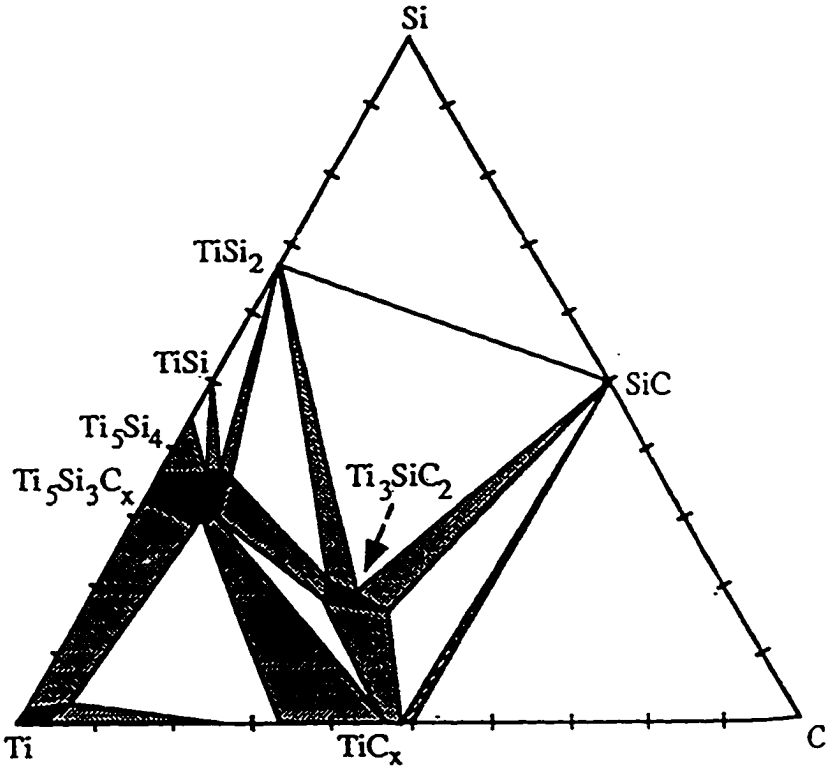

Figure 6. Isothermal section of the Ti-Si-C ternary system at 1200 °C [20].

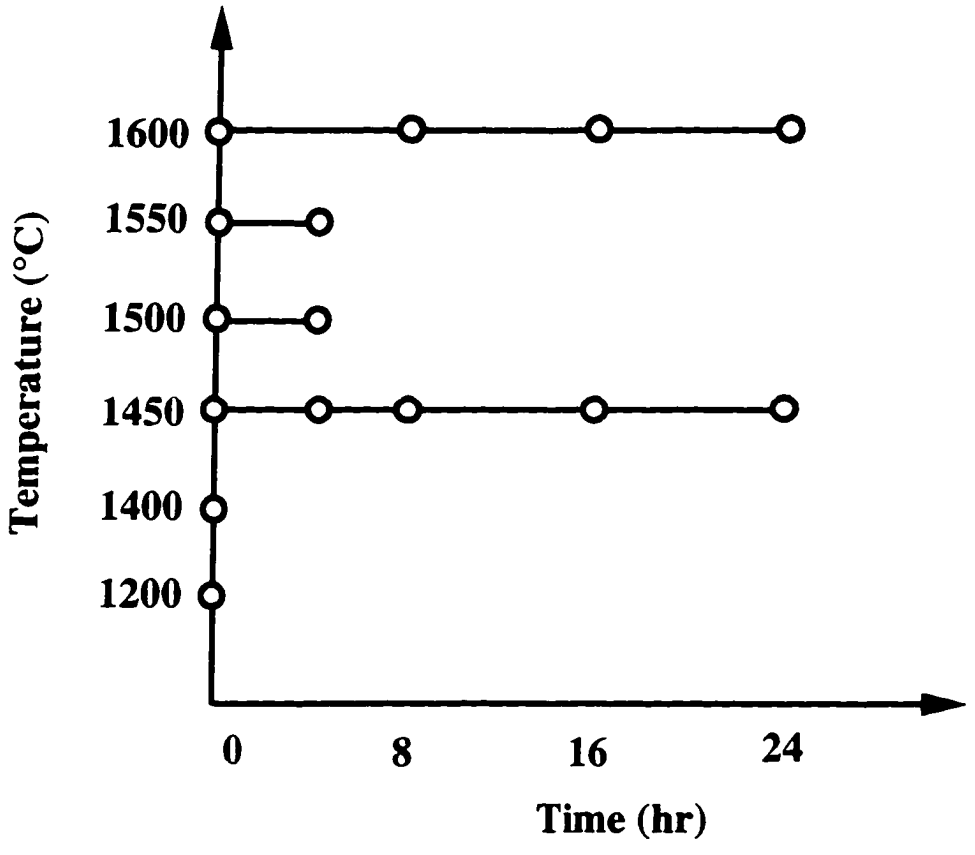

Figure 7. Summary of HIP runs (each circle represents a seperate run).

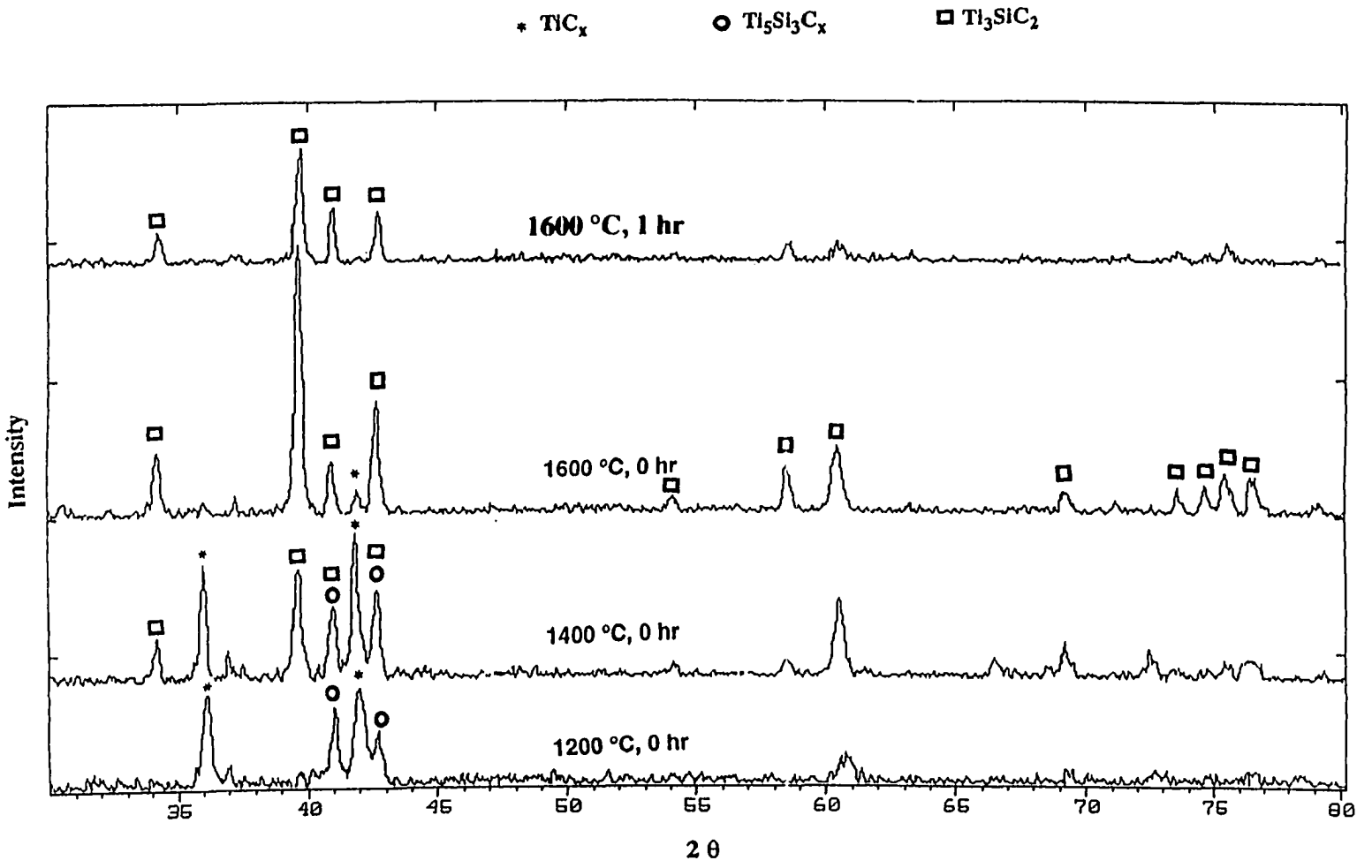

Figure 8. X-ray diffraction patterns at different stages during the processing of single phase Ti_3SiC_2

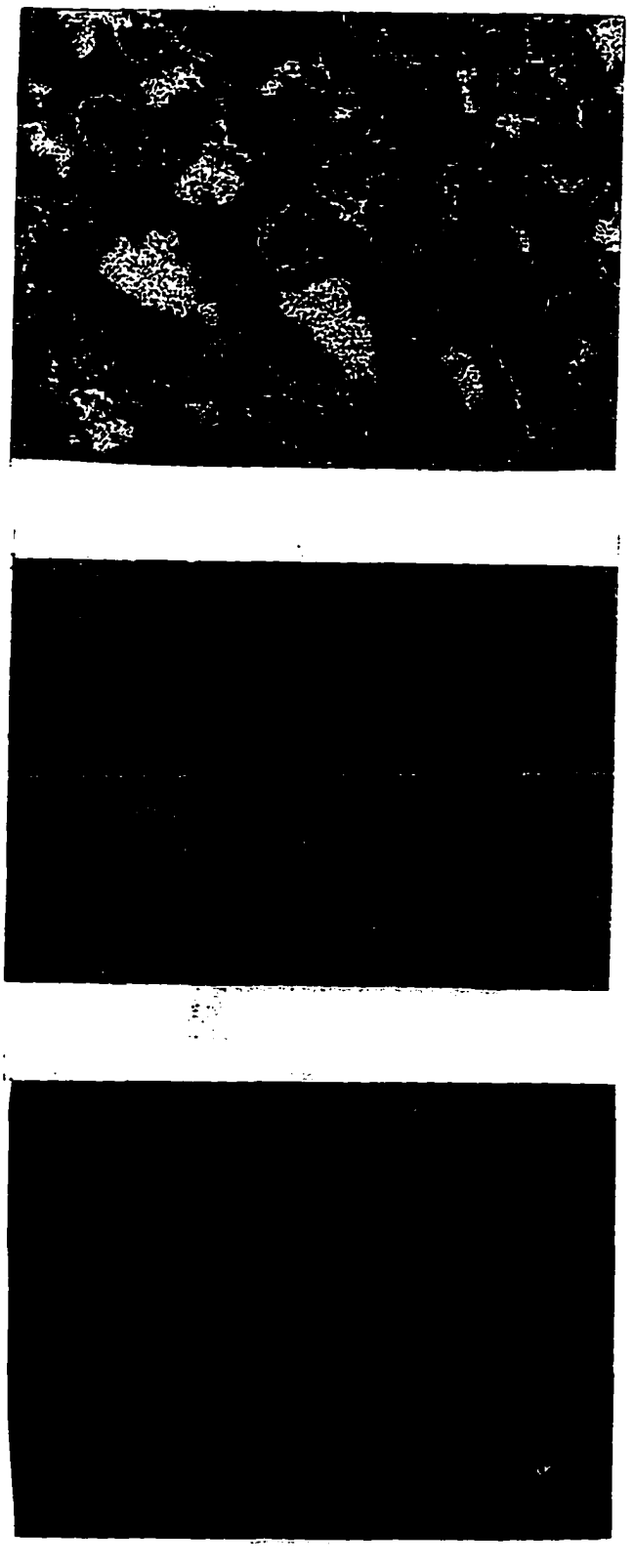

Figure 9. a) A back scattered SEM image; b) Ti EDS mapping; and c) Si EDS mapping of an interrupted HIP run at 1200 °C (no soaking time).

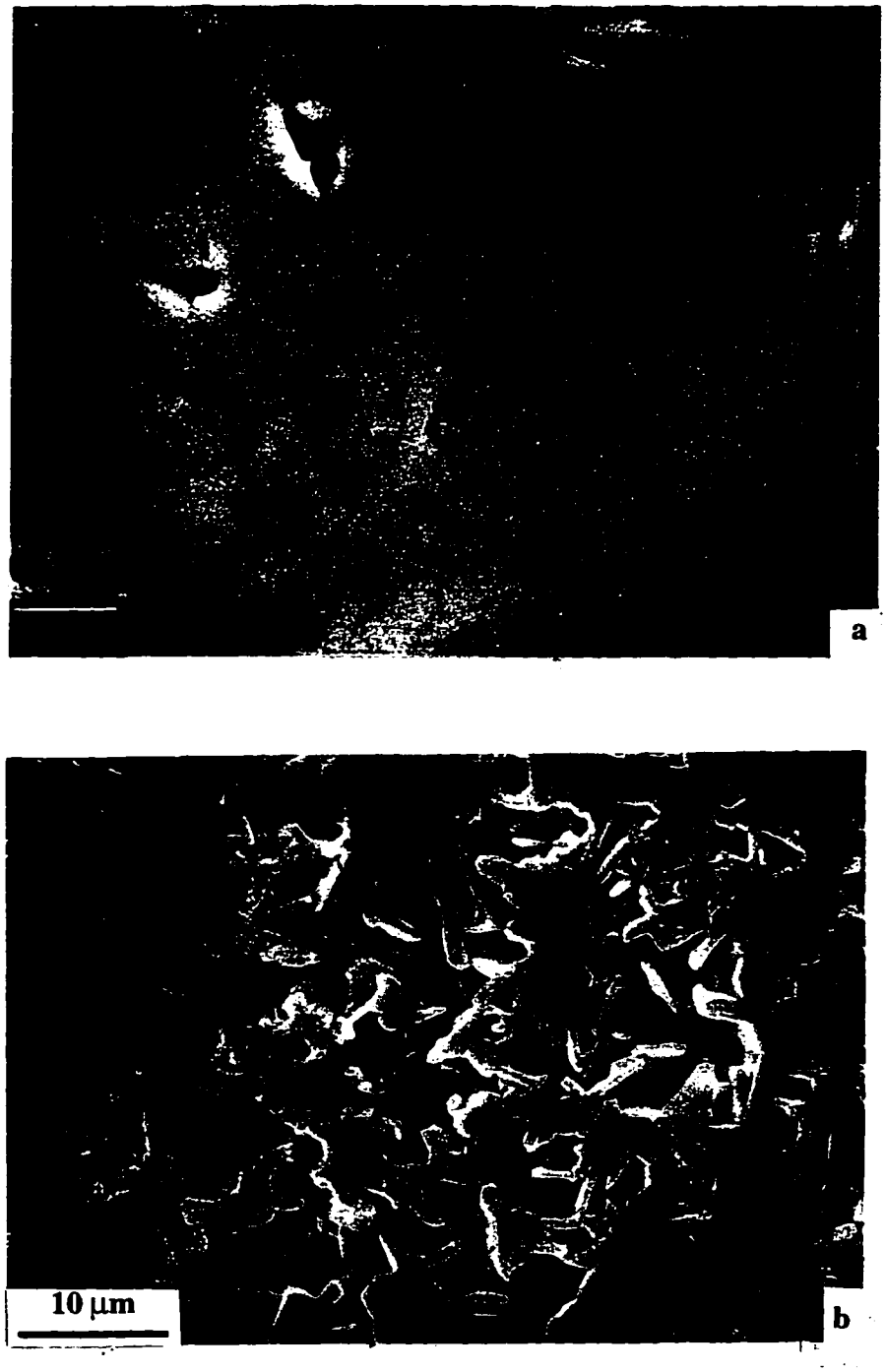

Figure 10. a) A back scattered SEM image showing the nucleation and growth of Ti_3SiC_2 in $Ti_5Si_3C_x$ field. b) A similar area after etching ($Ti_5Si_3C_x$ was leached)

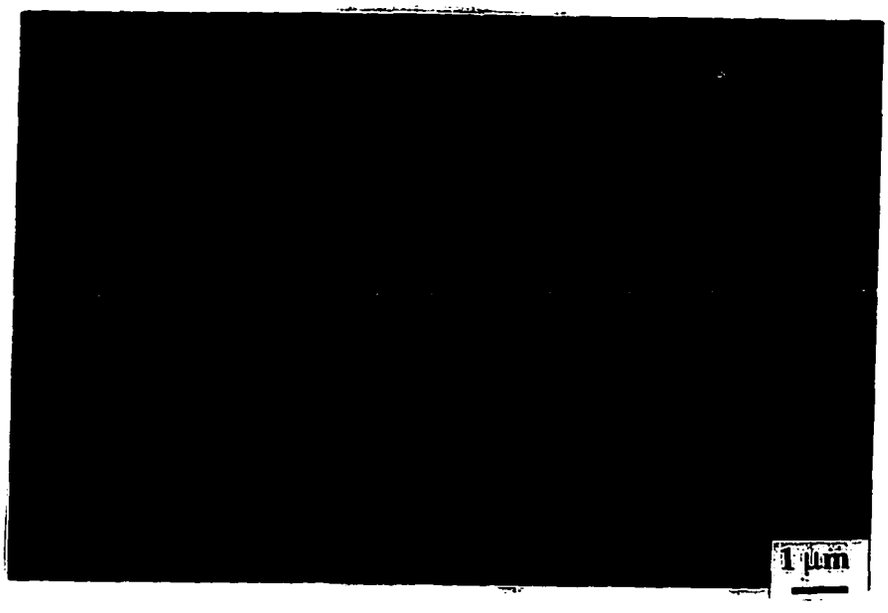

Figure 11. A back scattered SEM image showing that Ti_3SiC_2 is the only present phase.

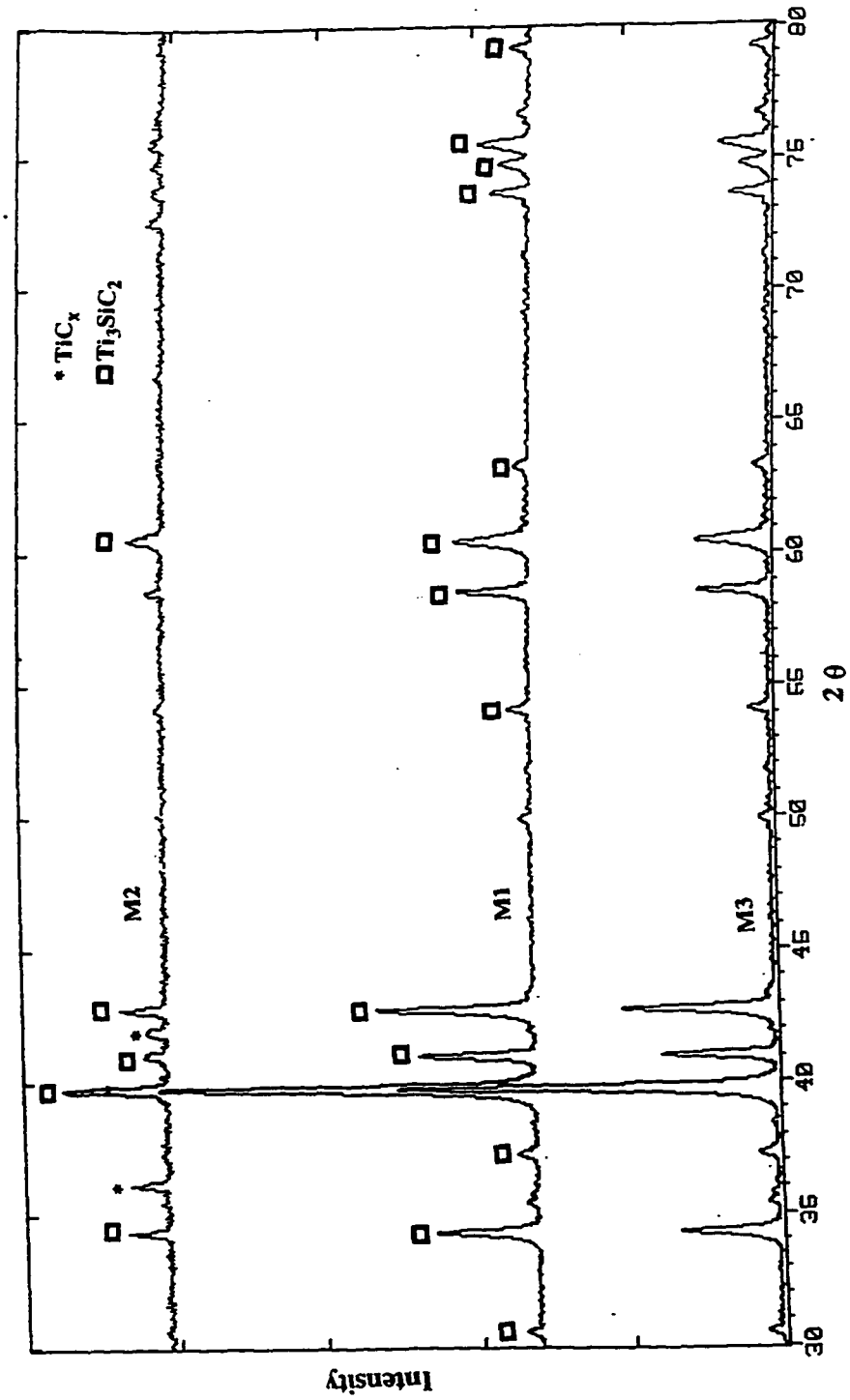

Figure 12 X-ray diffraction patterns of the resulting phases obtained by heating of powder mixtures M1, M2, and M3.

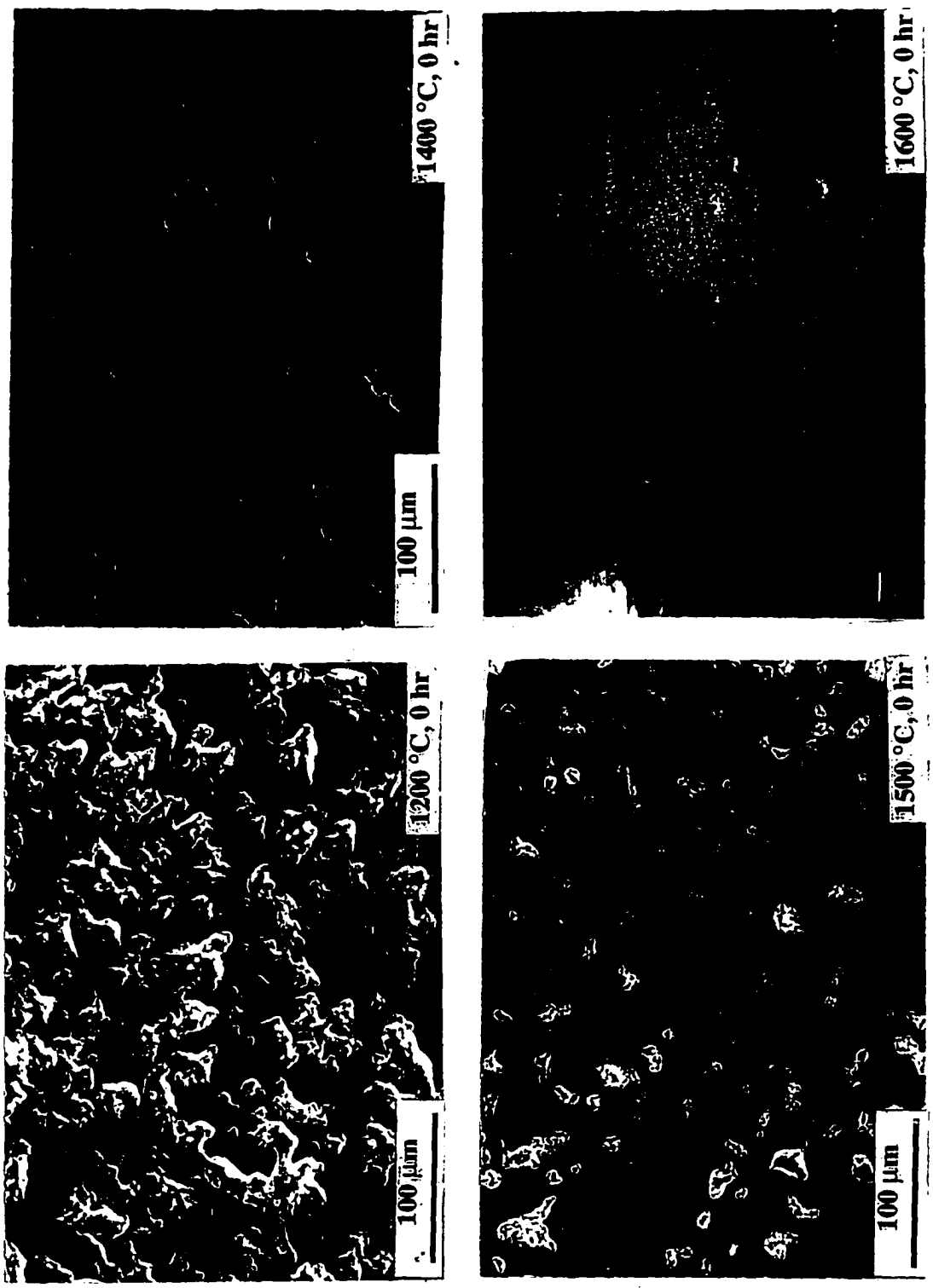

Figure 13. A secondary SEM images at different stages showing the densification progress during the process

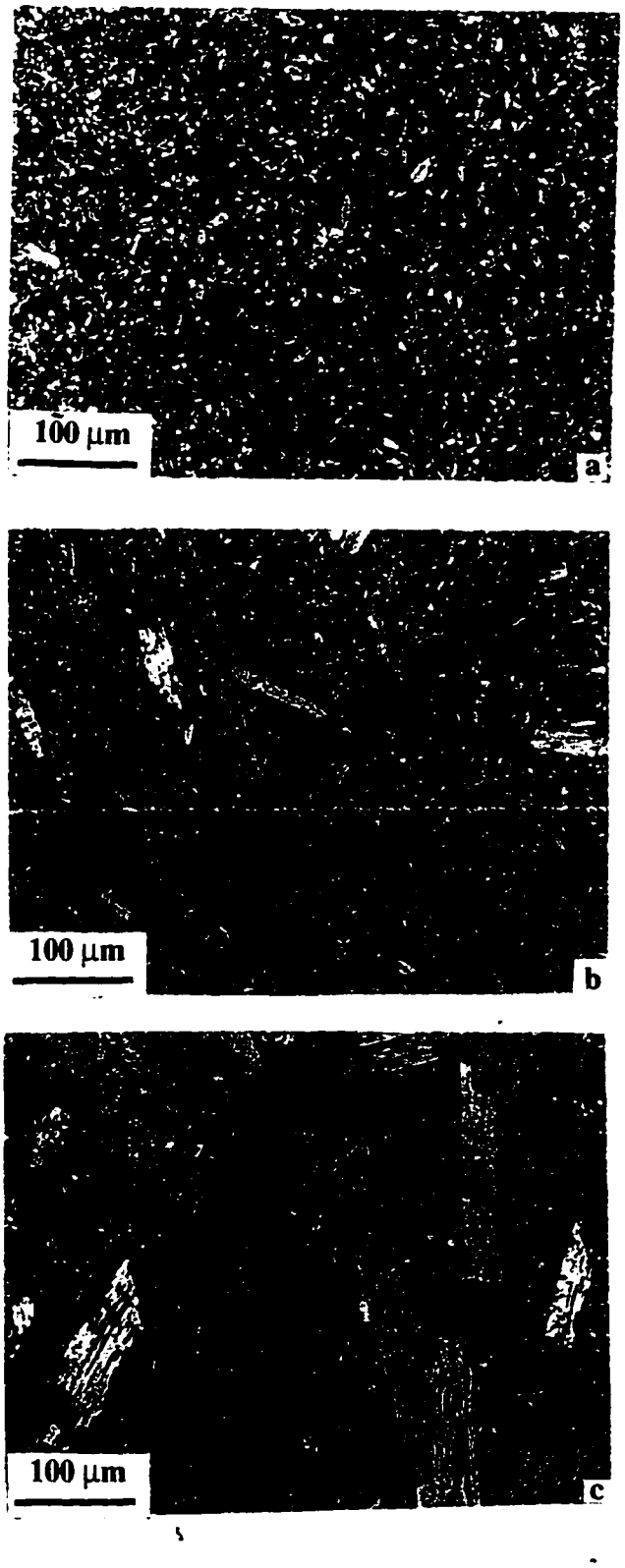

Figure 14. Optical micrographs (unpolarized light) showing the effect of the soaking time at 1450 °C on the microstructure : a) after 8 hr, b)after 16 hr, and c) after 24 hr.

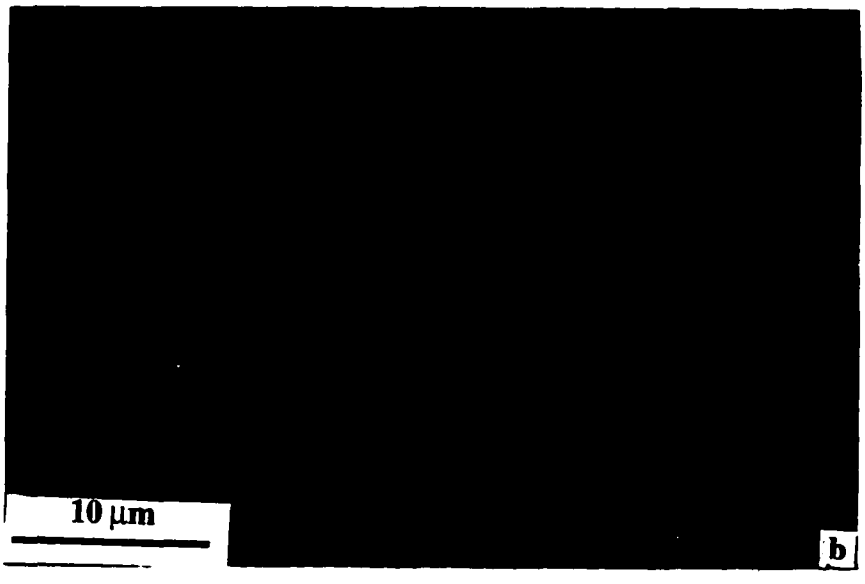

Figure 15. a) wide attacked grain boundaries in the case of fine grained microstructure.
b) Thin grain boundary in the case of coarse grained microstructure.

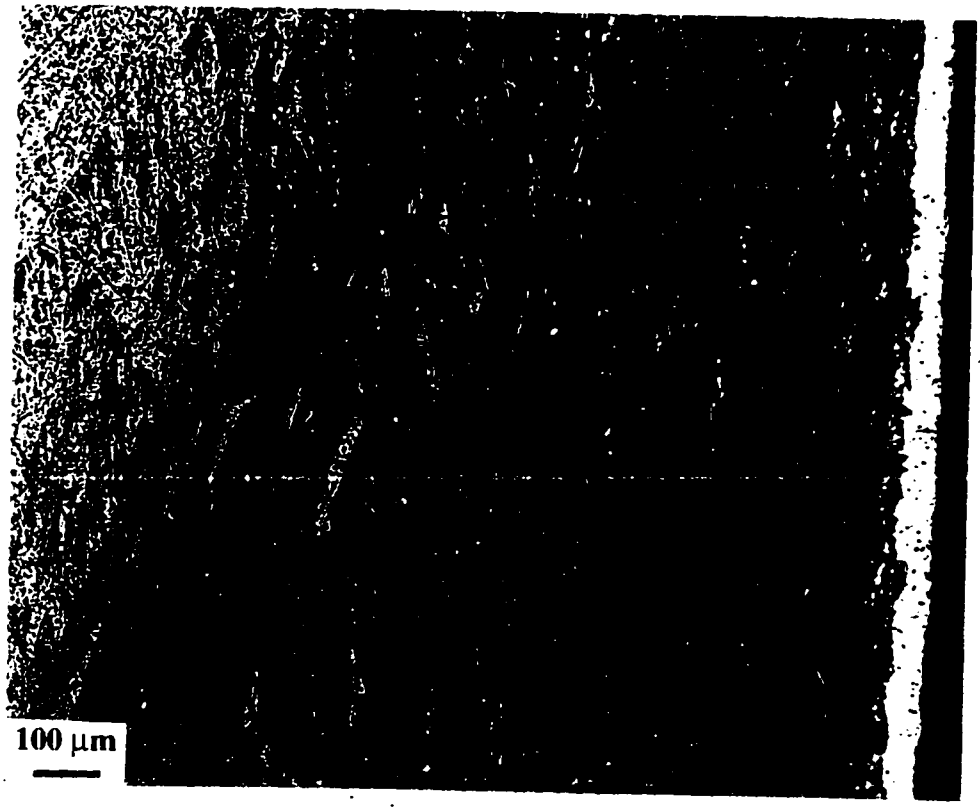

Figure 16. The effect of TiC_x on the inhibition of grain growth.

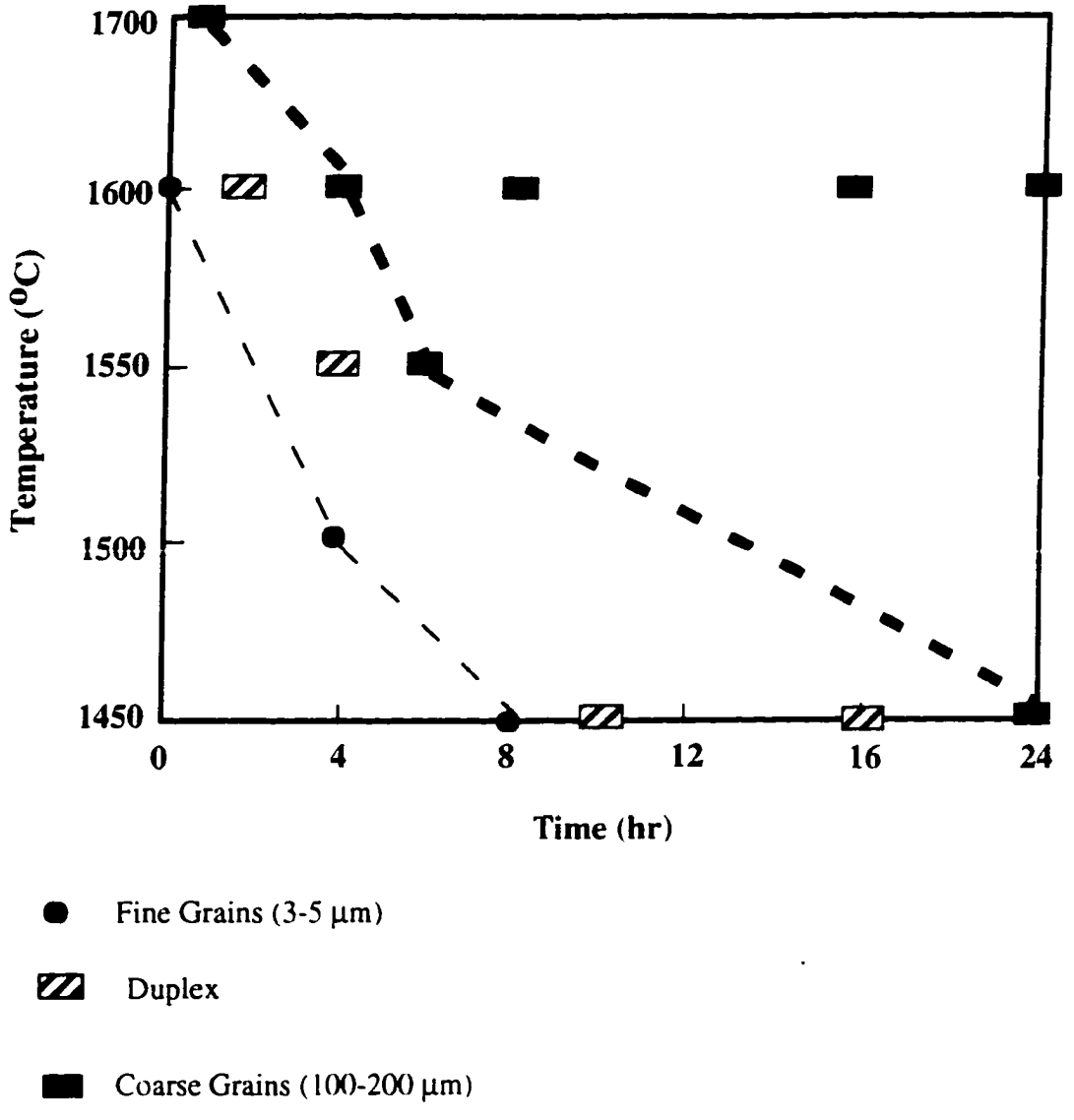

Figure 17. Processing domains that resulted in different microstructures.

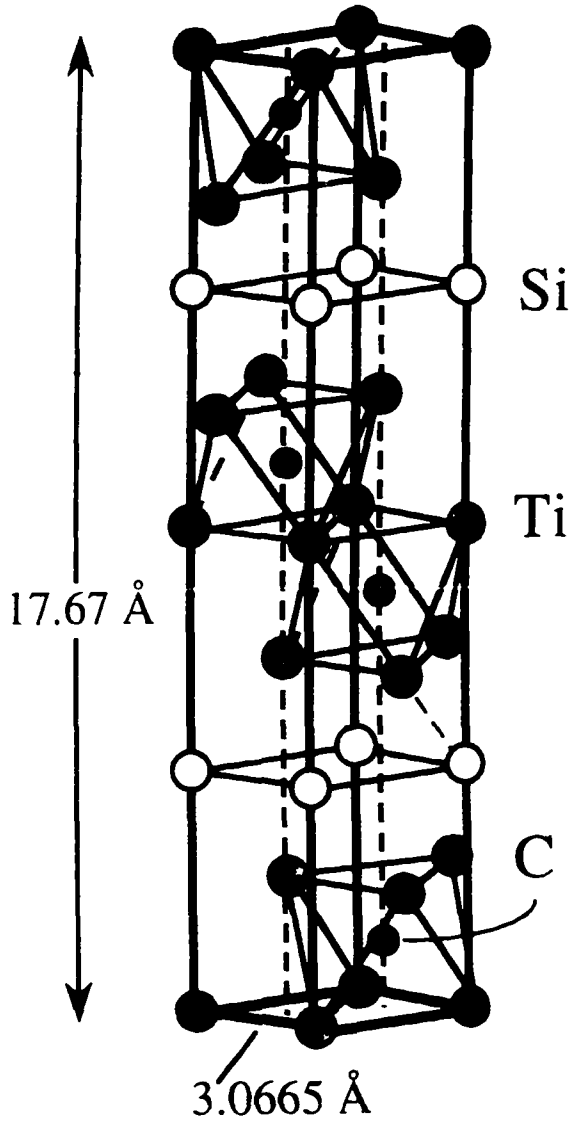

Figure 18. Unit cell of Ti_3SiC_2 according to Ref. [1].

Figure 19. Polished and etched scanning micrograph of as-fabricated Ti_3SiC_2 .

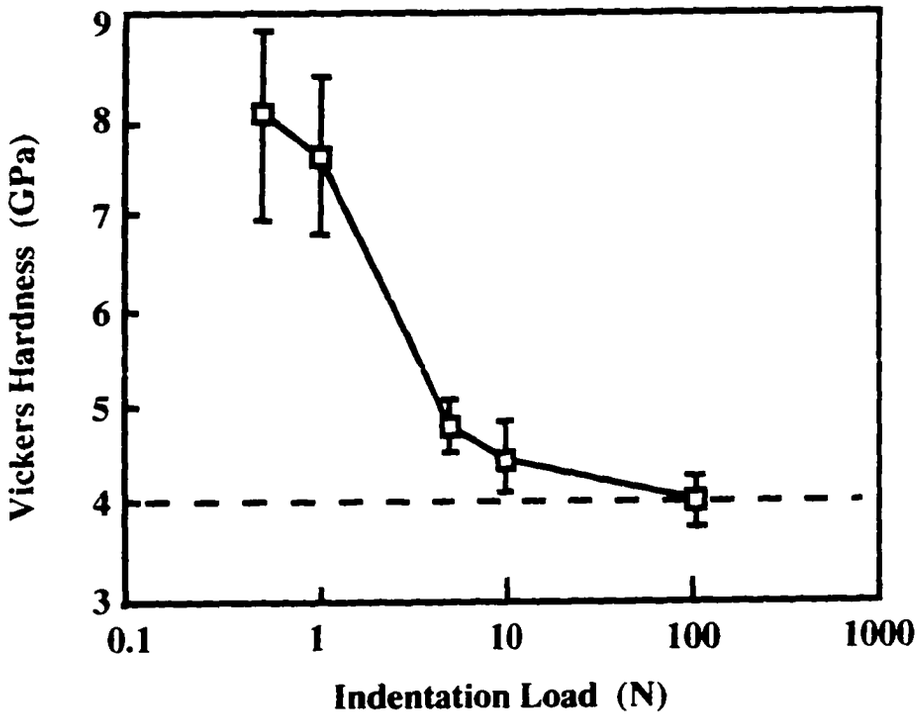

Figure 20. Vickers hardness versus indentation load (N).

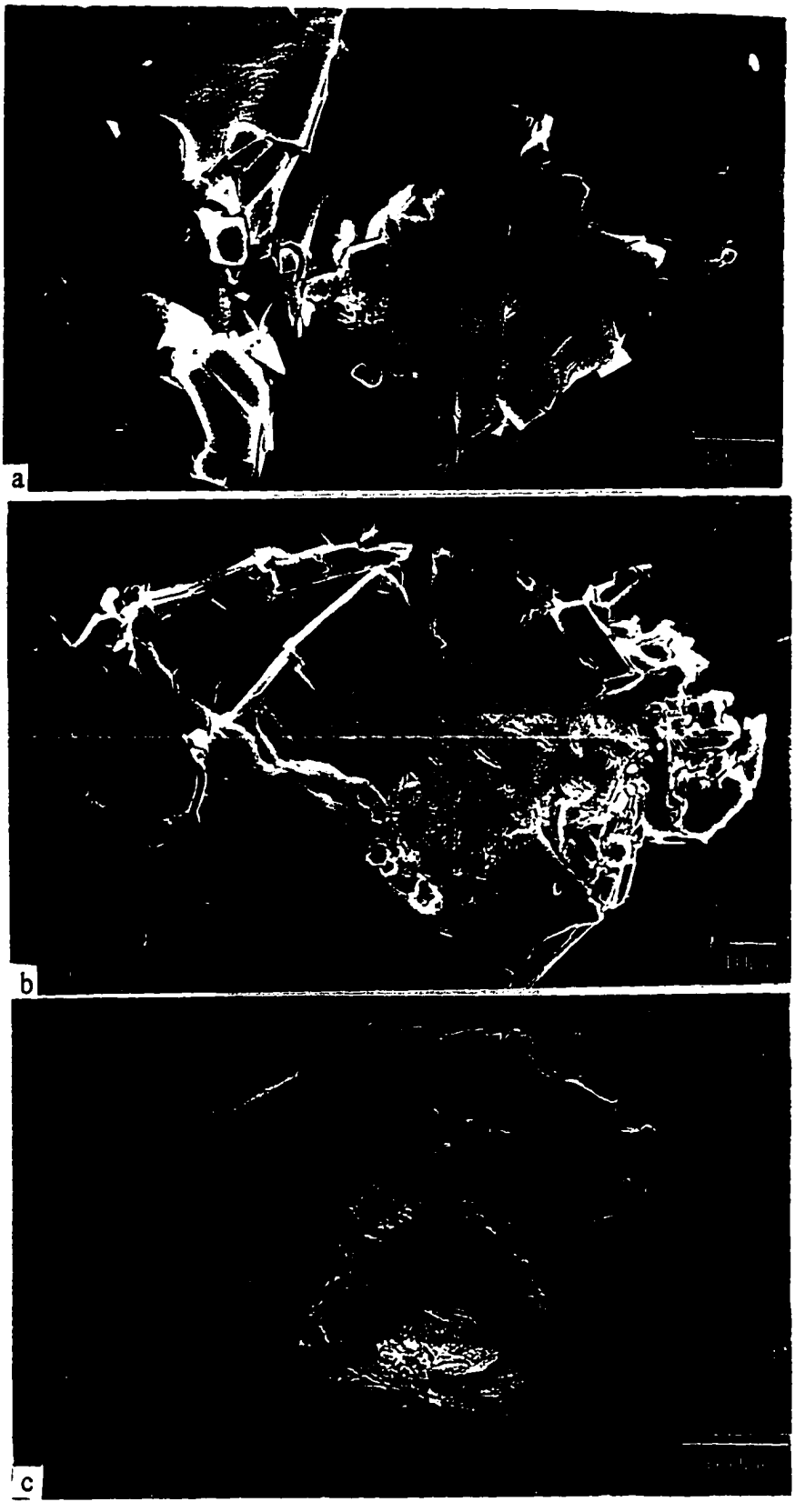

Figure 21. Vickers indentation marks for (a) 3 N, (b) 10 N, (c) 100 N. Each point is the average of at least 10 separate measurements.

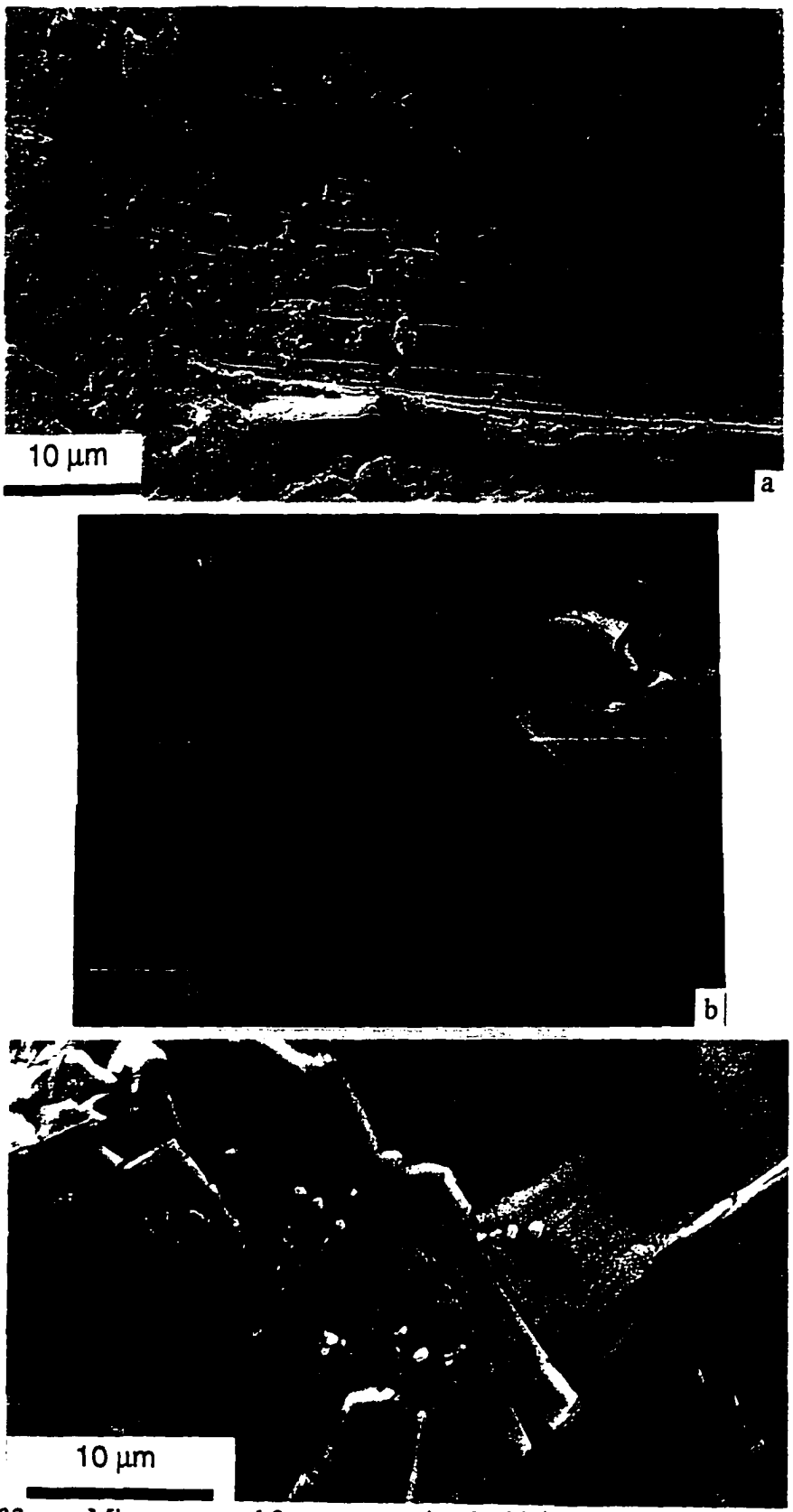

Figure 22. Microstructural features associated with indentation damage; a) laminate fracture, b) grain pullout and deformation, c) grain buckling.

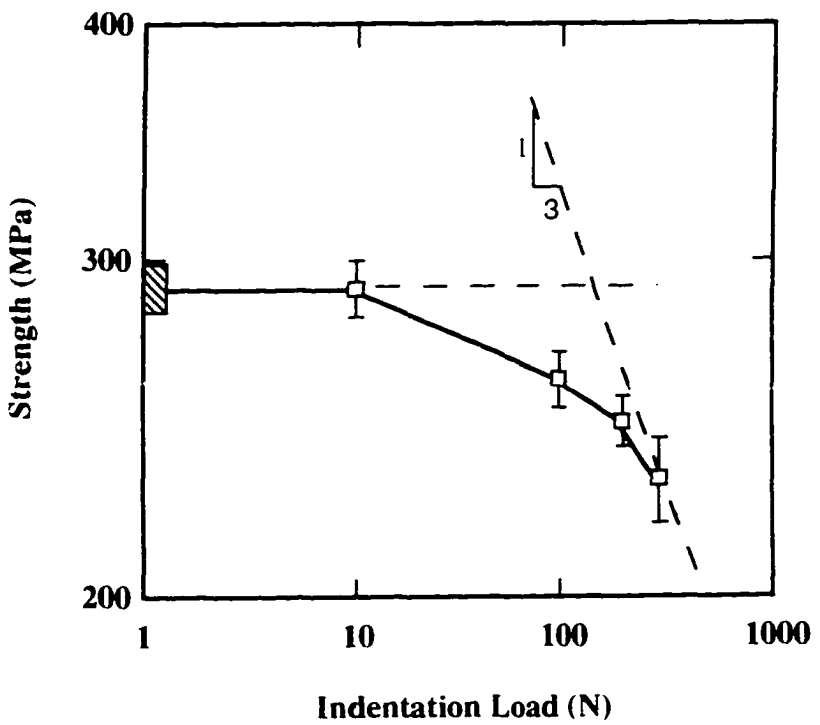

Figure 23. Four-point flexural strength versus indentation loads. Each point represents an average of at least 3 measurements. The inclined dashed line has a slope of - 1/3, which is the expected behavior for a brittle material [17].

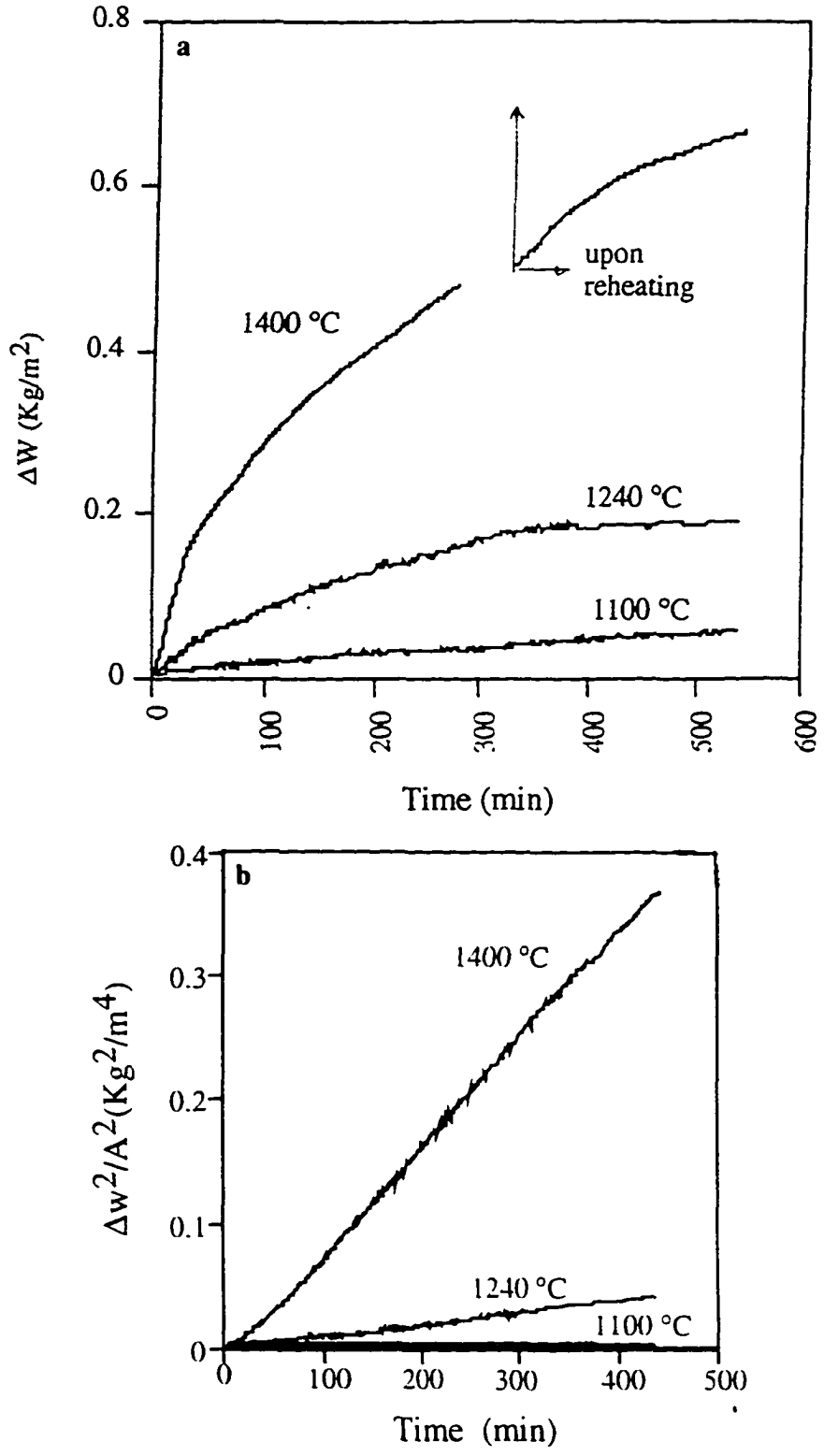

Figure 24. a) Functional dependence of normalized weight gain on time and temperature of oxidation for the M1 samples. b) Same data as in a, but plotted as the square of the normalized weight gain versus time confirming the parabolic nature of the oxidation.

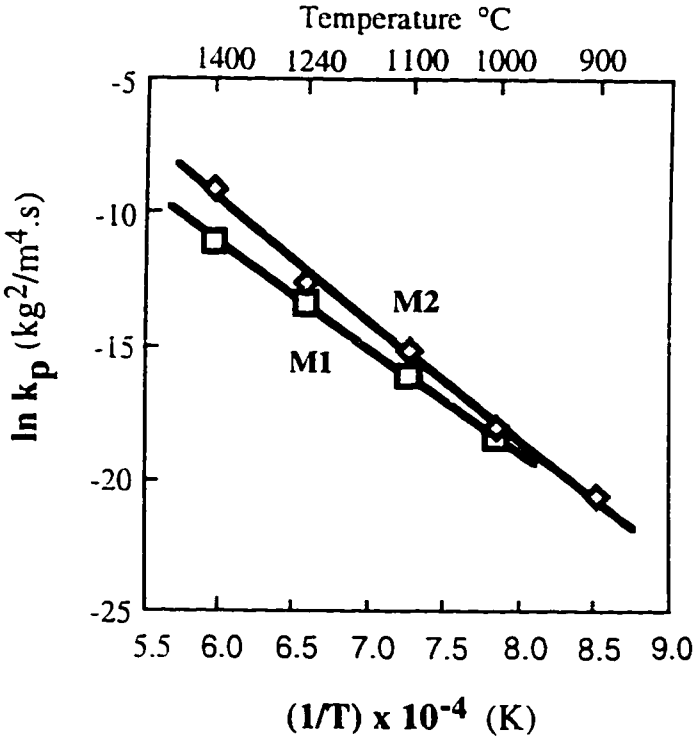

Figure 25. Effect of initial powder purity and processing route on oxidation kinetics at 1240 °C. The hot isostatically pressed samples and those made with the less pure SiC powders had better oxidation resistances than the purer samples or the hot pressed samples.

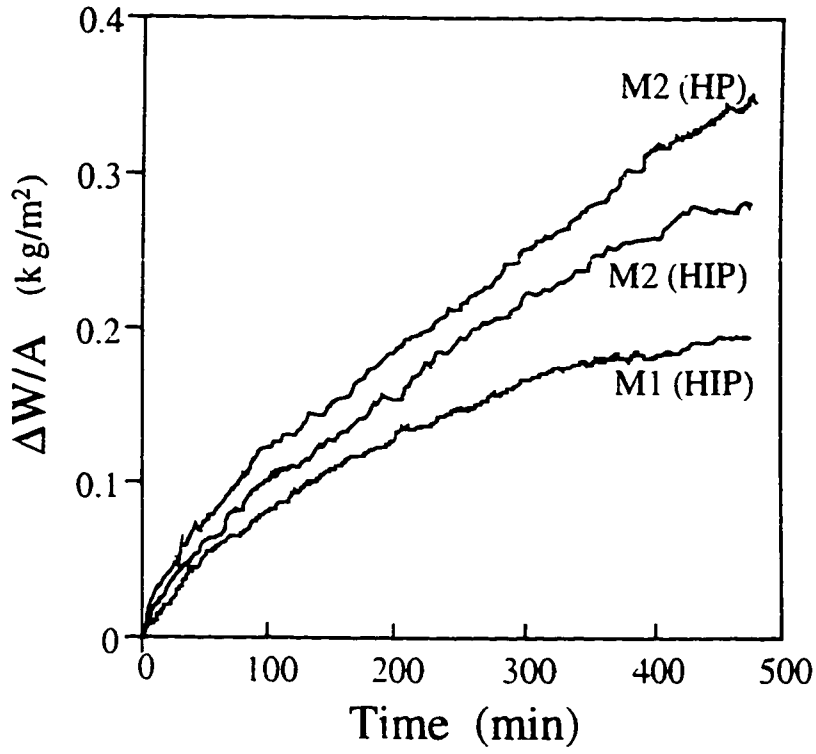

Figure 26. Effect of temperature and purity of initial powders on the parabolic rate constants of Ti_3SiC_2 oxidized in air.

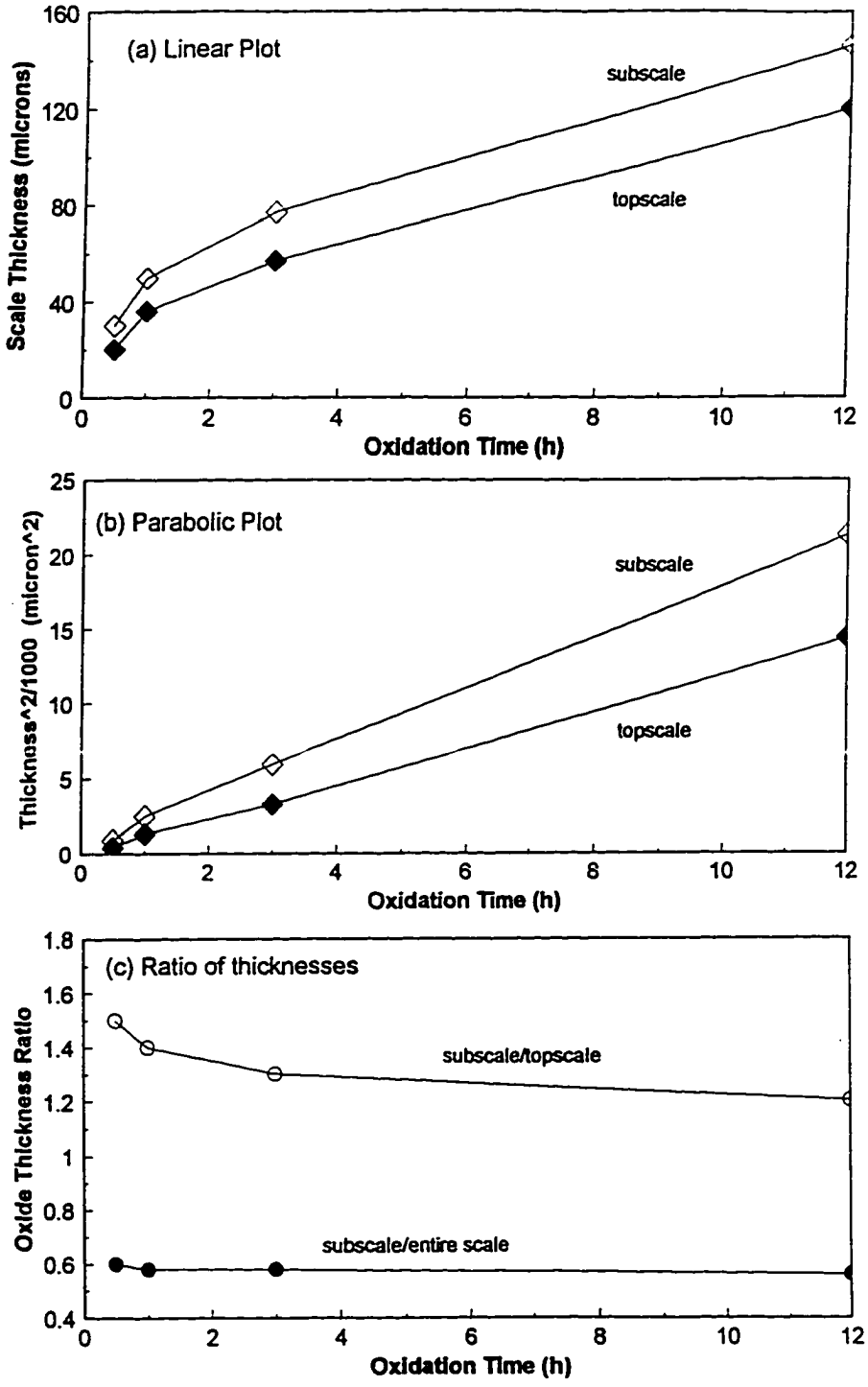

Figure 27. a) Growth rates of oxide sublayers on Ti_3SiC_2 at 1240 °C. b) Same data as a but plotted as the square of the normalized oxide thickness versus time. c) Ratio of subscale to topscale and subscale to entire scale thicknesses. The subscale was always thicker than the top rutile scale.

Figure 28. Morphology of oxide layer that forms after an isothermal anneal of Ti_3SiC_2 samples (M2) for 96 hrs at 900 °C.

Figure 29. Morphology of oxide layer that forms after an isothermal anneal of Ti_3SiC_2 samples (M2) for 96 hrs at 1000 °C.

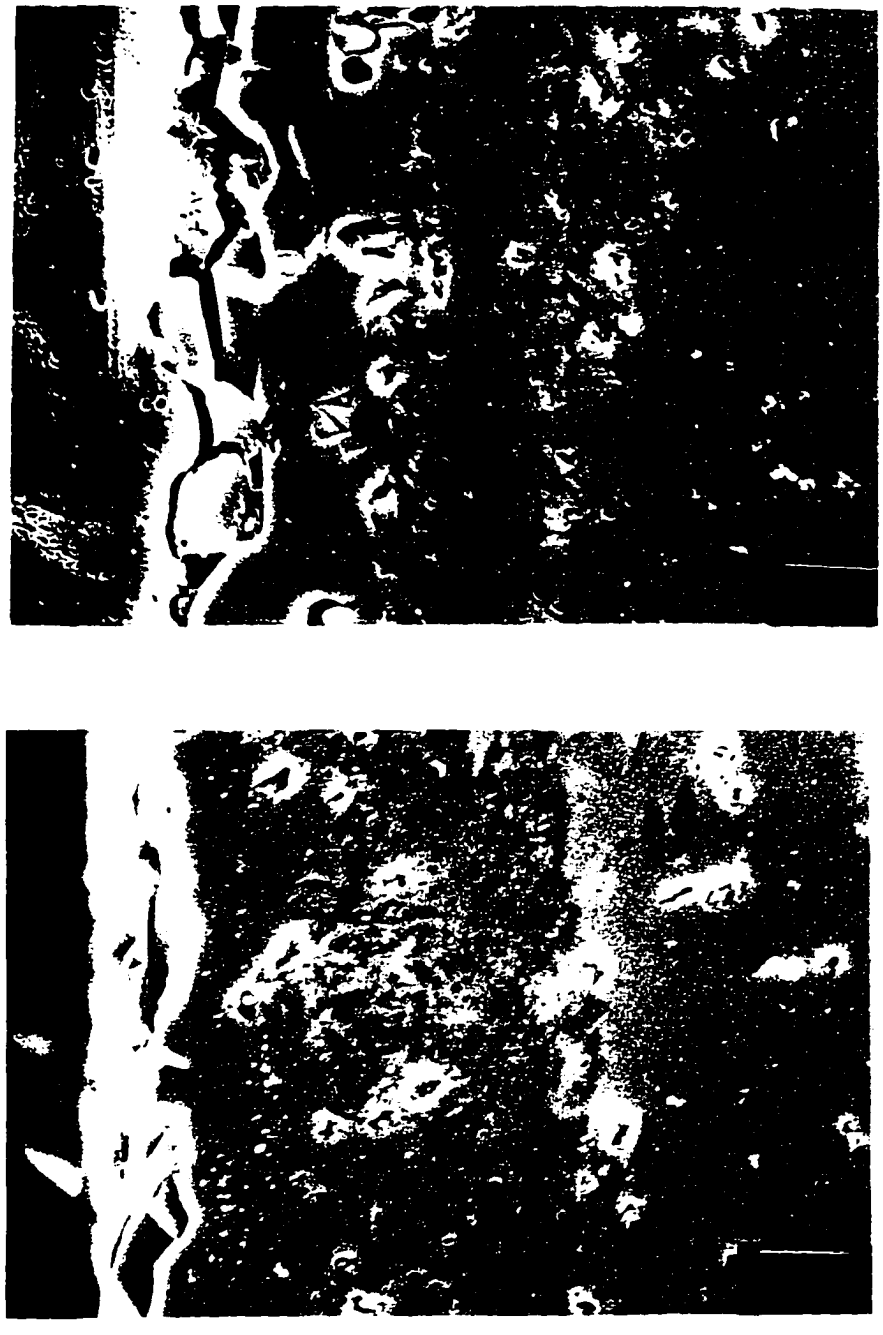

Figure 30. a) Morphology of oxide layer that forms after an isothermal anneal of Ti_3SiC_2 samples (M2) for 12 hrs at 1100 °C. b) Morphology of oxide layer that forms after cycling sample from 1100 °C to room temperature six times. The total time the sample spent at 1100 °C is the same as in a.

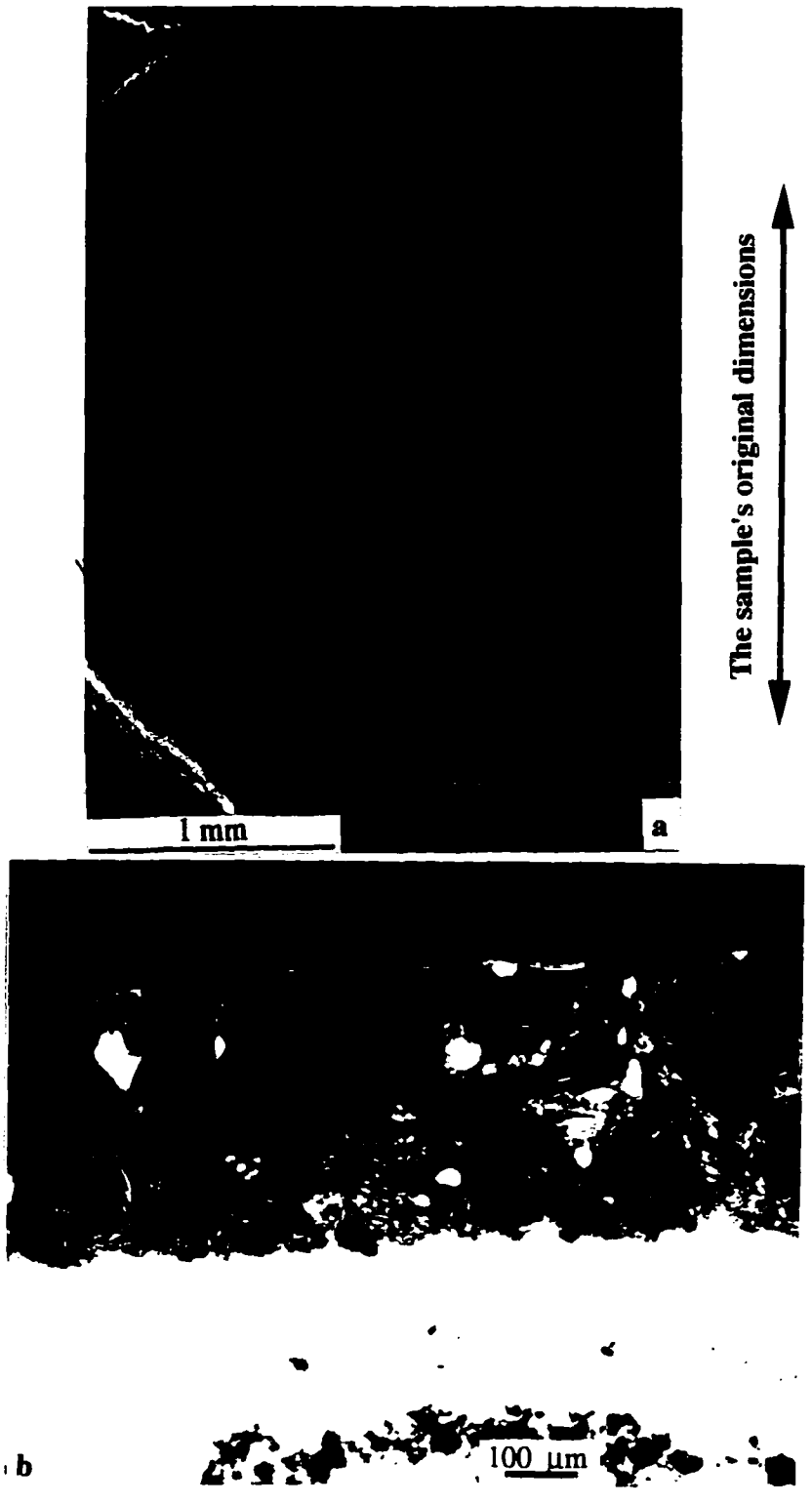

Figure 31. a) Morphology of oxide layer that forms after an isothermal anneal of Ti_3SiC_2 samples (M2) for 12 hrs at 1400 °C. b) Dark-field optical micrograph of oxidation layer at same temperature showing large titania grains in the topscale.

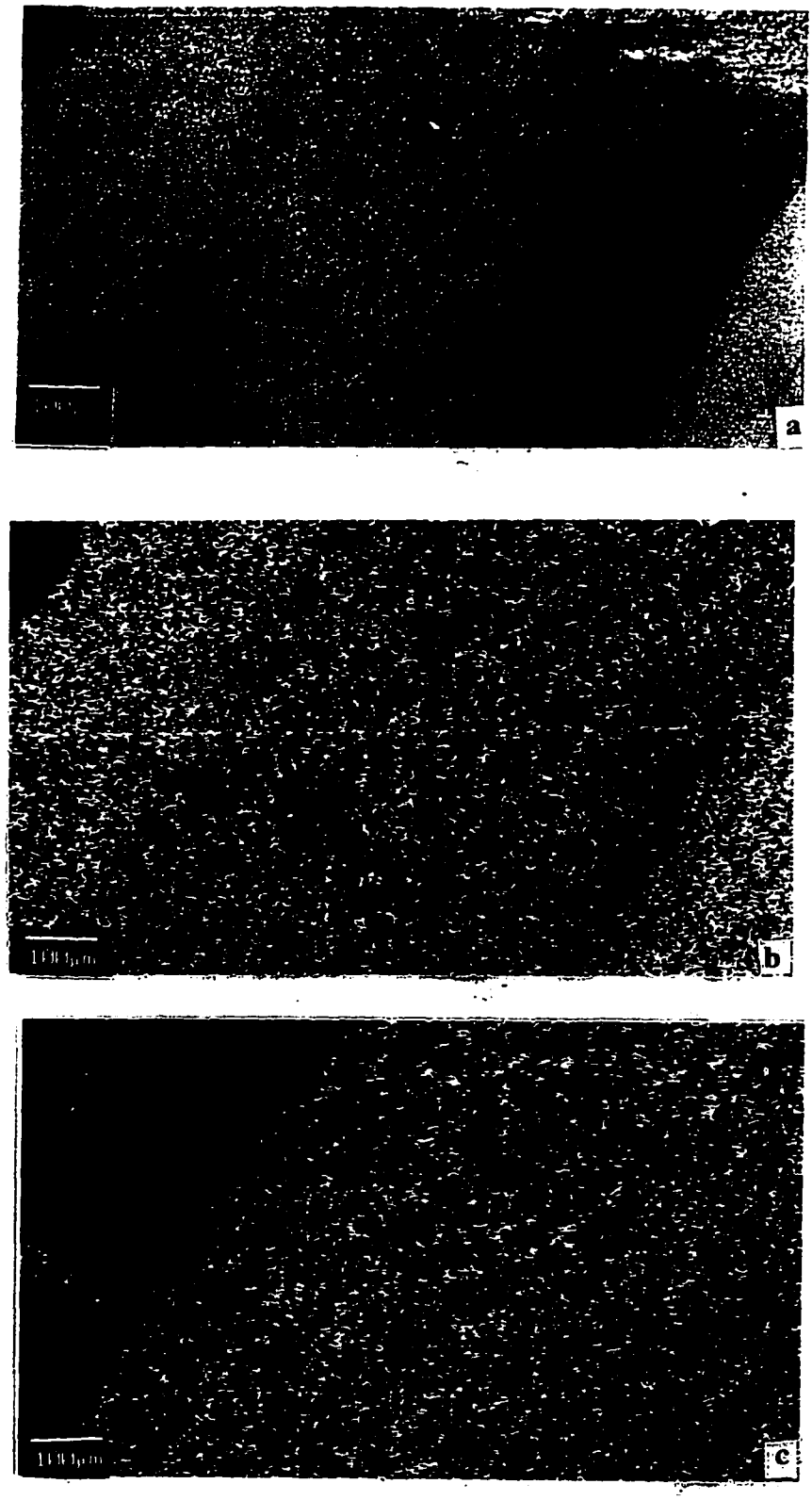

Figure 32.a) Back scattered image of sample oxidized at 1400 °C for 12 hours; b) Ti map of same image; c) Si map of same image

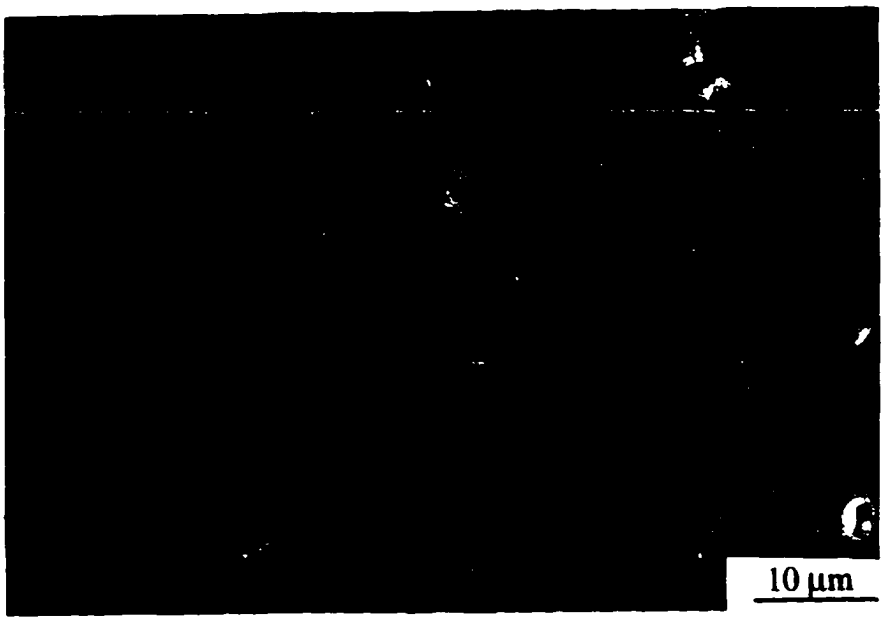

Figure 33. Back scattered SEM of inner scale formed in air for 12 hrs. at 1240 °C. Light areas are titania, gray areas are silica and the darkest areas are pores.

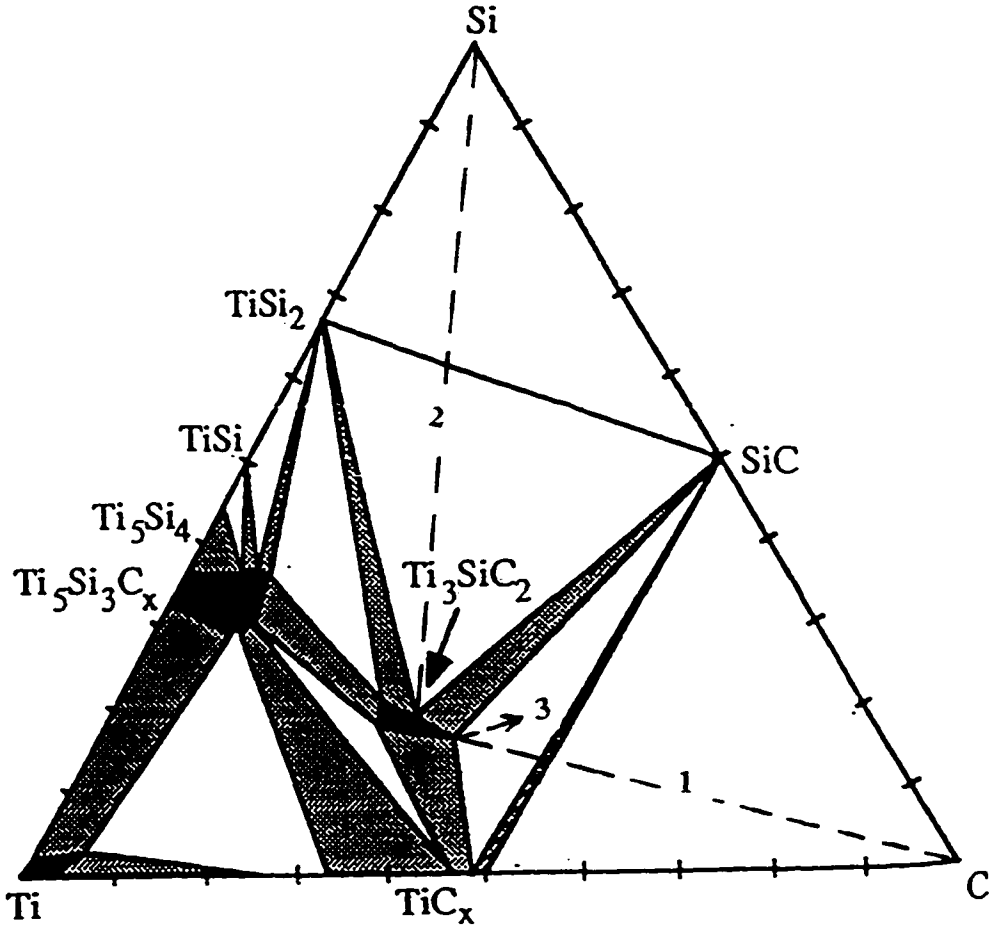

Figure 34. Isothermal section of the ternary system Ti-Si-C at 1200 °C showing the (1) carburization, (2) siliconization, and (3) nitridation paths.

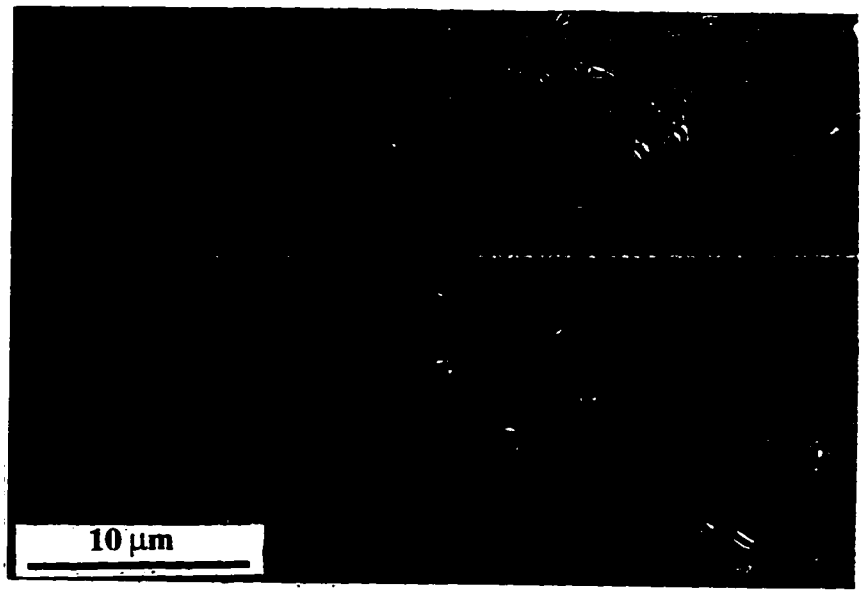

Figure 35. The carburized layer at 1600 °C for 16 hr.

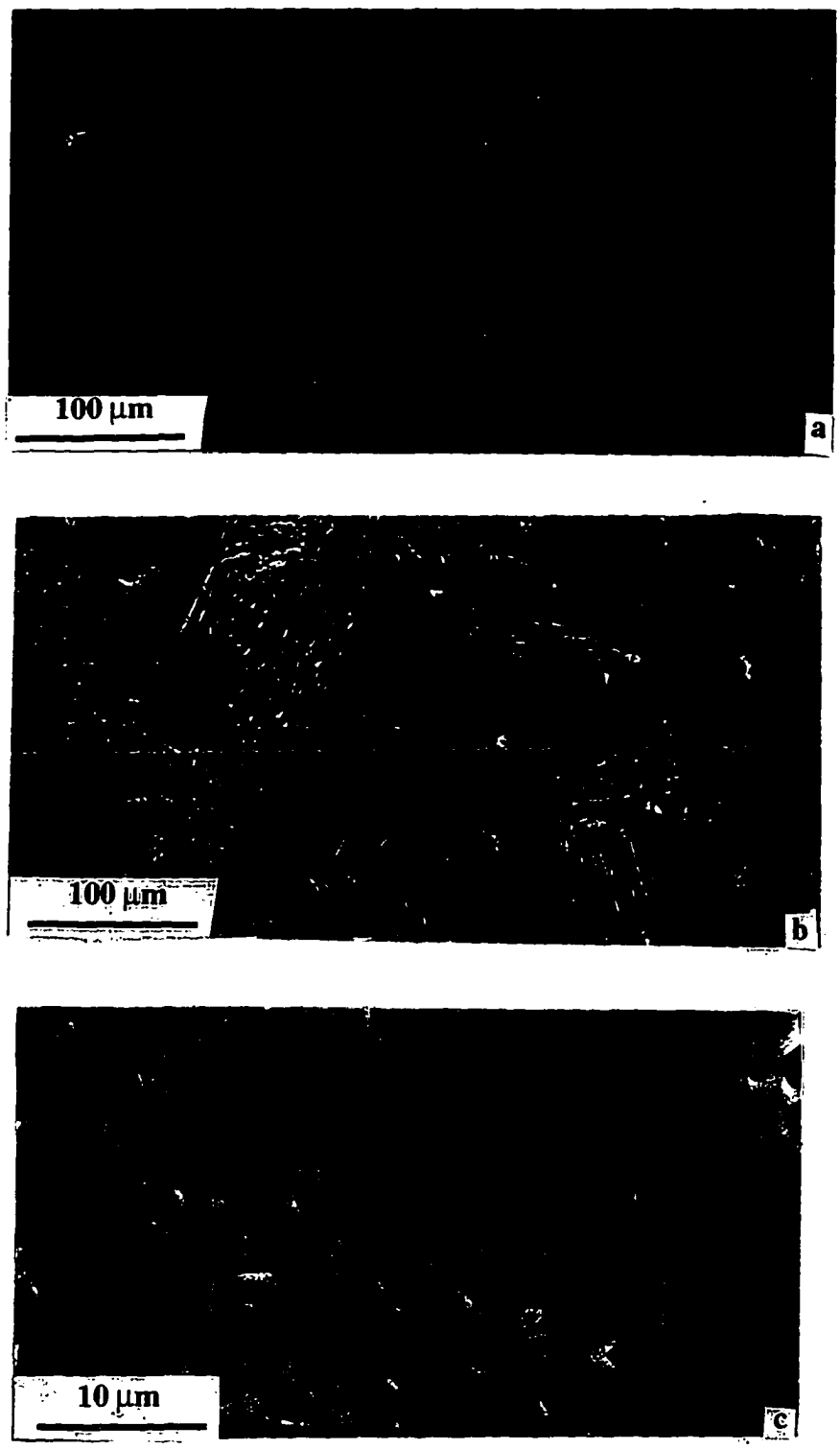

Figure 36. a) A secondary SEM image of an etched microstructure of uncarburized surface.
b) A top view of the carburized layer (as is).
c) A top view of the carburized layer shown in b) at higher magnification.

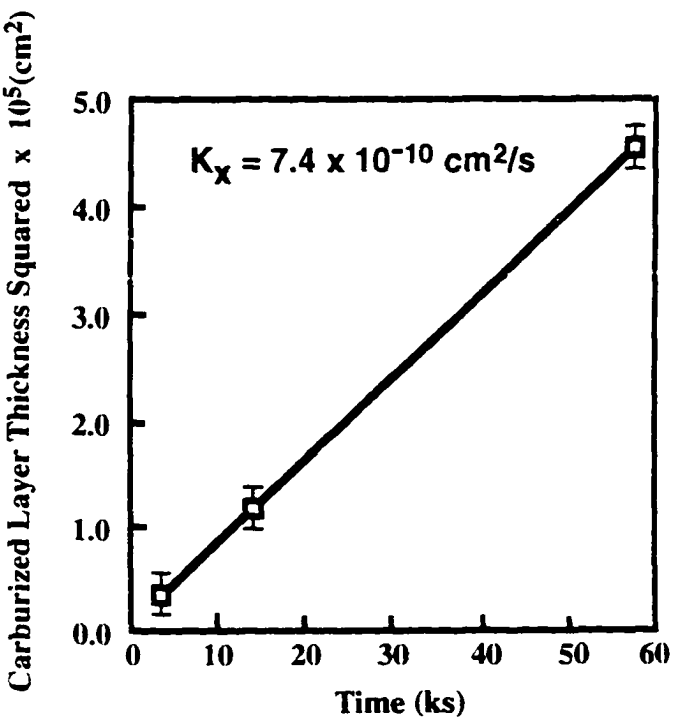

Figure 37. The squared of the carburized layer thickness as a function of carburization time at 1600 °C.

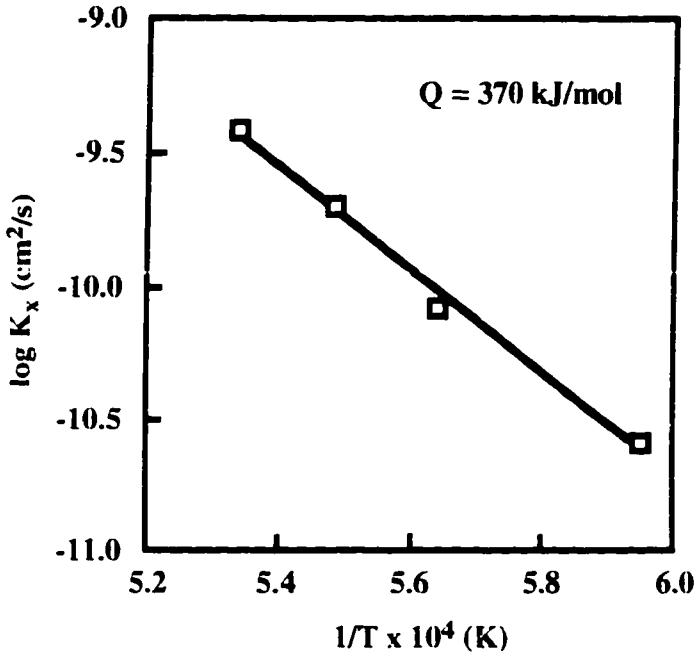

Figure 38. Arhenius plot of the parabolic rate constants for carburization.

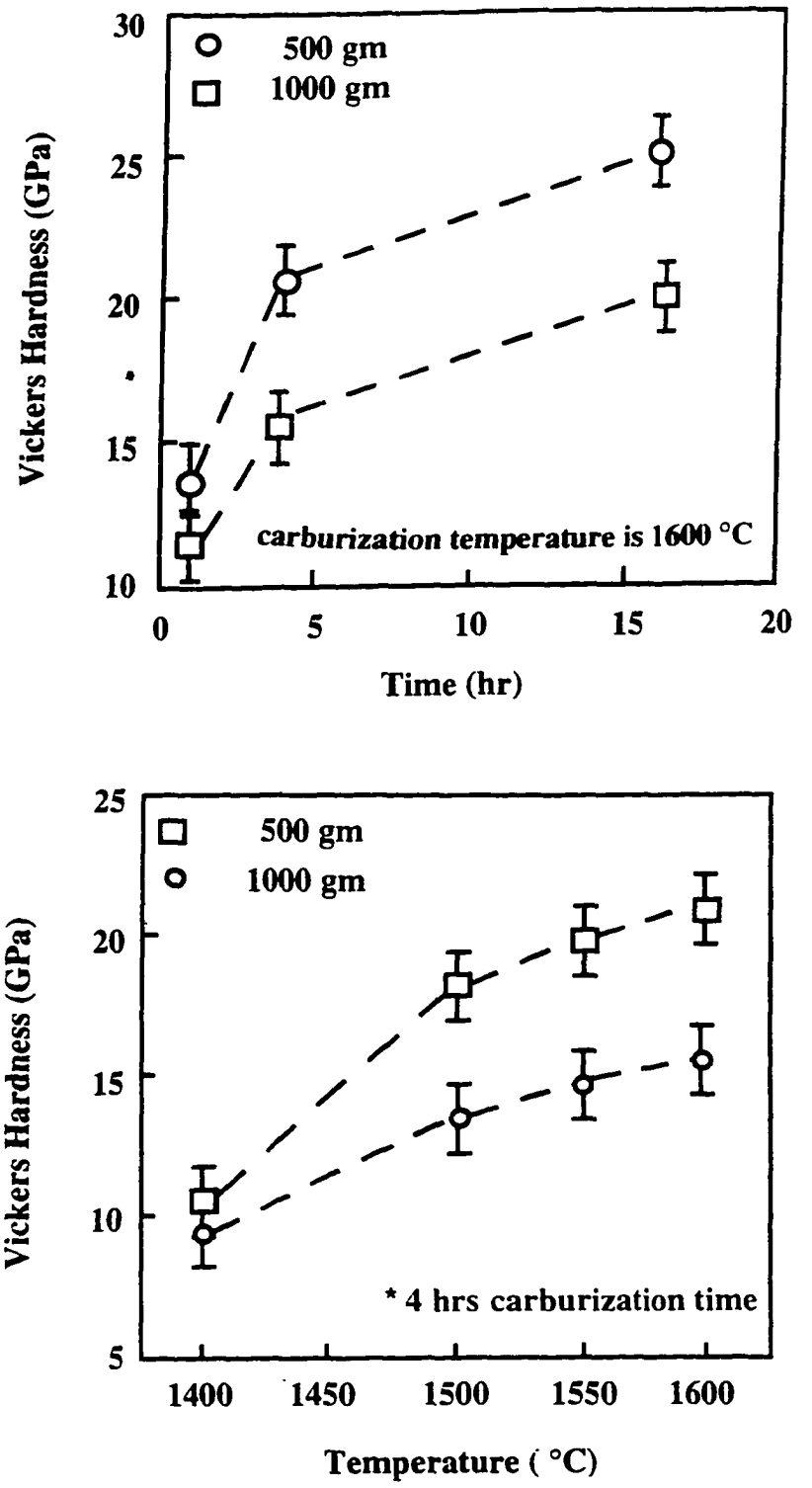

Figure 39. The effect of carburization : a) time and b) temperature on the surface microhardness

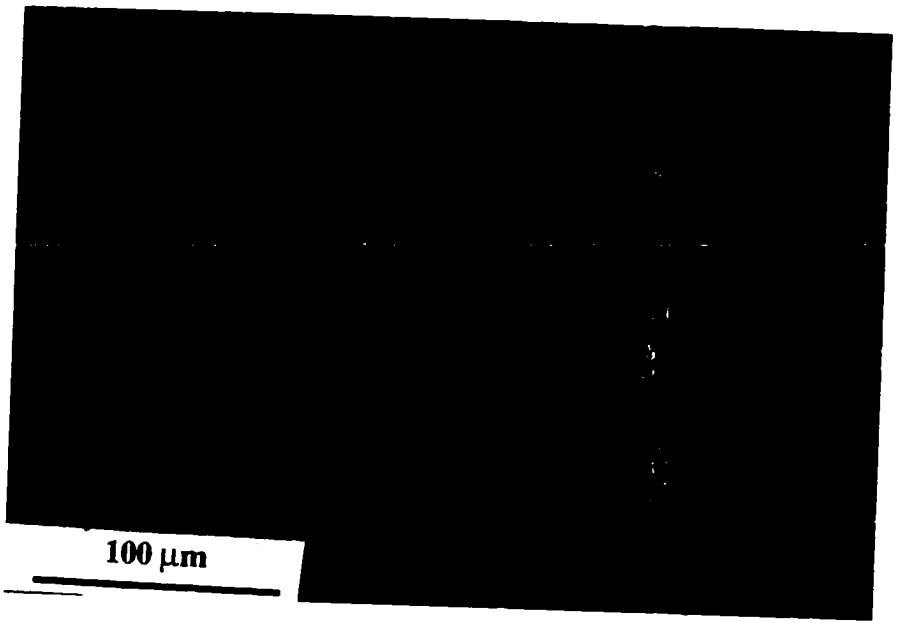

Figure 40. The carburized layer at 1600 °C for 24 hr under a pressure of 40 MPa.

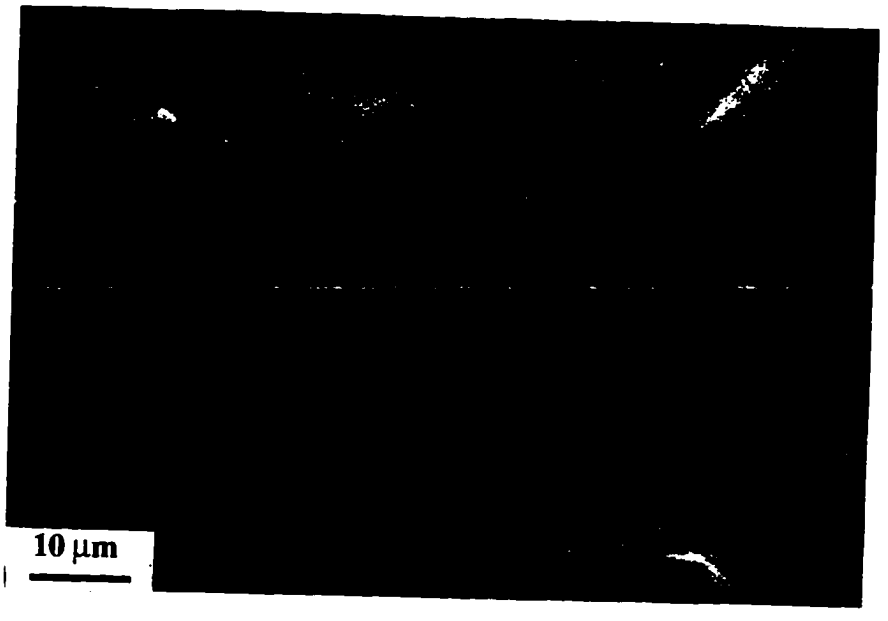

Figure 41. A top view of a siliconized layer (as is).

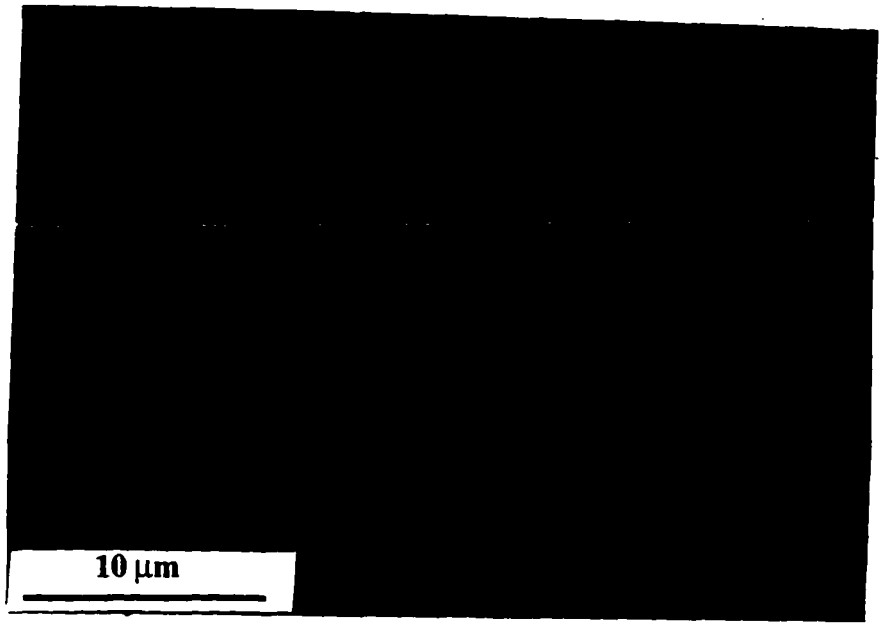

Figure 42. The siliconized layer at 1350 °C for 2 hr.

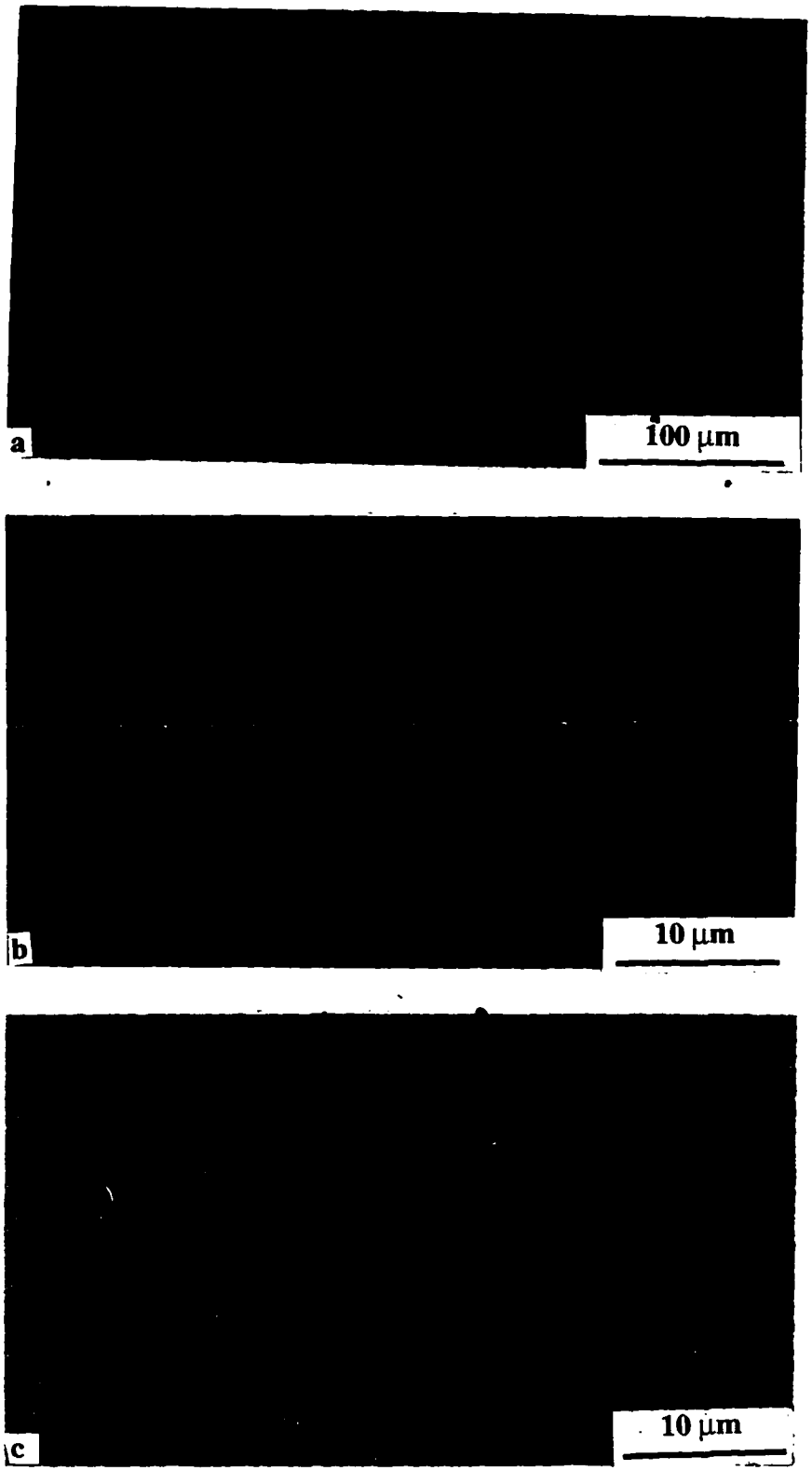

Figure 43. The siliconized layer at 1350 °C for 16 hr: a) total layer, b) inner sublayer, and c) outer sublayer.

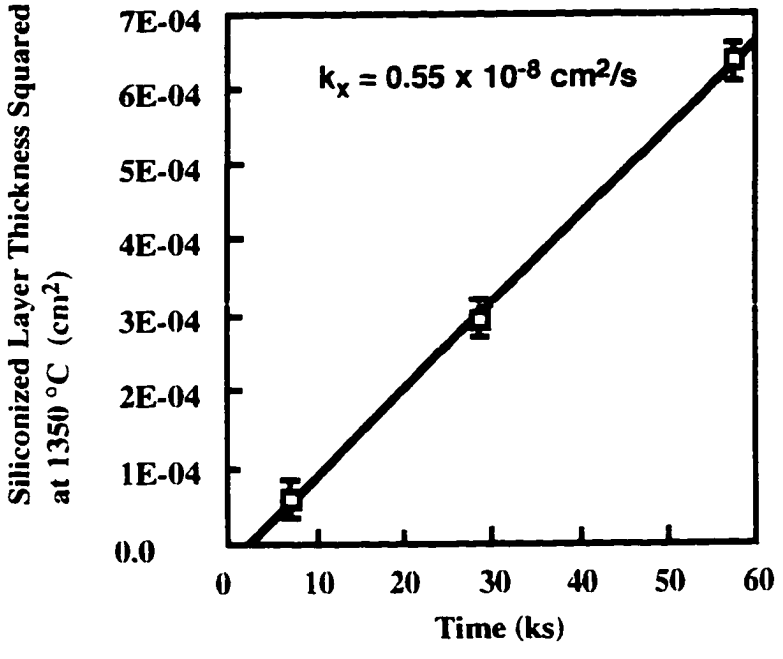

Figure 44. The squared of the siliconized layer thickness as a function of siliconization time at 1350 °C.

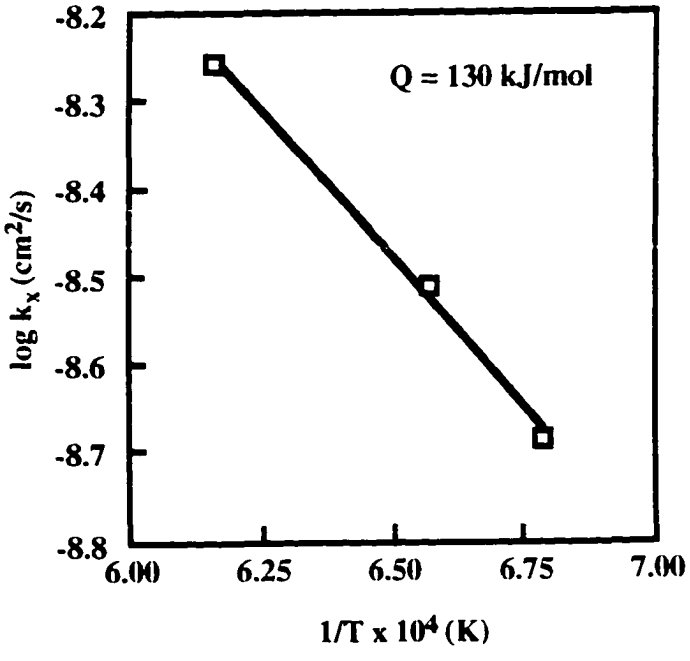

Figure 45. Arhenius plot of the parabolic rate constants for siliconization.

Figure 46. The nitrided layer at 1500 °C for 4 hr.

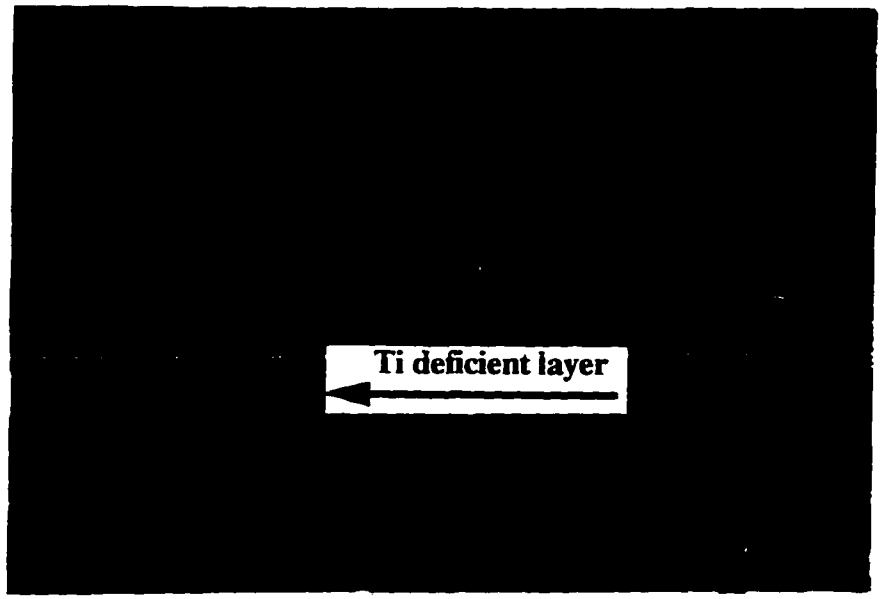

Figure 47. A Ti deficient layer around a grain in the subnitrided layer.

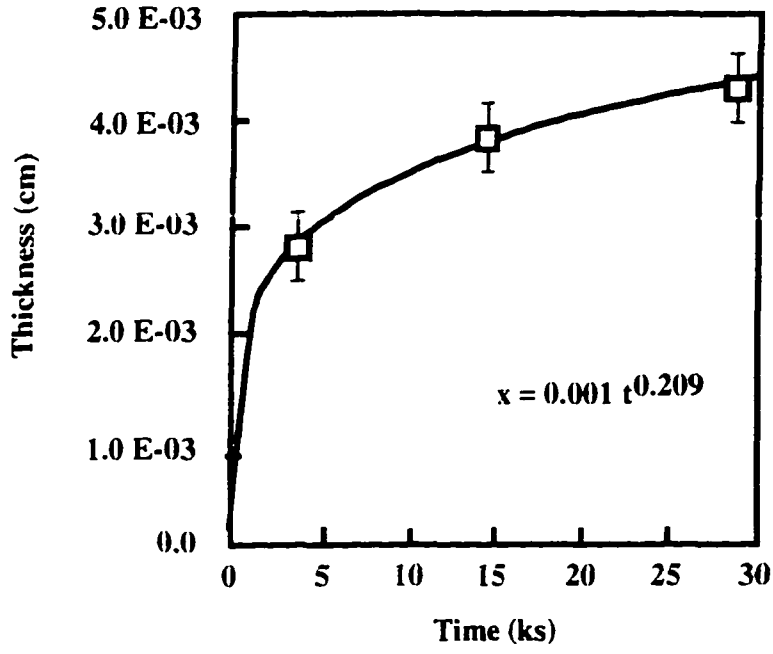

Figure 48. The effect of time on the nitrided layer thickness at 1400 °C.

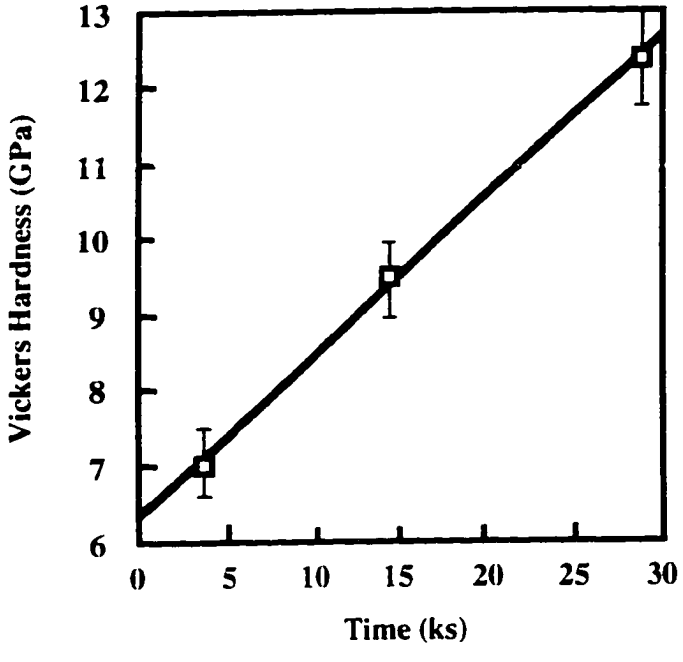

Figure 49. The effect of nitridation time at 1400 °C on the surface microhardness.

Figure 50. Optical micrographs (unpolarized light) of : a) Fine grained microstructure, and b) Coarse grained microstructure.

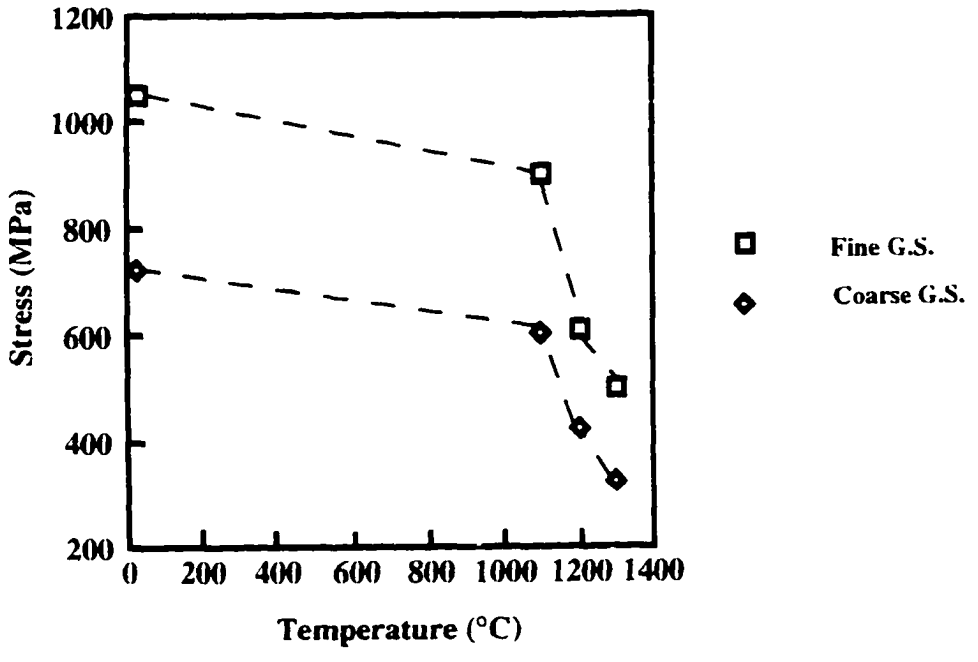

Figure 51. The functional dependence of the compressive strength on grain size and temperature.

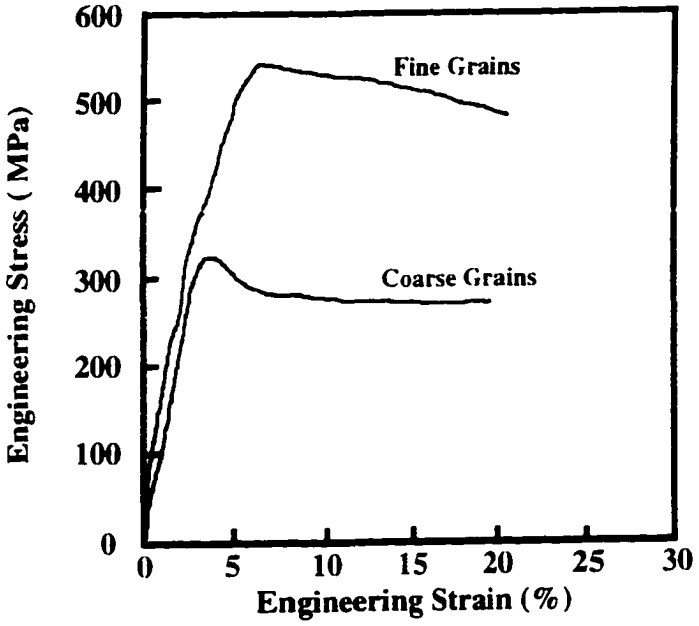

Figure 52. The engineering stress-strain curves at 1300 °C for the fine and coarse grained materials.

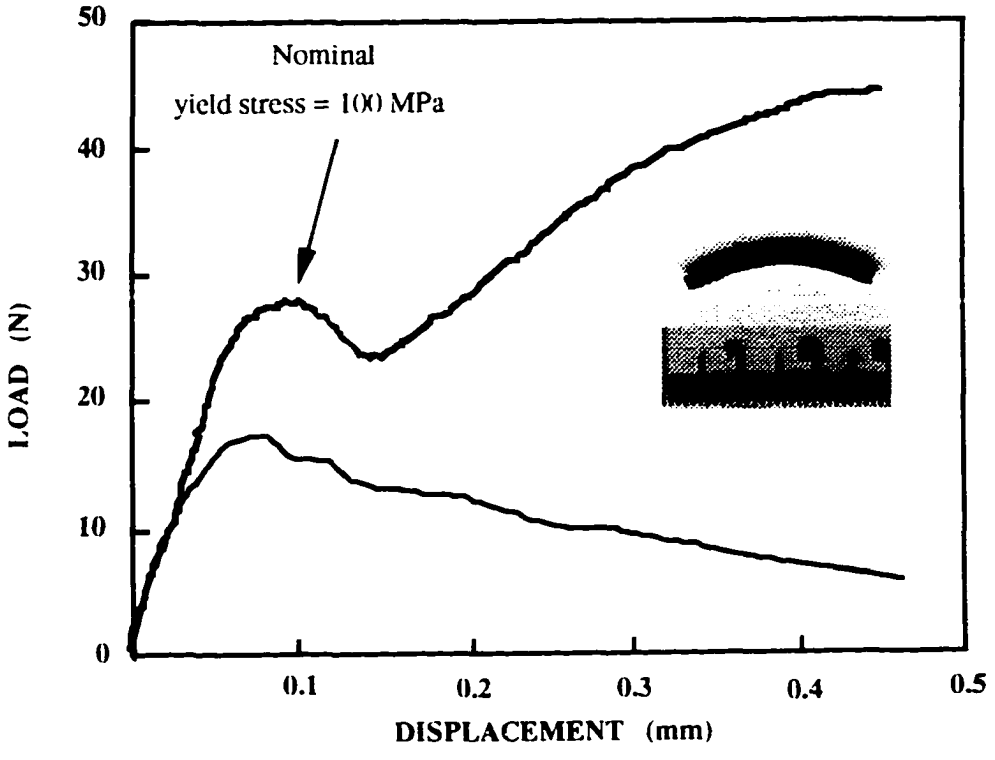

Figure 53. Load-displacement curves (effect of purity) and a bent sample (M1).

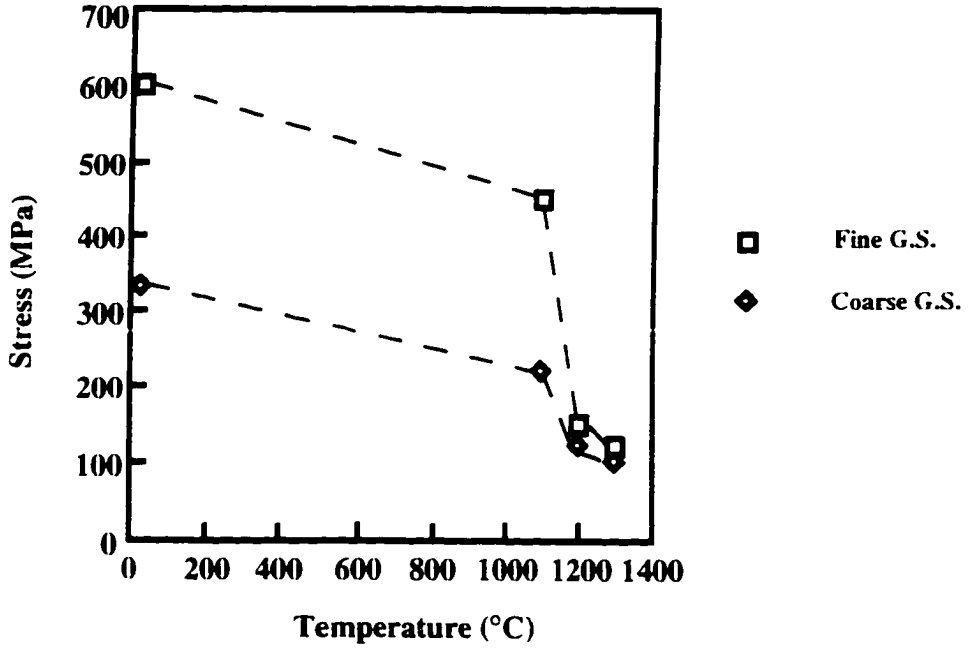

Figure 54. The effect of grain size on the four-point-bending strength as a function of temperature.

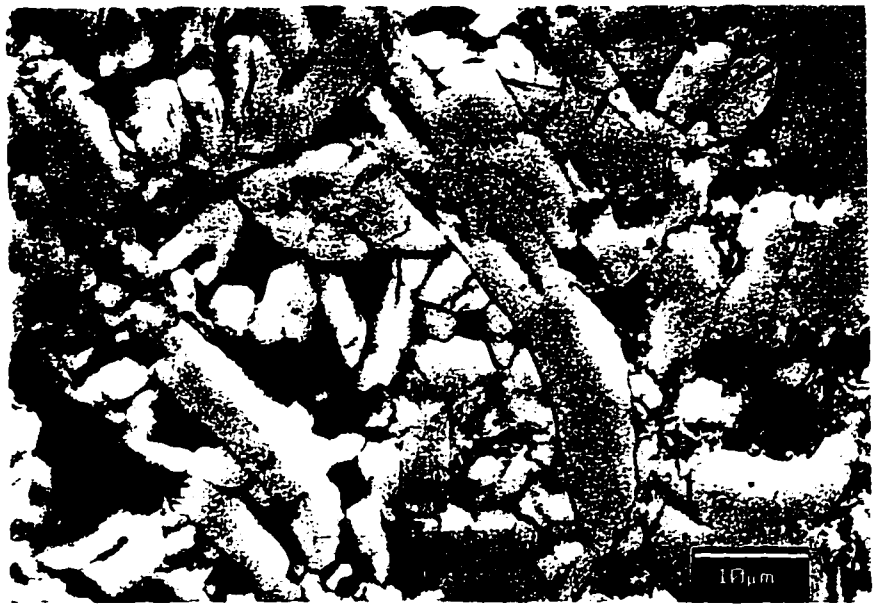

Figure 55. Optical micrograph of the deformed sample (the coarse grained one shown in Fig. 52) showing a) grains buckling and b) grain bending and break-up.

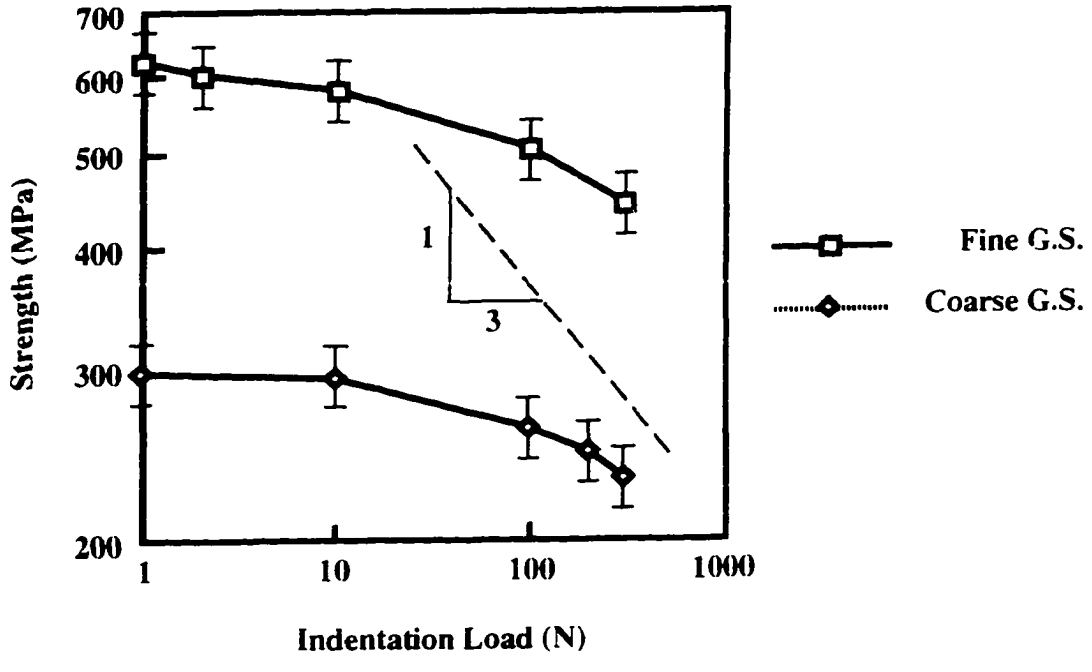

Figure 56. The retained flexural strength as a function of the indentation load.

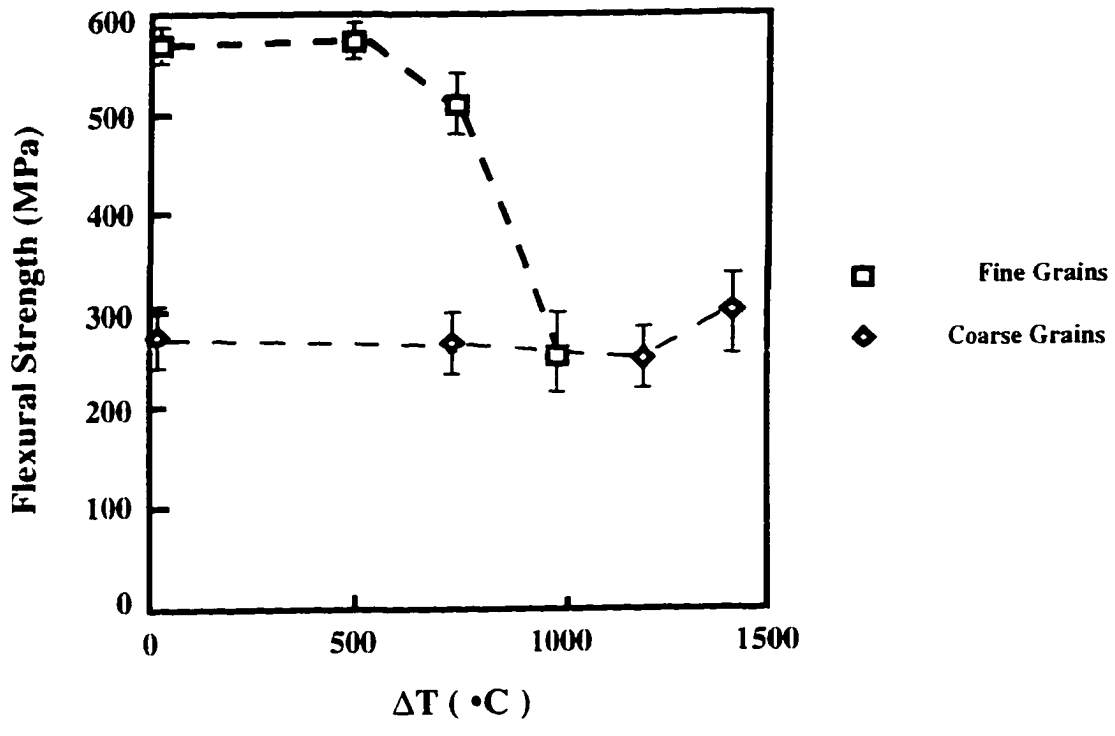

Figure 57. The effect of grain size on the retained flexural strength as a function of quenching temperature.

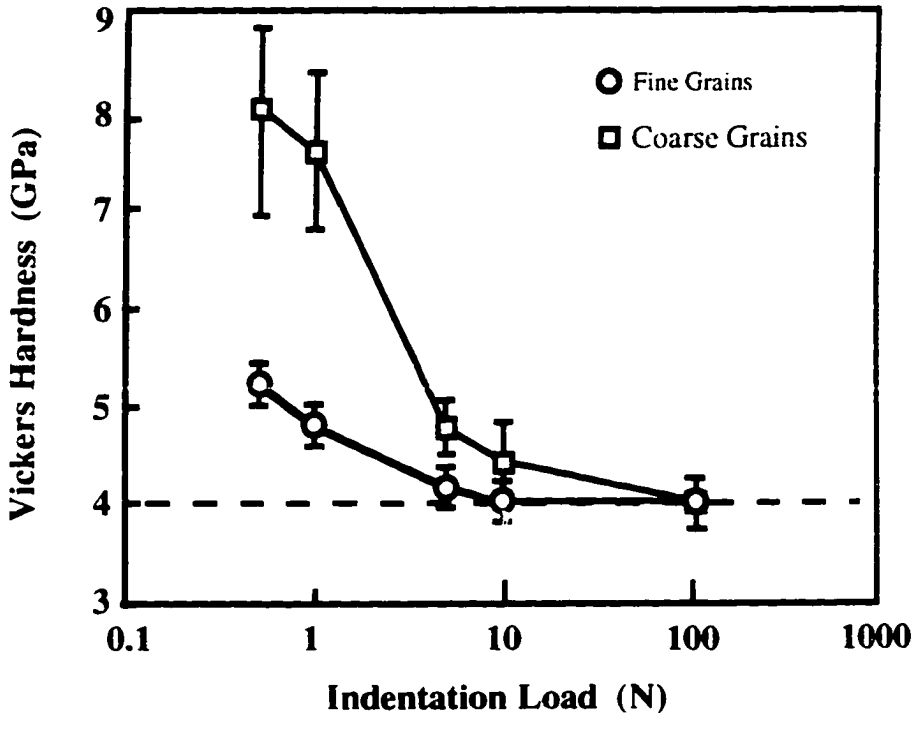

Figure 58. The effect of grain size on the Vickers hardness as a function of the applied load.

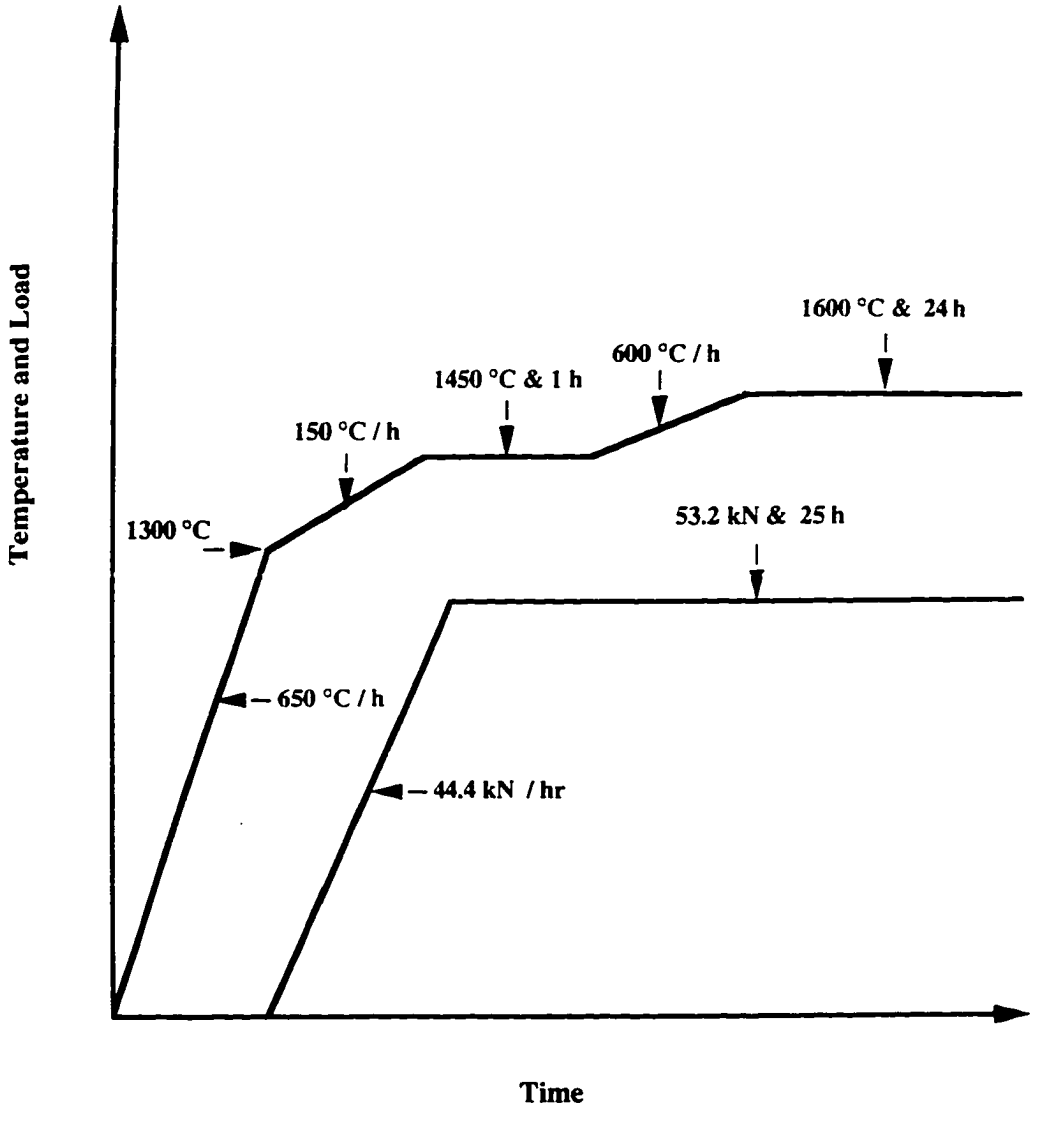

Figure 59. The heating and loading protocols that were followed in the processing of the oriented grains.

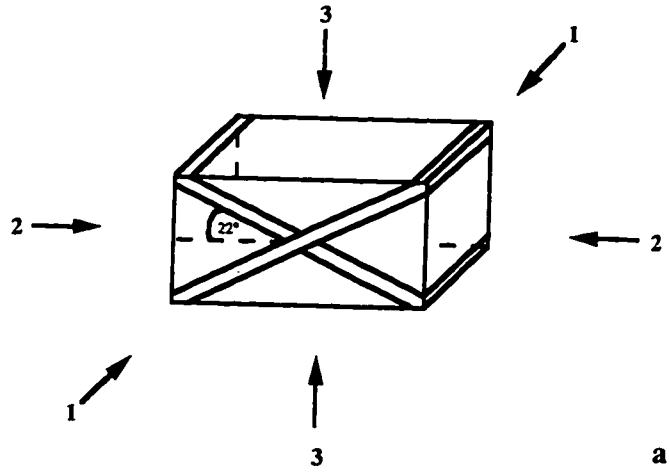

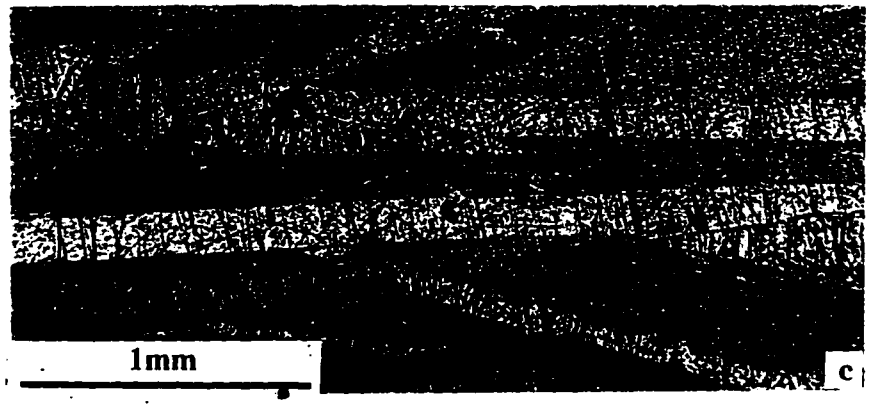

Figure 60. a) Schematic diagram shows the directions of the grains and the different planes. b) Micrograph of plane 23. c) Micrograph of plane 13.

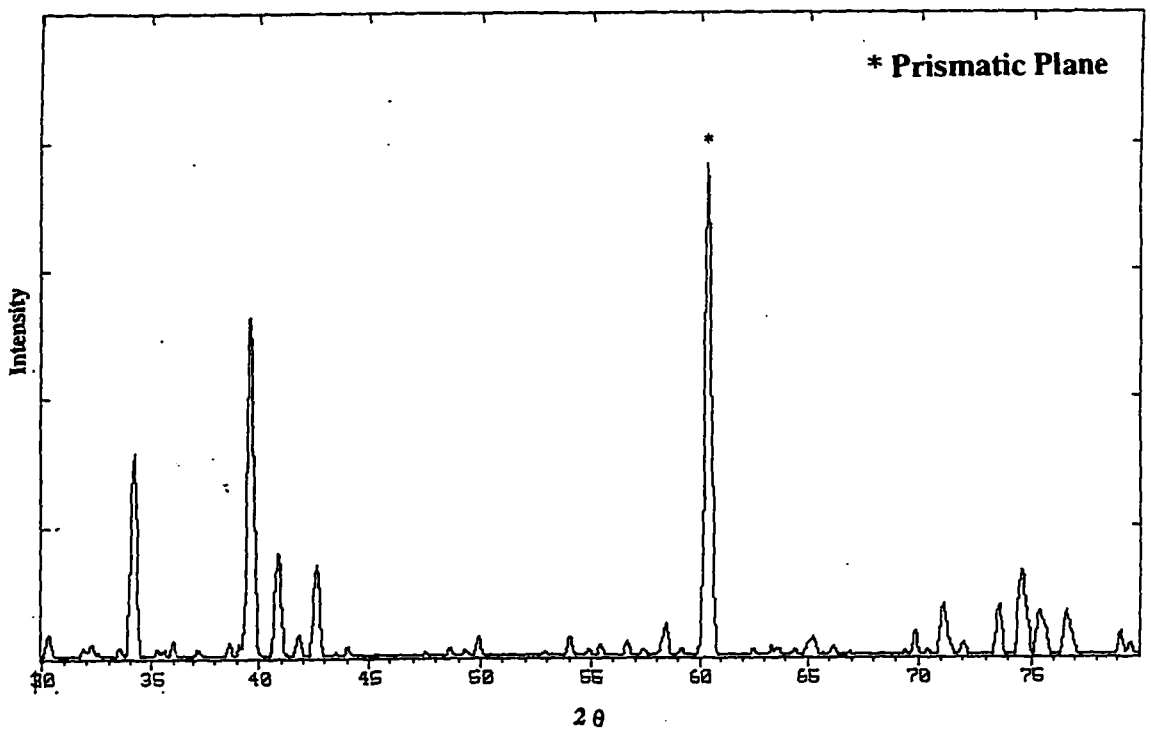

Figure 61. a) X-ray diffraction pattern of the 23 plane . b) Fracture surface showing the cleavage parallel to the basal planes.

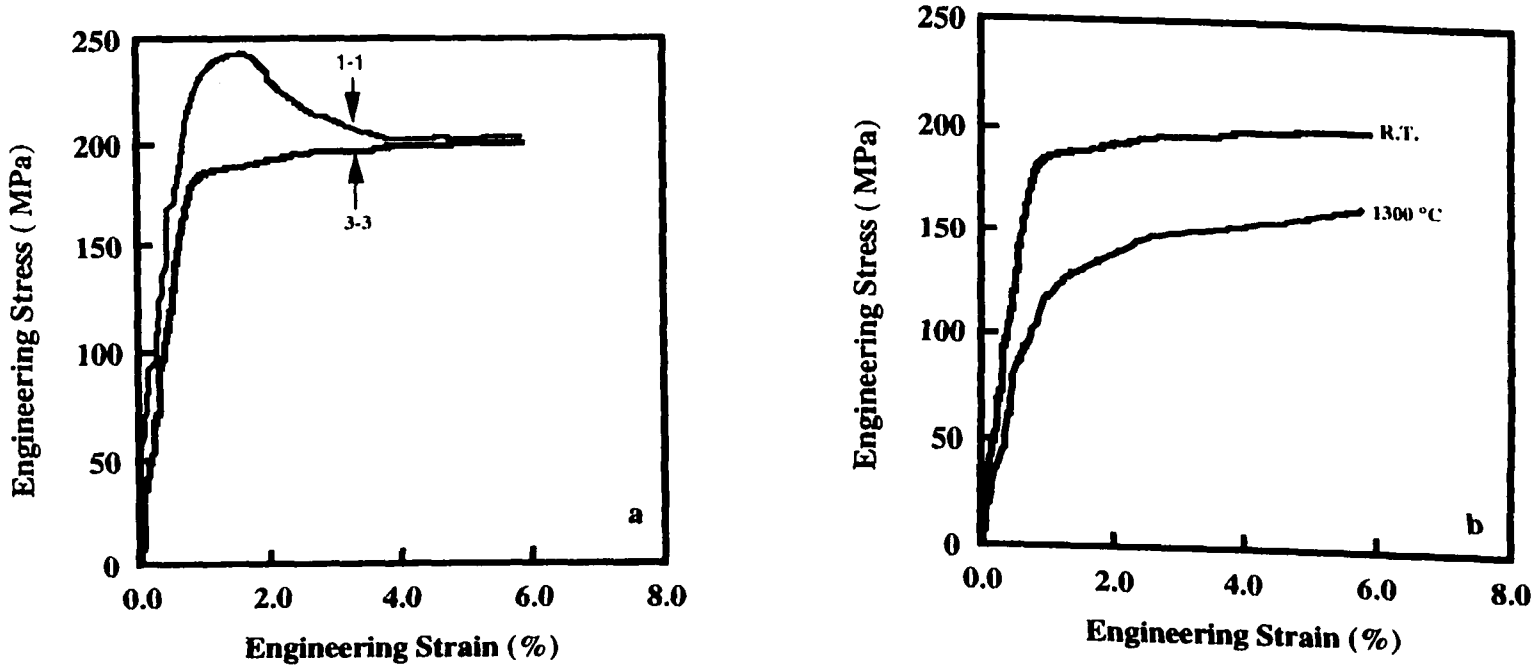

Figure 62 a) The effect of direction (1-1 vs. 3-3) on the compressive strength at room temperature. b) The effect of temperature (direction 3-3) on the compressive strength

Figure 63 Optical micrograph showing a compressed sample in the 1-1 direction at room temperature

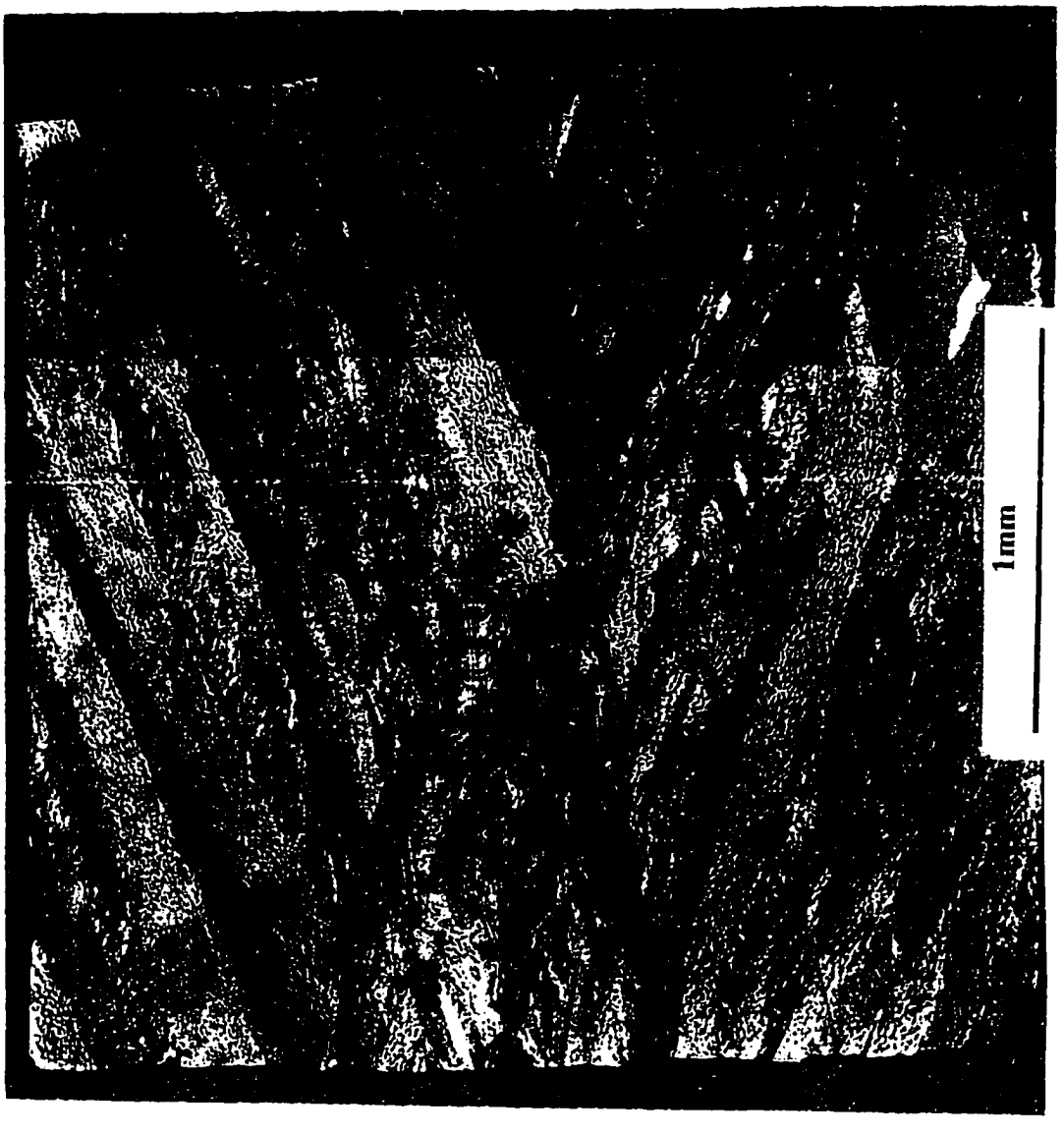

Figure 64 Optical micrograph showing a compressed sample in the 3-3 direction at room temperature

Figure 65 Optical micrograph showing a compressed sample in the 3-3 direction at 1300 °C.

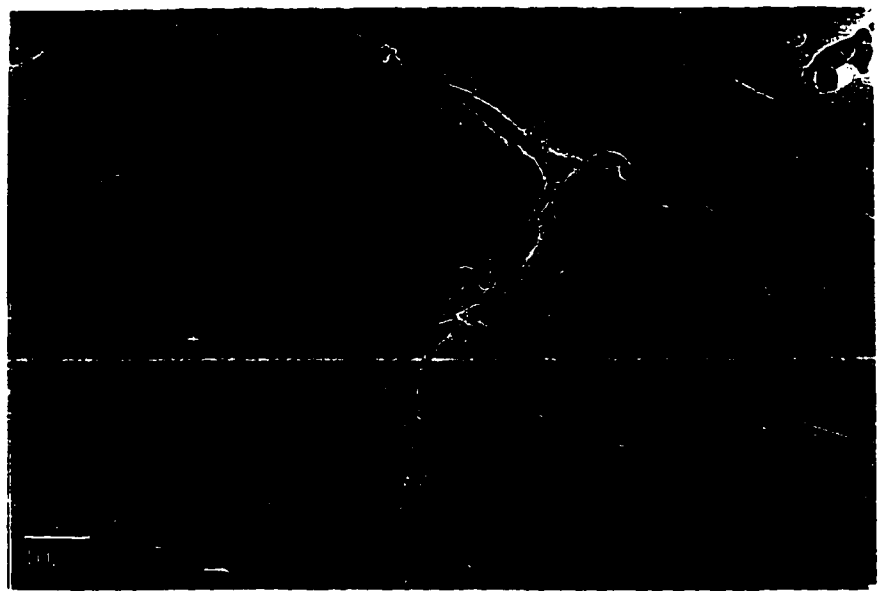

Figure 66. A secondary SEM micrograph showing a cavity formation at the grain boundaries.

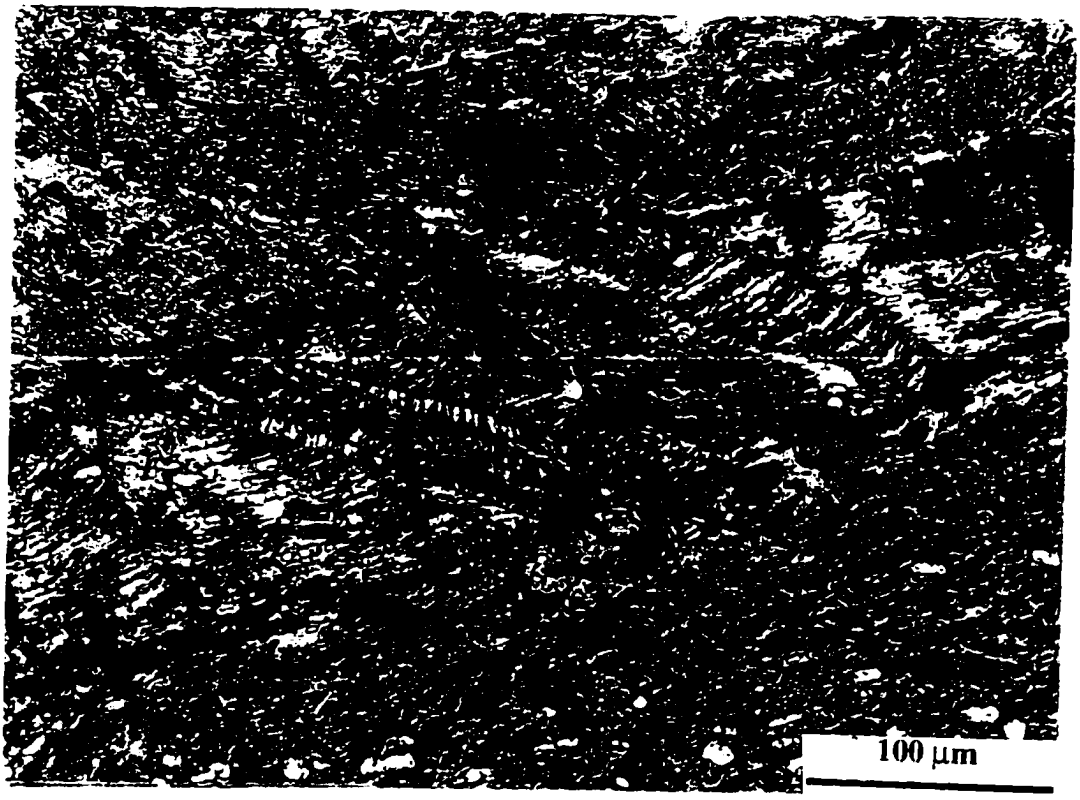

Figure 67. Optical micrograph showing a kinked grain.

Figure 68. Optical micrograph showing a curled grain.

Appendix C

APPENDIX C

Assuming the overall oxidation reaction is:

$$Ti_3SiC_2 + 4.5\ O_2 = 3\ TiO_2 + SiO_2 + 2\ CO\ (g)$$

The molar volumes of Ti_3SiC_2, TiO_2 and SiO_2 (density = 2.5 gm/cm^3) are, respectively, 43.5, 18.8 and 24 cm^3/mole. The total molar volume of the oxides is thus 80.4 cm^3/mole, for a Pilling-Bedworth ratio of 1.85. After oxidation at 1240 °C for 1 hour, according to Table 3, the thicknesses of the inner and outer layers would be, respectively, 75 μm and 58.6 μm. Assuming that the silica and titania do not dissolve in each other and taking a basis of 1 cm^2, the volumes associated with the inner and outer layers are, respectively, 75 x 10^{-4} and 58.6 x 10^{-4} cm^3. These volumes are distributed as:

$$V_{silica} + V_1\ (\text{inner layer}) = 75 \times 10^{-4}\ cm^3$$

$$V_2\ (\text{outer layer}) = 58.6 \times 10^{-4}\ cm^3$$

where V_{silica}, V_1 and V_2 are the volumes of silica, titania in the inner and outer layer, respectively. According to the oxidation reaction the overall volume of titania to silica is ≈ 2.

$$V_{TiO_2}\ (\text{total}) / V_{silica} \approx 2.35$$

Combining these equations and solving for V_{silica} and V_{TiO2} one obtains:

$V_{silica} = 40 \times 10^{-4}$ cm^3, V_{TiO_2} (total) = 93.7 x 10^{-4} cm^3,

It follows that the volume fraction of silica in the inner layer should be about 0.53. The corresponding mass of silica and titania are, respectively, 0.01 g and 0.04 g.

The total mass gained is thus 0.05 g. This value has to be corrected to account for the C lost. Based on the oxidation reaction, for every 3 moles of titania formed 2 moles of

C are lost. Thus mass of C lost is 0.004. The net weight gained is thus 0.046. Since the net gain occurs in one hour, on a 1 cm^2 area the parabolic rate constant equals 46 mg/cm^2 hr or 1.28×10^{-6} kg^2/m^4 s.

At that temperature the overall parabolic rate constant calculated from the thickness measurements is 2950 $\mu m^2/h$. Combining the two results in the conversion factor given in text.

Vita

TAMER S. EL-RAGHY **DOB: 08/19/70**
Citizenship: Egyptian

Education

Ph.D. in Materials Engineering, Drexel University, Philadelphia, PA, June 1997.
M.Sc. in Metallurgical Engineering, Cairo University, Egypt, September 1994.
B.Sc. in Metallurgical Engineering, Cairo University, Egypt, September 1992.

Experience

Research Assistant, Dept. of Materials Engineering, Drexel University
January 1995 - present
Teaching Assistant, Dept. of Metallurgical Engineering, Cairo University, Egypt
September 1992 - 1994

Patents

- M. Barsoum, T. El-Raghy, D. Brodkin, A. Zavaliangos, and S. Kalidindi " Synthesis of 312 Compounds and Composites Thereof ", Patent Pending

- M. Barsoum, T. El-Raghy, and D. Brodkin, " Synthesis of H-Phases Products ", Patent Pending

- M. Barsoum, and T. El-Raghy, " Transient and Non-Transient Liquid Phase Sintering of 312 Compounds and the H-Phases ", Patent Pending

- M. Barsoum, and T. El-Raghy, " Surface Treatment of 312 Compounds and H-Phases ", Patent Pending

Awards

- Drexel University Chapter of Sigma Xi, First Presidential Award, May 1996.
- Best B.Sc. Project From the Egyptian Engineering Syndicate, September 1992.
- 4 Honor Awards From the Egyptian Ministry of Education for Outstanding Academic Performance, 1988 - 1992.

Publications

Nine archival journal papers and six conference presentations.